Dissertation zur Erlangung des Doktorgrades

der Fakultät für Chemie und Pharmazie

der Ludwig-Maximilians-Universität München

Ammonothermal Synthesis of Functional Nitride Oxides And Ternary Nitrides

Niklas Cordes

aus

Bremen, Deutschland

2019

E r k l ä r u n g

Diese Dissertation wurde im Sinne von § 7 der Promotionsordnung vom 28. November 2011 von Herrn Prof. Dr. Wolfgang Schnick betreut.

E i d e s s t a t t l i c h e V e r s i c h e r u n g

Diese Dissertation wurde eigenständig und ohne unerlaubte Hilfe erarbeitet.

München, den 20.05.2019

…….....

(M. Sc. Niklas Cordes)

Dissertation eingereicht am	23.05.2019
1. Gutachter	Prof. Dr. W. Schnick
2. Gutachter	Prof. Dr. O. Oeckler
Mündliche Prüfung am	19.07.2019

Acknowledgements

An dieser Stelle möchte ich Herrn Schnick danken. Die Aufnahme in das *Ammono-FOR* Team hat mir zahlreiche interdisziplinäre Einblicke während meiner Promotion verschafft. Ich halte dies für eines der wichtigsten Erfahrungen in der Zeit meiner Promotion. Ich möchte Ihm zudem für die Möglichkeit zur Teilnahme an Tagungen in Obergurgl, Hirschegg, Bremen, Leipzig und den USA danken.

Ganz besonderer Dank gilt zudem Herrn Prof. Dr. Oliver Oeckler für die Übernahme des Koreferats meiner Dissertation. Weiterhin danke ich für die tolle Zusammenarbeit, sowie die große Hilfe bei jeglichen Diskussionen und Fragestellungen wissenschaftlicher Natur.

Herrn Prof. Dr.-Ing. Eberhard Schlücker, Herrn Prof. Dr. Hans-Christian Böttcher, Herrn Prof. Dr. Konstantin Karaghiosoff und Herrn Prof. Dr. Joost Wintterlin danke ich herzlich für Ihre Bereitschaft als Teil der Prüfungskommission meiner Doktorarbeit zur Verfügung zu stehen.

Großer Dank gilt auch meinen Laborkollegen Jonas Häusler, Peter Wagatha, Philipp Strobel, Mathias Mallmann und Lisa Gamperl. Darüber hinaus, möchte ich Lucien Eisenburger, Markus Nentwig, Christian Maak, Robin Niklaus und Adam Slabon für die tolle Zusammenarbeit danken, hieraus sind einige sehr spannende Projekte entstanden. Ich danke außerdem, meinen Praktikanten Florian Zoller, Arne Goldenbaum, Andreas Hess, Lukas Bauer und Elena Schubert für ihre Hilfe im Labor.

Vielen Dank an meine Kooperationspartner Anna Kimmel, Thomas Steigerwald und Dr. Saskia Schimmel in Erlangen für die unermüdliche Hilfe bei Fragestellungen bezüglich der Autoklaven. Des Weiteren, möchte ich mich bei den Projektpartnern Dr. Meissner, Prof. Dr. Niewa, Prof. Dr. Wellmann und Prof. Dr.-Ing. Schlücker für spannende Diskussionen in unseren Ammonothermalbesprechungen bedanken. Ich bin dankbar für das Arbeiten in dieser professionellen Gruppe und bin gespannt, was die Zukunft bringt.

Den Mitarbeitern des Departments Chemie möchte ich an dieser Stelle ebenfalls danken und vor allem die unentwegte Arbeit der Feinmechanik loben, ohne ihre umgehende Hilfe wäre Vieles nicht in dieser Art und Weise möglich gewesen.

Nicht zuletzt, möchte ich meinen Freunden Doro, Börnie, Marc, Laura, Yvi, Marthe, Angi, Aurelia, Simon B., Steffi, Johannes, Michael S., Claudia, Felix, Tanja, Philipp K., Andi, Paul, Mona, Martin, Mano, Markus, Michael K., Anna, Patrick, Sarah, Philipp P., Jenny, Torben und Albi danken. Besonders möchte ich die Unterstützung von Kerstin während meiner Promotion hervorheben. Ihr alle habt dafür gesorgt, dass es in der Uni und darüber hinaus nie langweilig wurde und so die nötige Abwechslung sichergestellt.

Mein allergrößter Dank gilt meinen Eltern und meinem Bruder. Ich wünschte, ich könnte sagen, dass ich euch nicht etwas schulde. Doch dann würde ich nicht an dieser Stelle in meinem Leben stehen. Eure Unterstützung sucht seinesgleichen.

„Das Ganze ist mehr als die Summe seiner Teile."

(Aristoteles)

Table of Contents

1 Introduction

The Earth Overshoot Day demonstrates a calculated date on which humanity's resource consumption for the current year exceeds Earth's capacity to regenerate those resources in the same year. In 2018 this day was August 1st.[1] This fact demonstrates the massively growing demand for energy and resources. Global population growth requires environmental-friendly alternatives for conventional fossil fuel based energy sources as well as ecological solutions for everyday life and sustainable mobility. Therefore, research is focused on new advanced functional materials with unique optical and electronic properties.[2] Important components of this everyday life technology are semiconductors. They are used in a lot of devices of daily life such as computers, data storage media, cell phones, photovoltaics and to a greater extent in cars. More importantly, such materials have the ability to produce hydrogen and oxygen from water with the support of sunlight. This photocatalytic water splitting provides a renewable energy source without the use of coal-based raw materials and therefore does not produce any anthropogenic greenhouse gas emissions like CO_2. Fortunately, water and solar energy resources are abundantly available on earth.[3, 4] Before irreversible damage in the environment occurs by a due to fossil fuel based economy, further research for earth-abundant semiconductors with electronic and optical properties as well as suited alternatives for commonly used materials is required.

In the past 30 years nitrides attracted great interest. BN and Si_3N_4 are used for high-performance applications due to their high level of hardness and temperature resistance. Besides these two often used nitrides, there are several other prominent representatives used as refractory materials, corrosion- and mechanical wear-resistant coatings, hard materials and magnets.[5] Chemical tuning of nitrides may be done by cation doping or exchange of the respective metal, but, the large diversity of compounds further increases by anion substitution. Conversely, anion substitution is less explored. This is a consequence of the high stability of metal-oxygen bonds and the bond energy of O_2 and N_2 (see Table 1) which in many cases required use of less straightforward and often more laborious synthesis methods.[6, 7] By exchange of anions e.g. nitrogen in pure oxygen compound properties become even more useful.[6]

Table 1. Properties of nitrogen and oxygen.[8]

	N	O
Anion charge (z)	-III	-II
Electronegativity	3.0	3.4
Atomic polarizability/Å³	1.10	0.80
Electron affinity (A → A^{z-}/kJ mol^{-1}	1736	601
Bond energy A–A (kJ mol^{-1})	941	499
Ionic radii/A (for CN = IV)	1.46	1.38
Coordination number (CN)	II-VIII	II-VIII
Ionization energy (kJ/mol)	1402.3	1313.9

One of the most abundant and well investigated substance classes are perovskites. Perovskites have been discovered by the Russian mineralogist G. Rose in mineral deposits in the Ural and are named after the Russian mineralogist C. L. A. von Petrovski. The general formula ABX_3 represents ionic compounds, where *A* is usually a large cation, *B* is usually a smaller-sized cation and *X* is an anion.[9]

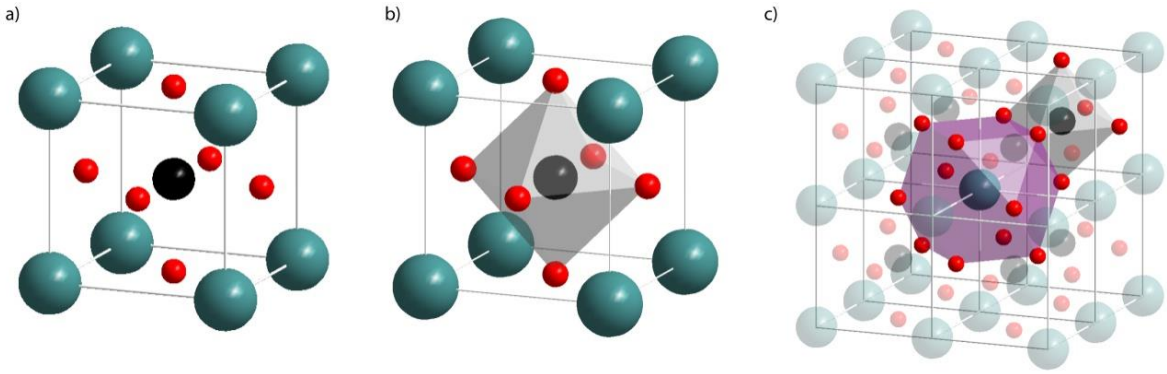

Figure 1. a) Ideal perovskite structure of $SrTiO_3$ with Ti^{4+} (black) in the centre b) TiO_6 octahedral coordination (grey) c) perovskite super cell (2x2x2) with Sr^{2+} in the centre with cuboctahedral cage (pink) and TiO_6 octahedral coordination (grey) connected with an common face.[10]

One measure of the stability and distortion of perovskites is presented by the Goldschmidt tolerance factor. Goldschmidt suggested that the likelihood that a pair of ions would form a perovskite structure phase when

$$t = \frac{(r_A + r_B)}{(\sqrt{2}\,(r_B + r_X))} \qquad \text{(Eq. 1)}$$

is, where t is called tolerance factor, r_A is the ionic radius of the cuboctahedrally coordinated cation, r_B is the radius of the octahedrally coordinated cation and r_X is the radius of the anion.[11] For the ideal cubic structure there is a geometric value of $t = 1$. In fact, this structure is observed when $0.89 < t < 1.1$. Distorted perovskites can be found, if $0.8 < t < 0.89$, hexagonal perovskites in general possess values with $t > 1$, whereas values below $t = 0.8$ lead to the Illmenite-type. Apart from its simplicity, the tolerance factor has reasonable predictive power, especially for many oxides.[10, 12, 13] Still, perovskites are no pure ionic compounds and the result of the tolerance factor depends on the ionic radii. Therefore, the Goldschmidt tolerance factor is only a rough estimation.[9]

The first nitride oxide* perovskites with the general formula $ABO_{2-x}N_{1+x}$ were obtained by Marchand et al. in 1986.[14] After the first discovery, many different nitride oxide perovskite compounds were synthesized. Usually, ternary oxide precursors, which have been prepared from the binary oxides are used. This route is called hard chemistry approach. Another possibility, using a sol-gel process, is the so-called Pechini method. The starting materials are dissolved in citric acid and mixed. Afterwards, the precursor is dried, so that the organic matrix is burned. This yields a highly reactive precursor, which is subsequently heated in an ammonia stream. At temperatures above 500 °C ammonia dissociates into the reactive gases N_2 and H_2.[15] Interestingly, directly applying an equivalent mixture of nitrogen and hydrogen has no effect on oxides under the same conditions. In the Pechini method, additive salts are widely used as flux to promote the diffusion of the starting materials.[16]

Numerous nitride oxide perovskites including alkaline earth metals (Ca, Sr, Ba) or lanthanides (e.g. La, Pr, Nd) in combination with transition metals (e.g. V, Nb, Ta, W) were discovered in recent years.[7, 17] Generally, these materials are synthesized at temperatures between 650 – 1050 °C in flowing ammonia. This so-called ammonolysis

*: nitride oxide is correct according to IUPAC. In the following publications “oxonitride” or “oxynitride” was formerly used.

can easily be performed, though also has its limits. Regrinding of the starting materials, different flow rates and thermodynamic formation of stable residual side phases, just to mention a few difficulties, which lead to limited product yields.

Sometimes oxygen can only partly be exchanged by nitrogen in ammonolysis gas flow reactions. $SrMoO_{2.6}N_{0.4}$ was obtained from $SrMoO_4$ in flowing ammonia at 750 °C. Later the corresponding $SrWO_2N$ was successfully synthesized at 900 °C and a higher nitrogen amount was achieved for $SrMoO_{2.5}N_{0.5}$ by Fawcett et al.[18] Remarkably, in $LaWO_{0.6}N_{2.4}$, a significantly larger proportion of nitrogen can be incorporated by ammonolysis.[19] It is possible to partially substitute Ca^{2+} for La^{3+}, resulting in solid solutions like $Ca_{0.25}La_{0.75}TiO_{2.25}N_{0.75}$.[20]

The findings described above demonstrate that a whole series of nitride oxide perovskites have been displayed with the help of ammonolysis. However, this reaction path has some difficulties The synthesis at ambient pressures could sometimes be difficult because of the formation of thermodynamic stable side phases.[17] Therefore, new synthetic approaches were used applying increased pressure and innovative solution-based processes. The first high pressure synthesis of $BaNbO_2N$ using BaO, BaO_2 and NbN was performed in 1995 by Troyanchuk et al. Remarkably, no gas was necessary for the synthesis at 1000°C and a pressure of 5 GPa.[21] However, the new nitride oxide perovskites $RZrO_2N$ (*R* = Pr, Nd, Sm) were synthesized *via* a direct solid-state reaction of R_2O_3 with Zr_2ON_2 at 1200°C – 1500 °C under 2 – 3 GPa pressure using the multi-anvil technique.[22]

In general, the morphology of the nitride oxide perovskite crystals obtained by high pressure techniques and ammonolysis is undefined and random. By using a KCl flux for the synthesis of $BaTaO_2N$ submicron-sized cube-like crystals were obtained[23] and rectangular crystals of $Sr_{1-x}Ba_xTaO_2N$ were grown with the help of $BaCN_2$ flux.[24] Further examples, where defined crystals are accessible are $LaTaON_2$[25] and $LaTiO_2N$, synthesized by ammonolysis reactions.[26, 27]

Despite the difficulties concerning the methods to obtain nitride oxide perovskite crystals nitride oxide perovskite crystals and films are of strong interest due to their special properties such as ferroelectricity and dielectricity. $LaTiO_xN_y$ thin films were prepared by a reactive magnetron sputtering technique using reactive plasma and an oxide target.[28] $SrMoO_{3-x}N_x$ has been fabricated by pulsed laser deposition of $SrMoO_4$ in hydrogen.[29] $BaTaO_2N$ thin films were grown by pulsed laser deposition using a

[100]-cut $SrTiO_3$ substrate.[30] Thick films of nitride oxide perovskites ($LaTiO_2N$, $NbTiO_2N$, $SrNbO_2N$ and $SrTaO_2N$) were synthesized by nitridation of single of the corresponding oxides with general composition $ABO_{3.5}$ crystals in flowing ammonia. Another possibility is to use reactive magnetron sputtering of powdered $La_2Ti_2O_7$ target under N_2-rich plasma to synthesize $LaTiO_2N$ films.[31] Different thin film synthesis are modified molecular-beam epitaxy (MBE)[32] and plasma-assisted pulsed laser deposition (NPA-PLD).[33-35] A more recently developed explosion reaction type is an intense exothermic reaction between $Ba(OH)_2$, $NbCl_5$ and $NaNH_2$ to produce $BaNbO_2N$ in seconds.[36]

As illustrated above, many nitride oxide perovskites are only accessible by explorative reaction approaches. Besides many different synthesis methods, versatile properties of the nitride oxide perovskite family lead to tailor-made wide spectrum of applications. They have been reported as non-toxic pigments,[37] colossal magnetoresistive materials, [8, 38] high permittivity dielectrics[39-41] and photocatalysts.[8, 42, 43]

The possibility to introduce nitrogen as a substitute for oxygen within the anionic network of perovskites allows a significant enrichment of possible perovskites. Metal nitride oxides are emerging materials that may exhibit properties of oxides and nitrides at the same time. For example, the introduction of nitrogen reduced the band gap of colorless oxygen compounds.[44]

Nevertheless, the consequence of the high stability of the metal-oxygen bond is that the synthesis of anion-substitution compounds is elaborate and requires the use of less straightforward methods. All aforementioned synthesis routes have in common that the obtained films are only several micrometers thin and that substrates for successful growth are required. The accompanying lattice mismatch has many disadvantages. Powders synthesized by ammonolysis are microcrystalline and defined crystals are scarcely obtained. This demonstrates the importance of innovative explorative synthesis methods, which could enable access to novel functional nitride oxides and nitride compounds.

Considering that, the ammonothermal method represents a highly promising technique in this field. It is derived from hydrothermal synthesis, but uses ammonia instead of water as reaction medium. Rather moderate temperatures in combination with high pressured ammonia provide suitable reaction conditions for many inorganic substances. Ammonia is often present in supercritical form, where distinct liquid and

gas phases do not exist. It is very similar to water in many respects, but it is less explored within research and commercial application fields due to the less straightforward handling. Ammonia is polar, protic, subject to autoprotolysis, has a low specific conductivity, but provides only small solubility for many inorganic compounds, which frequently yields poorly crystallized and amorphous solids. Solubility can be increased by pressurized supercritical ammonia due to higher permittivity and the deployment of mineralizers.[45]

During the last decade, the ammonothermal approach attracted great attention. Several concepts of the hydrothermal can be adapted to the ammonothermal method, since both are solvothermal methods.[45, 46] This method includes temperature, pressure, mineralizer, chemical transport and crystal growth mechanism in a modified way for the synthesis of nitrides and nitride oxides. The ammonothermal method also gained great attention because of the lack of useful growth techniques of large GaN single crystals, however it is still a challenge.[47] For ammonothermal crystal growth, the nutrient polycrystalline GaN is dissolved in the presence of different mineralizers under the formation of well-soluble complex intermediate species.[48] Three different mineralizer classes (neutral, ammonobasic and -acidic) can be differentiated. Typically, alkali metal amides and ammonium halides are employed as mineralizers. An applied temperature gradient leads to convection of the intermediates inside the pressure vessel, which are transported to the growing seed crystal. The crystal growth is therefore achieved by dissolution and recrystallization based transport reactions. Intermediates have a major impact on solubilities, mass transport, growth rates, growth faces as well as predominant growth directions and are thus essential to elucidate and optimize crystal growth. The autoclave contains a baffle plate (Figure 2a) that regulates the mass transport (Figure 2b, 2c) and limits heat transfer between dissolution and growth zones. In that way, formation of defects is minimized by providing constant temperatures in seed zone (Figure 2c). Numerous parameters such as fluid temperature, pressure, autoclave and baffle geometry, fluid convection, type of nutrient and seeds, type and concentration of mineralizer as well as impurities lead to a very complex system for an effective crystal growth.[45, 49]

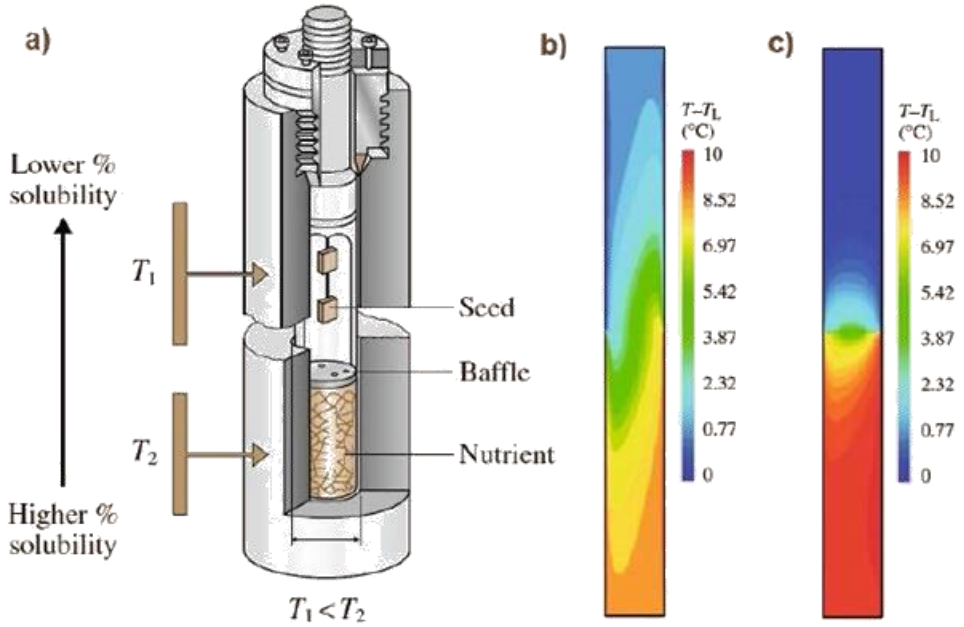

Figure 2. Schematic structure of the temperature gradient method (a) the temperature distribution in the autoclave without (b) and with baffles (c) with ΔT = 10 °C.[50]

Baffle plates mounted in the autoclave are used to regulate mass and heat transport between dissolution and growth zones. Using this method crystal growth can be effectively controlled and additionally formation of defects is minimized by constant temperatures around the seed.[49]

Although the ammonothermal synthesis is derived from the hydrothermal synthesis, it is much less explored. This fact can primarily be explained due to the history of ammonothermal synthesis. Since the 1950s Herbert Jacobs and its coworkers were focusing on the explorative synthesis of metal amides, imides and ammoniates.[45] In the last decade the main focus of the ammonothermal research has been based on the development of large GaN crystals, while the explorative synthesis of new compounds fell literally behind. In 2011 the *Ammono-FOR* research group was found by an interdisciplinary team of chemists, engineers and crystallographers of the Universities of Erlangen, Stuttgart and Munich. The aim of this group is to reestablish the ammonothermal technology as a powerful synthetic tool to investigate various nitrogen (and oxygen)-containing compounds in supercritical ammonia and the subsequent characterization in terms of typical solid-state methods.[51] Nowadays, commercially available autoclave systems barely provide the required parameters for the ammonothermal synthesis in supercritical ammonia. This challenging demand for

new autoclaves can be sufficiently supplied by the *Ammono-FOR* group itself to synthesize new and well crystalline nitride and nitride oxide materials and investigate crystallization processes *in situ*. With regard to previous findings and theoretical calculations in the field of these compounds, innumerable unprecedented nitride oxides materials still await their discovery. The aforementioned tolerance factor predicts many other compounds of the type $ABO_{2-x}N_{1+x}$ which crystallize in the perovskite type.[12] In addition, there are nitrides with the perovskite[52] and delafossite structure[53] which are predicted. The complete substitution of oxygen against nitrogen will form pure nitride perovskites. Possible compounds are $LaReN_3$, $YReN_3$ and $LaWN_3$. $LaWN_3$ is a semiconductor and displays a large ferroelectric polarization.[52]

Moreover, such materials are essential for the evolution of photocatalytical hydrogen production providing renewable energy sources without collateral formation of greenhouse gases. The increasing scarcity of industrially important elements like gallium or indium further demands the search for earth-abundant semiconductors with similar electronic and optical properties as well as suited alternatives for commonly used materials. Regarding this wide range of applications, the exploration of new functional materials is an important aspect in solid-state chemistry enabling development of innovative and novel devices that can promote a sustainable future.

This thesis covers the evaluation of the required interacting parameters and customization of newly developed autoclave systems. The close cooperation with the *Ammono-FOR* group improved the design of the autoclave system to efficiently obtain access to multinary nitride (oxides). High pressure autoclaves are made of a nickel based superalloy deliver eminent chemical stability against supercritical ammonia in combination with corrosive mineralizers as well as a high yield and tensile strength at maximized process temperatures of up to 1100 K. Therefore, the potential of the ammonothermal synthesis has astonishingly promoted the formation of highly crystalline multinary nitrides and nitride oxides from supercritical ammonia solutions. Crucial steps for this goal were the systematic investigation of suitable reaction conditions (temperature and pressure), different mineralizer systems as well as highly reactive precursor species in combination with new liner-systems under ammonothermal reaction conditions.

By comparing hydrothermal and ammonothermal synthesis and its commercial application fields, the latter is far less explored. The oxide perovskite synthesis within the hydrothermal method is well established.[54, 55]

Since, nitrogen and oxygen have similar chemical properties (see Table 1), the introduction of oxygen in nitride compounds and vice versa have particular difficulties.[56] The affinity of most elements for oxygen is higher than those of the corresponding nitrogen compounds. Besides that, the formation of oxides is problematic because the bond enthalpies are also higher and the formation of oxides is thus an important side reaction.[57] The ammonothermal approach for nitrides requires therefore the rigorous exclusion of oxygen and water. But, GaN[47] and InN[58] obtained by the ammonothermal synthesis for example often possess not negligible amounts of oxygen in their lattice.[59] Whereas, the formation of nitride oxide perovskites with the gas flow ammonolysis is easy to perform.[15] The dissociation is appreciable at temperatures higher than 500°C where many metal oxides significantly begin to react with NH_3. The reaction follows the general equation:

$$ABO_3 + x\ NH_3 \rightarrow ABO_{3-x}N_x + H_2O + \tfrac{1}{2}\ H_2 \qquad \text{(Eq. 1)}$$

Any formation of the nitride oxides is supported by the dissociation of NH_3 into N_2 and H_2 and the removal of water in the gas flow tube furnace (Eq. 1).[7] However, the ammonothermal approach of nitride oxides encounters challenges. The dissociation is predominant in the closed autoclave[60] during the ammonothermal synthesis, but the removal of water is not possible in this self-contained system. The use of oxygen containing starting materials is problematic, because of the above mentioned chemical behavior of oxygen and nitrogen. Watanabe though only used $NaNH_2$ for the synthesis and stated that it was contaminated with NaOH to a considerable extent.[61] Consequently, the use of a certain amount of oxygen is necessary. By the use of a deficient amount of NaOH the formation of oxides is hampered and small amounts of residual phases can be extracted.[62-64]

Facing these problems, the advantages of solution-based methods are low temperatures and the control of crystal size and shape by means of crystal growth. The ammonothermal synthesis of nitride oxide perovskites is built on this basis. At the moment, ammonothermal synthesis pools most efforts on the crystal growth of GaN,

and since the retiring of Jacobs, only a few studies focused on the ammonothermal studies of multinary nitride oxides were published. Since there is sparse information about solubility and crystallization behavior of inorganic compounds in supercritical ammonia, the demand for valuable information about the ammonothermal synthesis is important. The demand for high quality autoclave materials is a key requirement because supercritical fluids like ammonia in combination with added salts are highly corrosive. High temperature and high pressure impede the selection of autoclave material. From this technical point of view, the ammonothermal approach is quite challenging, as there are only a few heat resistant materials available and commercially autoclaves barely provide the required reaction parameters. As a result, the *Ammono-FOR* research group, especially the Chair of Process technology and machinery at University of Erlangen-Nuremberg, developed own autoclave systems to investigate the holistic ammonothermal approach. Over the years the design was improved to efficiently obtain access to multinary nitride oxides and nitrides. Since first autoclaves only withstand 600 °C, new autoclaves had been needed to enhance the potential of the ammonothermal synthesis at elevated temperatures.[60] The above mentioned further development of autoclave systems expands the accessibility of novel compounds and the crystals growth of known nitride oxides.[62-64]

On the basis of newly developed autoclaves and in close collaboration with other *Ammono-FOR* group members, this thesis deals with the synthesis and characterization of new nitride oxides by means of ammonothermal synthesis. This area of inorganic solid-state chemistry is in its infancy. As the ammonia gas flow ammonolysis reaction produces, in rare cases, crystals of nitride oxides, the ammonothermal approach provides a sophisticated method to grow µm-sized crystals with the targeted use of starting materials and mineralizers.

This thesis starts with the ammonothermal synthesis of known compounds of the alkaline earth metals with the transition metals Nb and Ta resulting in Sr/BaNb/TaO_2N and the ^{14}N NMR investigation of the *AM*(O_2N) with *A* = Ca, Sr, Ba, La and *M* = Nb, Ta was performed. Furthermore, the publication of *Ln*TaON_2 with *Ln* = La, Ce, Pr, Nd, Sm, Gd is demonstrated and the obtained products are investigated by typical solid-state methods. The attempted synthesis of the europium nitride oxide perovskite (Eu$Ta(O,N)_3$) resulted in the novel Ruddlesden-Popper phase $Eu_3Ta_2N_4O_3$. Another chapter is about the ammonothermal synthesis of the *A*TaN_2 with *A* = Na, K ,Rb, Cs nitrides and their electronic and optical properties. The last part covers the

ammonothermal synthesis of $PrNb(N,O)_3$ and the mineralizer conditions in the system of $PrTaN_2O$.

[1] M. Wackernagel, A. Galli, L. Hanscom, D. Lin, L. Mailhes, T. Drummond, *Routledge Handbook of Sustainability Indictors*, Routledge International Handbooks, **2018**.

[2] T. W. Brown, T. Bischof-Niemz, K. Blok, C. Breyer, H. Lund, B. V. Mathiesen, *Renewable Sustainable Energy Rev.* **2018**, *92*, 834-847.

[3] S. Y. Tee, K. Y. Win, W. S. Teo, L. D. Koh, S. Liu, C. P. Teng, M. Y. Han, *Adv. Sci. (Weinheim, Ger.)* **2017**, *4*, 1600337.

[4] A. Kudo, Y. Miseki, *Chem. Soc. Rev.* **2009**, *38*, 253-278.

[5] R. Dronskowski, S. Kikkawa, A. Stein, *Handbook of Solid State Chemistry*, Wiley-VCH, Weinheim, **2017**.

[6] A. Fuertes, *J. Mater. Chem.* **2012**, *22*, 3293-3299.

[7] A. Fuertes, *Prog. Solid State Chem.* **2018**, *51*, 63-70.

[8] A. Fuertes, *Dalton Trans.* **2010**, *39*, 5942-5948.

[9] U. Müller, *Anorganische Strukturchemie*, Teubner, Wiesbaden, **2008**.

[10] R. J. D. Tilley, *Perovskites: Structure–Property Relationships*, Wiley, United Kingdom, **2016**.

[11] V. M. Goldschmidt, *Naturwissenschaften* **1926**, *14*, 477-485.

[12] W. Li, E. Ionescu, R. Riedel, A. Gurlo, *J. Mater. Chem.* **2013**, *1*, 12239-12245.

[13] O. Bock, U. Muller, *Acta Crystallogr. Sect. B* **2002**, *58*, 594-606.

[14] R. Marchand, F. Pors, Y. Laurent, *Rev. Int. Hautes Temp. Refract.* **1986**, *23*, 11-15.

[15] S. G. Ebbinghaus, H.-P. Abicht, R. Dronskowski, T. Müller, A. Reller, A. Weidenkaff, *Prog. Solid State Chem.* **2009**, *37*, 173-205.

[16] R. Marchand, Y. Laurent, J. Guyader, P. L'Haridon, P. Verdier, *J. Eur. Ceram. Soc.* **1991**, *8*, 197-213.

[17] Y.-I. Kim, P. M. Woodward, K. Z. Baba-Kishi, C. W. Tai, *Chem. Mater.* **2004**, *16*, 1267-1276.

[18] I. D. Fawcett, K. V. Ramanujachary, M. Greenblatt, *Mater. Res. Bull.* **1997**, *32*, 1565-1570.

[19] P. Bacher, P. Antoine, R. Marchand, P. L'Haridon, Y. Laurent, G. Roult, *J. Solid State Chem.* **1988**, *77*, 67-71.

[20] A. Kasahara, K. Nukumizu, G. Hitoki, T. Takata, J. N. Kondo, M. Hara, H. Kobayashi, K. Domen, *J. Phys. Chem. A* **2002**, *106*, 6750-6753.

[21] I. O. Troyanchuk, N. V. Kasper, O. S. Mantytskaya, E. F. Shapovalova, *Mater. Res. Bull.* **1995**, *30*, 421-425.

[22] M. Yang, J. A. Rodgers, L. C. Middler, J. Oró-Solé, A. B. Jorge, A. Fuertes, J. P. Attfield, *Inorg. Chem.* **2009**, *48*, 11498-11500.

[23] M. Hojamberdiev, K. Yubuta, J. J. M. Vequizo, A. Yamakata, S. Oishi, K. Domen, K. Teshima, *Cryst. Growth Des.* **2015**, *15*, 4663-4671.

[24] A. Hosono, Y. Masubuchi, T. Endo, S. Kikkawa, *Dalton Trans.* **2017**, *46*, 16837-16844.

[25] Y.-I. Kim, *Ceram. Int.* **2014**, *40*, 5275-5281.

[26] M. Hojamberdiev, A. Yamaguchi, K. Yubuta, S. Oishi, K. Teshima, *Inorg. Chem.* **2015**, *54*, 3237-3244.

[27] S. Pokrant, S. Dilger, S. Landsmann, *J. Mater. Res.* **2016**, *31*, 1574-1579.

[28] L. Le Gendre, C. Le Paven-Thivet, J. Pinel, D. Fasquelle, J.-C. Carru, F. Cheviré, F. Tessier, R. Marchand, *Silic. Indus.* **2004**, *69*, 165-171.

[29] I. C. Lekshmi, A. Gayen, M. S. Hegde, *Mater. Res. Bull.* **2005**, *40*, 93-104.

[30] Y.-I. Kim, W. Si, P. M. Woodward, E. Sutter, S. Park, T. Vogt, *Chem. Mater.* **2007**, *19*, 618-623.

[31] Y. Lu, C. Le Paven, H. V. Nguyen, R. Benzerga, L. Le Gendre, S. Rioual, F. Tessier, F. Cheviré, A. Sharaiha, C. Delaveaud, X. Castel, *Cryst. Growth Des.* **2013**, *13*, 4852-4858.

[32] A. David, S. Guérin, B. E. Hayden, R. Noble, J.-P. Soulié, C. Vian, I. P. Koutsaroff, S. i. Higai, N. Tanaka, T. Konoike, A. Ando, H. Takagi, T. Yamamoto, T. Fukura, H. Ieki, *Cryst. Growth Des.* **2014**, *14*, 523-532.

[33] D. Oka, Y. Hirose, T. Fukumura, T. Hasegawa, *Cryst. Growth Des.* **2014**, *14*, 87-90.

[34] D. Oka, Y. Hirose, H. Kamisaka, T. Fukumura, K. Sasa, S. Ishii, H. Matsuzaki, Y. Sato, Y. Ikuhara, T. Hasegawa, *Sci. Rep.* **2014**, *4*, 4987.

[35] M. Sano, Y. Hirose, S. Nakao, T. Hasegawa, *J. Mater. Chem. C* **2017**, *5*, 1798-1802.

[36] J. Odahara, A. Miura, N. C. Rosero-Navarro, K. Tadanaga, *Inorg. Chem.* **2018**, *57*, 24-27.

[37] M. Jansen, H. P. Letschert, *Nature* **2000**, *404*, 980-982.

[38] M. Yang, J. Oró-Solé, A. Kusmartseva, A. Fuertes, J. P. Attfield, *J. Am. Chem. Soc.* **2010**, *132*, 4822-4829.

[39] Y. Masubuchi, F. Kawamura, T. Taniguchi, S. Kikkawa, *J. Eur. Ceram. Soc.* **2015**, *35*, 1191-1197.

[40] Y. R. Zhang, Y. Masubuchi, T. Motohashi, S. Kikkawa, K. Hirota, *Ceram. Int.* **2013**, *39*, 3377-3380.

[41] J. Ahchawarattaworn, D. P. Thompson, F. Azough, R. Freer, *J. Ceram. Sci. Tech.* **2016**, *7*, 39-46.

[42] B. Siritanaratkul, K. Maeda, T. Hisatomi, K. Domen, *ChemSusChem* **2011**, *4*, 74-78.

[43] S. Balaz, S. H. Porter, P. M. Woodward, L. J. Brillson, *Chem. Mater.* **2013**, *25*, 3337-3343.

[44] M. Ahmed, G. Xinxin, *Inorg. Chem. Front.* **2016**, *3*, 578-590.

[45] T. Richter, R. Niewa, *Inorganics* **2014**, *2*, 29-78.

[46] A. Rabenau, *Angew. Chem.* **1985**, *97*, 1017-1032; *Angew. Chem. Int. Ed. Engl.*, **1985**, *24*, 1026-1040.

[47] J. Häusler, W. Schnick, *Chem. Eur. J.* **2018**, *24*, 11864-11879.

[48] S. Zhang, F. Hintze, W. Schnick, R. Niewa, *Eur. J. Inorg. Chem.* **2013**, *2013*, 5387-5399.

[49] D. Ehrentraut, E. Meissner, M. Bockowski, *Technology of Gallium Nitride Crystal Growth*, Springer-Verlag GmbH Heidelberg, **2010**.

[50] K. Byrappa, M. Yoshimura, *Handbook of Hydrothermal Technology*, Elsevier Science, **2012**.

[51] Ammono-FOR, *http://www.ammono-for.de/* **2019**.

[52] R. Sarmiento-Pérez, T. F. T. Cerqueira, S. Körbel, S. Botti, M. A. L. Marques, *Chem. Mater.* **2015**, *27*, 5957-5963.

[53] A. Miura, M. Wessel, R. Dronskowski, *J. Ceram. Soc. Jpn.* **2011**, *119*, 663-666.

[54] Y. Hu, H. Gu, Z. Hu, W. Di, Y. Yuan, J. You, W. Cao, Y. Wang, H. L. W. Chan, *Cryst. Growth Des.* **2008**, *8*, 832-837.

[55] D. R. Modeshia, R. I. Walton, *Chem. Soc. Rev.* **2010**, *39*, 4303-25.

[56] A. Fuertes, *Mater. Horiz.* **2015**, *2*, 453-461.

[57] W. Schnick, *Angew. Chem. Int. Ed. Engl.* **1993**, *32*, 806-818; *Angew. Chem.* **1993**, *105*, 846-858.

[58] J. Hertrampf, P. Becker, M. Widenmeyer, A. Weidenkaff, E. Schluecker, R. Niewa, *Cryst. Growth Des.* **2018**, *18*, 2365-2369.

[59] M. R. Amin, T. de Boer, P. Becker, J. Hertrampf, R. Niewa, A. Moewes, *J. Phys. Chem. C* **2019**, *123*, 8943-8950.

[60] S. Pimputkar, S. Nakamura, *J. Supercrit. Fluids* **2016**, *107*, 17-30.

[61] T. Watanabe, K. Tajima, J. Li, N. Matsushita, M. Yoshimura, *Chem. Lett.* **2011**, *40*, 1101-1102.

[62] N. Cordes, W. Schnick, *Chem. Eur. J.* **2017**, *23*, 11410-11415.

[63] N. Cordes, T. Bräuniger, W. Schnick, *Eur. J. Inorg. Chem.* **2018**, *2018*, 5019-5026.

[64] N. Cordes, M. Nentwig, L. Eisenburger, O. Oeckler, W. Schnick, *Eur. J. Inorg. Chem.* **2019**, *2019*, 2304-2311.

2 Ammonothermal Synthesis of *EAMO*$_2$N (*EA* = Sr, Ba; *M* = Nb, Ta) Perovskites and ^{14}N Solid-State NMR Investigations of *AM*(O,N)$_3$ (*A* = Ca, Sr, Ba, La)

Published in: *Chem. Eur. J.* **2018**, *2018*, 5019–5026.

Authors: Niklas Cordes, Thomas Bräuniger, Wolfgang Schnick

https://onlinelibrary.wiley.com/doi/full/10.1002/ejic.201800827

Keywords: Perovskite phases • Ammonothermal synthesis • Solvothermal synthesis • High-pressure chemistry • Solid-state chemistry

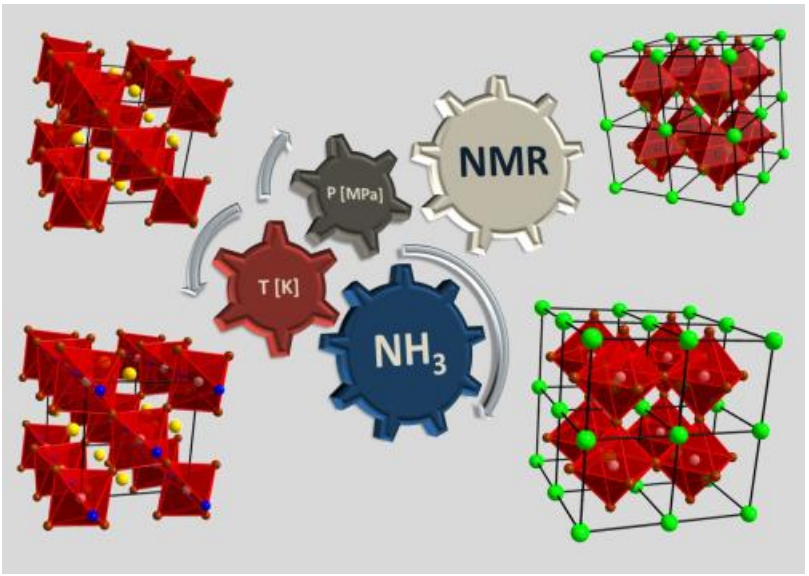

EAMO$_2$N (*EA* = Sr, Ba, *M* = Nb, Ta) oxonitride perovskites crystals were obtained in custom-built high-pressure autoclaves with the ammonothermal approach. Cube like crystals of up to 10 µm were analyzed with PXRD, SEM, EDX, UV/VIS. Furthermore, solid-state ^{14}N NMR measurements were performed on *AM*(O,N)$_3$ with *A* = Ca, Sr, Ba, La; *M* = Nb, Ta). A single resonance was recorded for each compound at about 270 ppm.

Abstract: Alkaline earth oxonitride perovskites *EAM*O_2N (*EA* = Sr, Ba; *M* = Nb, Ta) were synthesized with the ammonothermal method at temperatures of 900 K and maximum pressures of up to 300 MPa in custom-built autoclaves starting from Nb or Ta and Sr or Ba metals. The reactions were performed under ammonobasic conditions using NaN_3 and NaOH as mineralizers. Powder X-ray diffraction and Rietveld refinement were used to determine the crystal structures. The elemental composition and morphology of the obtained products were investigated by scanning electron microscopy and energy-dispersive X-ray spectroscopy. Crystals of 1 - 10 µm size were obtained. Optical band gap values were determined from UV/VIS measurements applying the Kubelka-Munk function with the Tauc method (E_g = 1.9 – 2.1 eV). In addition to that, *A*Nb/Ta(O,N)$_3$ with *A* = Ca, Sr, Ba, La were synthesized by ammonolysis reactions of the respective ternary oxide precursors. The products were investigated with ^{14}N solid-state (MAS) NMR spectroscopy all showing a single resonance at about 270 ppm.

2.1 Introduction

Oxonitrides with perovskite crystal structure are of considerable interest due to their materials properties and potential applications, e.g. as pigments,[1] photocatalysts,[2] dielectrics[3] or magnetic materials.[4] Typically, oxonitride perovskites are synthesized by nitridation in flowing NH_3 (ammonolysis).[5] For this approach, binary and ternary oxide precursors or carbonates can be used for a broad range of different compositions.[6] However, in the last decade new synthetic approaches have been further developed such as thin layer synthesis,[7, 8] plasma-assisted pulsed laser deposition,[9] high-pressure synthesis,[10-12] reactive sputtering,[13] explosive reaction[14] and ammonothermal synthesis.[15-19] Comparing these methods, each of them has their specific advantages. The ammonolysis is easy to perform and uses abundant starting materials like oxides. However, the products are usually obtained as microcrystalline powders and color as well as morphology are significantly depending on reaction temperatures, flowing rates and mineralizers.[2, 20] Only by using carbodiimides $SrCN_2$ and $BaCN_2$ as flux in ammonolysis reactions crystals of up to 1 µm length of $Sr_{1-x}Ba_xTaO_2N$ were obtained. These results underline the importance of the effect of a mineralizer or flux.[21, 22] Pulsed laser deposition for growth of thin films is challenging and product thickness of only several 100 nm or less is obtained. Apart from that, films possess high quality and crystallinity and atomically smooth surfaces that makes them suitable for the investigation of electronic properties.[23-25] High-pressure synthesis of oxonitride perovskites starting from R_2O_3 (*R* = Pr, Nd and Sm) with Zr_2ON_2 typically requires a multianvil setup yielding only small amounts of the product. Interestingly, for this approach no nitriding gas is required enabling new mixed-metal oxonitrides.[10] Very recently, a new reaction approach has been described by using reactive precursors $Ba(OH)_2$, $NbCl_5$ and $NaNH_2$. $BaNbO_2N$ was obtained by explosion reaction within seconds.[14] Recently, the ammonothermal approach was used to synthesize oxonitride perovskites *Ln*$TaON_2$ with *Ln* = La,[15] Ce, Pr, Nd, Sm and Gd.[18] By reacting powdery metals in supercritical ammonia with NaN_3 and NaOH as mineralizers in a high-pressure custom-built autoclave crystals with a cube-like habitus and sizes of several µm length were obtained. The benefits of the ammonothermal method[19] for crystal growth have recently been demonstrated for synthesis of nitrides $ZnSiN_2$ and $ZnGeN_2$,[26] $CaGaSiN_3$,[27] Mg-IV-N_2, Mn-IV-N_2, Li-IV$_2$-N_3 (IV = Si, Ge)[28] and $Ca_{1-x}Li_xAl_{1-x}Ge_{1+x}N_3$ ($x \approx 0.2$).[29]

Besides the synthesis of oxonitride perovskites, there are still challenges in this particular research field. The two anions, O^{2-} and N^{3-} have nearly the same X-ray scattering factors, which makes them difficult to differentiate. In literature different types of anion ordering have been discussed ranging from full crystallographic ordering over partial ordering to complete disorder.[3, 30, 31] On the other hand, solid-state NMR of ^{14}N (spin $I = 1$, natural abundance 99.63%) provides a promising approach for characterization of the local electronic environment of N^{3-}, since the local symmetry of the nitrogen sites in oxonitride perovskites is sufficiently high to avoid the effects of quadrupolar interaction.[32-35]

In this contribution, we report on synthesis of the oxonitride perovskites *EAM*O_2N (*EA* = Sr, Ba; *M* = Nb, Ta) by the ammonothermal approach and their characterization by PXRD, SEM and UV/VIS measurements to estimate the optical band gaps. Furthermore, we synthesized *AM*(O,N)$_3$ with *A* = Ca, Sr, Ba, La and *M* = Nb, Ta by ammonolysis reactions and measured ^{14}N solid-state NMR spectra.

2.2 Results and Discussion

2.2.1 Synthesis

The oxonitride perovskites with composition *EAM*O_2N (*EA* = Sr, Ba; *M* = Nb, Ta) were obtained by ammonothermal synthesis using custom-built autoclaves made of the nickel-based superalloy Inconel 718.[18, 19] Experimental parameters have been carefully optimized in order to obtain phase pure, highly crystalline products and suppress the formation of side phases. Contrary to other ammonothermal reactions leading to oxonitride perovskites,[15, 16] our approach comes along without elaborate precursors (e.g. amides or arc melted alloys).

The transition metals Nb and Ta were added in substoichiometric amount in order to suppress formation of undesired side products like $NaNbN_2$, $NaTaN_2$, NbH and TaH. However, in some of our reactions non-reacted Ta or TaH was found as side phases. We have used powdery metals Nb or Ta and Sr or Ba as starting materials and NaN_3 and NaOH as mineralizers.[18] NaOH is also the required oxygen source for the desired oxonitride perovskite. All of the starting materials were ground for better solubility, except for Sr and Ba, and subsequently placed in bottom sealed cylindrical Nb Ta

liners, respectively. These custom-built liners are an extra barrier to prevent the autoclave from corrosion and were used to facilitate isolation of the products from the autoclave. Under supercritical conditions, Sr and Ba are converted to the respective amides ($Sr(NH_2)$, $Ba(NH_2)_2$, $Na_2Sr_3(NH_2)_8$).[36-38] They decompose during the reaction and react with Nb / Ta. The nature of reaction intermediates which are relevant for the formation of oxonitride perovskites in supercritical ammonia are still a matter of debate.[18]

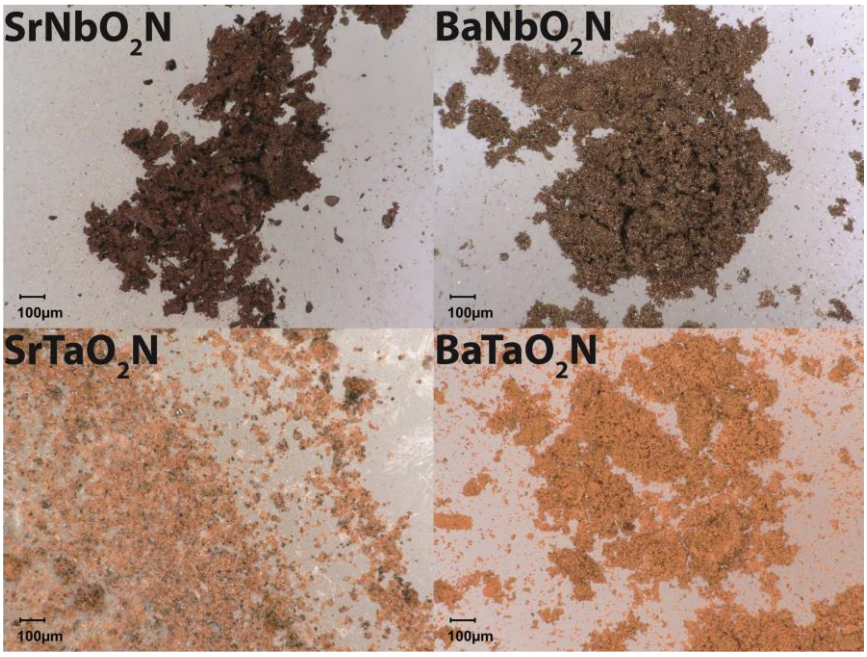

Figure 1. Optical pictures of synthesized oxonitride perovskites *EAM*O_2N with *EA* = Sr, Ba and *M* = Nb, Ta (all with magnification of 200x).

Na*EA*-amides, which are well investigated,[39] may be assumed as intermediates for the reactions discussed in this contribution. According to previously investigated ammonothermal syntheses of nitrides, amide or amide imide intermediates could be formed after dissolution of the metals in supercritical ammonia. Gradual polymerization of these intermediates by condensation of NH_3 and H_2O due to partial substitution of amide by hydroxide and imide by oxide would yield the respective oxonitrides.[17, 40] Non-condensed octahedral anions, like $Na*M*(O_{1-x},N_x)_{3-x}$ with *M* = Nb, Ta may occur as well,[18] this seems likely because the same coordination also occurs in the formed oxonitride perovskites as well. For the hydrothermal synthesis of $KTa_{1-x}Nb_xO_3$ the oxide intermediate $Na(Ta/Nb)O_{3-x}$ has been discussed as well.[41, 42]

We assume a dissolution/precipitation process because of the well developed habitus (Fig. 3) of the obtained cube like crystals of the products. The reaction process could take place at the bottom of the Nb/Ta liner in a melt of the $NaNH_2$/NaOH mineralizer. Druse-like agglomerations of the oxonitride perovskite crystals are found after the reaction and cracking of the liner. Furthermore, formation of an oxide precursor during the reaction may be possible. This intermediate could react to the desired oxonitride perovskite by nitridation in the presence of hydrogen resulting from dissociation of ammonia at high temperature and pressure within the autoclaves.[43, 44]

The obtained product contained negligible side phases of $NaNH_2$ and Sr/Ba$(NH_2)_2$. Residual mineralizers were removed easily by washing with water and EtOH. After washing with conc. HCl or aqua regia a single-phase product was obtained. The four products were successfully synthesized at temperatures of about 900 K and pressures up to 300 MPa. The autoclave was held for 80 h at the reaction temperature, but inner temperature of the reaction vessel might be lower due to temperature loss between furnace and inner wall of the autoclave. The pressure decreases over time because of hydrogen loss through the autoclave wall. The obtained products exhibit dark red ($SrNbO_2N$), brown ($BaNbO_2N$) and brick-red (Sr/$BaTaO_2N$) colors (Fig. 1), respectively. PXRD investigations proved the formation of crystalline single phase products (Fig. 2).

Still the Ca phases of the respective oxonitride perovskites could not be obtained which is maybe due to the lower solubility of Ca in supercritical ammonia.[45] By variation of the reaction parameters (temperature, reactive precursors) it might even be possible to successfully synthesize the Ca compounds as well.

2.2.2 Crystal-structure analysis

Crystal structures were analyzed and refined by powder X-ray diffraction (PXRD). Rietveld refinement (Fig. 2) was used to determine structural parameters, where literature known Wyckoff positions and atomic coordinates were used as starting values.[3] The crystallographic data are listed in table 2. The small peak widths of the reflections indicate highly crystalline products. In addition, no remarkable background was visible in the PXRD patterns, indicating the absence of amorphous phases. Due

to the nearly indistinguishable X-ray scattering factors of O and N there was no evidence for crystallographic ordering of oxide and nitride anions in the products.

$BaNbO_2N$ and $BaTaO_2N$ have regular cubic structure (space group $Pm\bar{3}m$) and therefore is no evidence for octahedral tilting. The resulting demonination in the Glazer system is $a^0a^0a^0$. By tilting of the octahedra in $SrNbO_2N$ and $SrTaO_2N$ a lower tetragonal symmetry (space group *I*4/*mcm*) is observed. This is expressed by the Glazer symbol $a^0a^0c^-$.[46, 47]

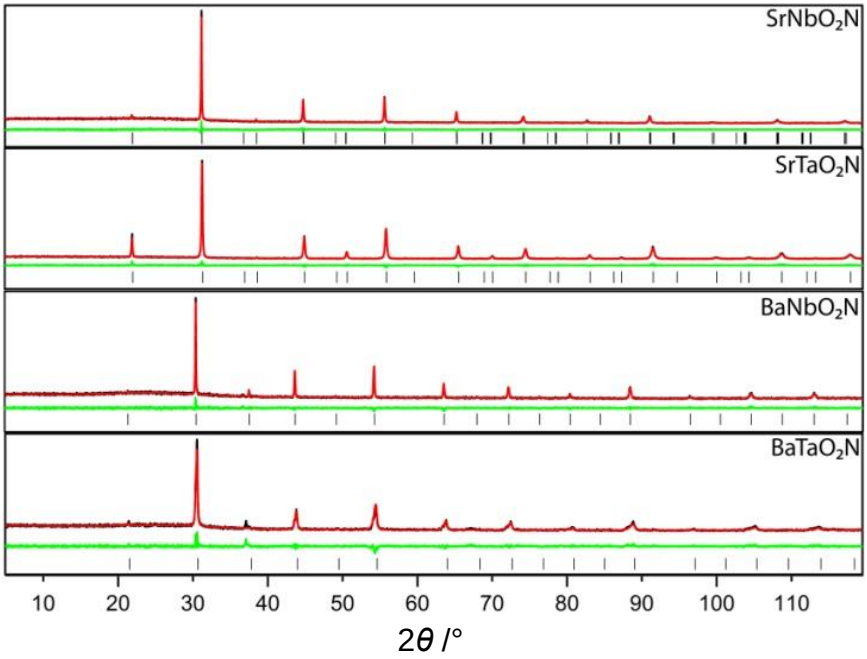

Figure 2. Rietveld refinements of $SrNbO_2N$, $SrTaO_2N$, $BaNbO_2N$ and $BaTaO_2N$ with experimental data (black lines, Cu-Kα_1, 1.54056 Å), calculated patterns (red lines), difference plot (green lines) and positions of Bragg reflections (black bars).

The lattice parameters and the corresponding volume of the unit cell are in very good agreement with values from literature.[3, 48] For $BaNbO_2N$ the cubic space group $Pm\bar{3}m$ (no. 221) was used to refine literature known lattice parameters which correspond as well.[5] Interestingly, the niobium compounds have larger unit cells than the tantalum oxonitride perovskites (Sr-compound: for $\Delta a = \Delta b = +0.4\%$, $\Delta c = +0.33\%$, $\Delta V = +1.04\%$; Ba-compound: $\Delta a = \Delta b = \Delta c = +0.48\%$, $\Delta V = +1.45\%$) though the ionic radii for both Nb^{5+} and Ta^{5+} are nearly identical.[49] The reason for this unit cell enlargement could be the introduction of small concentrations of charge carriers into

the conduction band resulting in a partial reduction of Nb^{5+}.[3] In general, the lattice parameters of the corresponding tantalum oxonitride perovskites are also in agreement with literature data.[3]

The PXRD pattern of $BaTaO_2N$ compound shows small shoulders of the reflections on their low angle side (see Figure 2, $BaTaO_2N$). These shoulders could be explained by a second phase of $BaTaO_2N$ with space group *P4/mmm* (no. 123),[50] where the reflections split by symmetry lowering. In addition to that, the combustion nitrogen analysis of our samples hint at nitrogen deficiency which would result in a phase width $BaTaO_{2+x}N_{1-x}$ containing both Ta^{5+} and a certain amount of Ta^{4+}. As a consequence, deviation from local symmetry would occur. It should be noted that during ammonothermal synthesis employing two mineralizers (NaOH and $NaNH_2$) local concentration variations may be possible resulting in slight differences of oxygen and nitrogen contents of the products.[51] However, the true crystal structure of $BaTaO_2N$ is still controversially discussed in literature.[51-57] The local symmetry in the crystals could be broken and space group $Pm\bar{3}m$ used in our Rietveld refinement represents the statistically averaged structure.[53, 54]

2.2.3 Electron microscopy

SEM images of the products were recorded to illustrate the cube-like crystal shape (Fig. 3). This observation is similar to other reported oxonitride perovskites synthesized by the ammonothermal approach.[15-18] All four products in this contribution were synthesized under the same ammonothermal conditions, but there is no clear correlation or discernible trend between the starting materials and the resulting composition and their observed crystal sizes (1 - 10 µm). A reason for that could be a local supersaturation. There is only a few data in literature for the solubility of the alkaline earth metals and their respective amides in supercritical ammonia, however both metals were reported to show good solubility.[45] On the other hand, $Sr(NH_2)_2$ was reported to be less soluble than $Ba(NH_2)_2$.[58] Therefore, larger crystals should be formed for the Ba compounds, if formation of the respective amide correlates with the crystallization process. Table 1 summarizes the EDX-measurements of the crystals. Analysis of light elements by EDX is challenging. Due to that problem the oxygen

content is slightly increased. In general the percentage is in good agreement with the stoichiometric formula (1:1:2:1) for each oxonitride compound.

Table 1. SEM EDX measurements of *EAM*O_2N with *EA* = Sr, Ba; *M* = Nb, Ta oxonitride perovskites of three crystals each in atom% and theoretical values in brackets.

Sr	**Nb**	**O**	**N**
16.3 (20)	18 (20)	46 (40)	19.7 (20)
Ba			
21 (20)	18.7 (20)	44.3 (40)	16 (20)
Sr	**Ta**		
18 (20)	18.7 (20)	44.7 (40)	18.6 (20)
Ba			
16.6 (20)	17.4 (20)	51.6 (40)	14.4 (20)

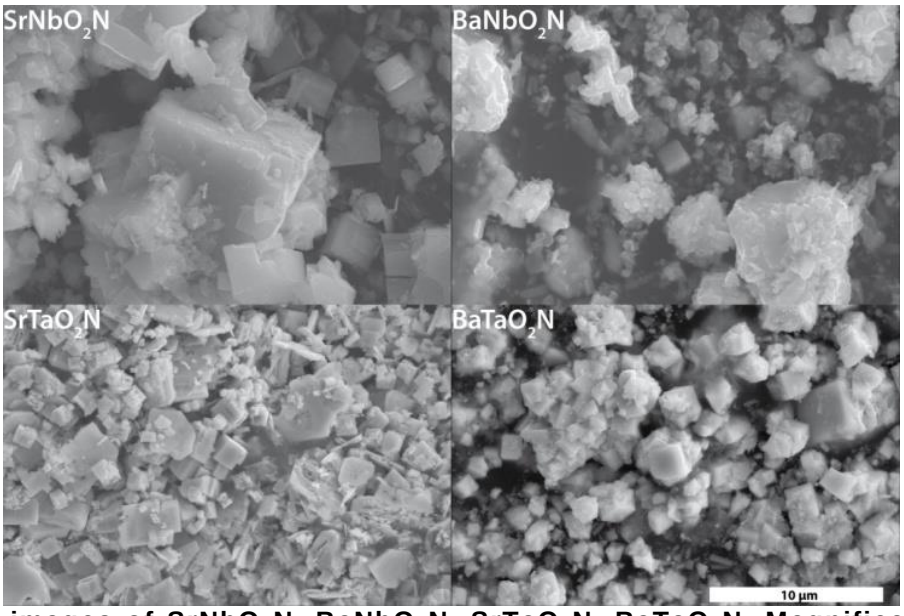

Figure 3. SEM images of $SrNbO_2N$, $BaNbO_2N$, $SrTaO_2N$, $BaTaO_2N$. Magnification of 8000x. Scale applies for all four images.

2.2.3.1 UV/VIS spectroscopy

UV/VIS measurements were performed to determine the optical properties and band gap values of the products. The oxonitride perovskites were ground and mixed with $BaSO_4$ (white standard). Diffuse reflectance was recorded and converted to absorption spectra with the Kubelka-Munk function.[59] By drawing a tangent (Fig. 4) at the inflection points optical band gap values were obtained (Tauc plot).[59] The measured

band gaps of the oxonitrides are: $SrNbO_2N$ (1.9 eV), $BaNbO_2N$ (2.0 eV), $SrTaO_2N$ (2.1 eV) and $BaTaO_2N$ (2.1 eV). The determined values are in good agreement with data from literature[3, 20, 60-66] which supports the accuracy of these measurements. However, small discrepancies of about 0.1 eV, compared to known band gap values of the four compounds, are attributed to different synthesis conditions due to the fact that the ammonothermal method was used instead of ammonolysis reactions.[2, 63, 67-69] The small band gap difference could be attributed to the differing synthesis conditions as already known from literature where a sintering process turned the sample black and subsequent ammonolysis red again.[51] Deviation of the band gap may occur due to a changing nitrogen content.[2] Therefore, different impurity concentrations or varying degrees of ordering may result in a small deviation of the band gap and thus the color of the products.

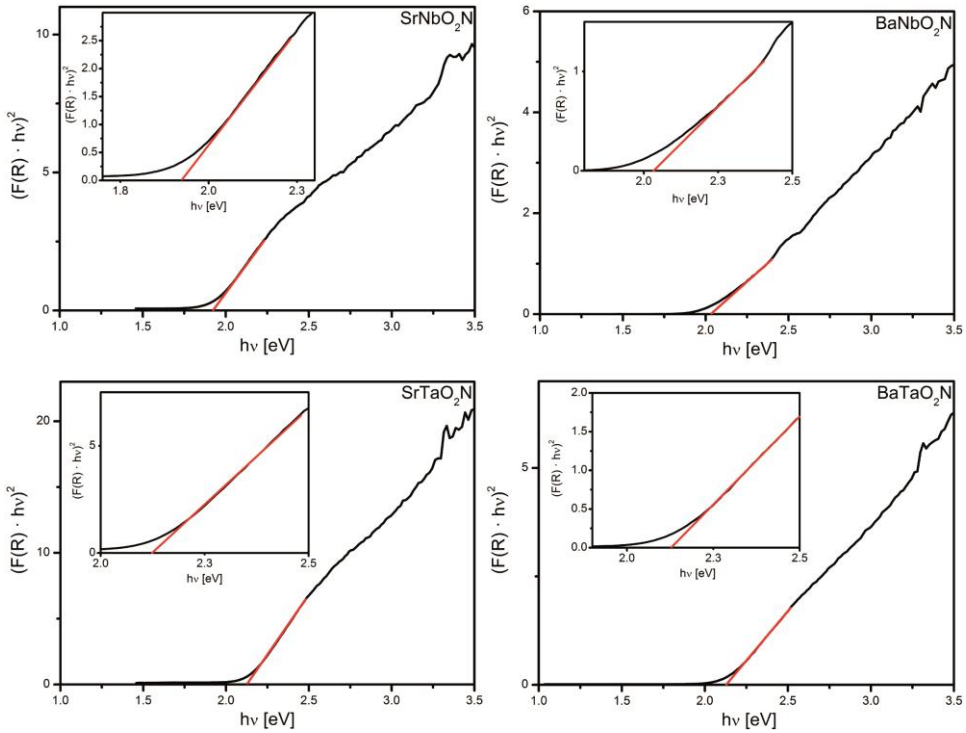

Figure 4. Tauc plots of Sr/BaNb/TaO$_2$N. Estimated band gaps of SrNbO$_2$N (1.9 eV), BaNbO$_2$N (2.0 eV), SrTaO$_2$N (2.1 eV) BaTaO$_2$N (2.1 eV). Insets show enlargement of the Tauc plots.

2.2.4 Solid-state ^{14}N NMR (MAS) spectroscopy

Because of its sensitivity to the local surroundings of the observed nuclei, nuclear magnetic resonance (NMR) spectroscopy is a useful complementary analytical technique for inorganic solids.[33, 35] In the context of oxonitrides, NMR of the nuclide ^{14}N (natural abundance 99.63%) has been shown to be helpful for structural characterization.[32, 34] In particular, the magnitude of the quadrupolar coupling of 14N (spin I = 1) can be evaluated to obtain information about the local symmetry of the nitride ions in the oxonitride perovskite structure, whereas the chemical shift provides information about the local electron density. In Fig. 5, ^{14}N spectra of *AM*(O,N)$_3$ with *A* = Ca, Sr, Ba, La and *M* = Nb, Ta are shown. They were recorded from samples made by ammonolysis reactions, because of the typically occurring metallic residual phases originating from the metallic liner used in the ammonothermal route and the quantity of the reaction product. All compounds show a single resonance at about 270 ppm (Fig. 5) (referenced to NH_4Cl, see Experimental Section). The spectra show no spinning side bands, which means that the quadrupolar interaction is absent, indicating high site symmetry for the nitride ions.[32] It has been noted before that the chemical shift of various perovskite oxonitrides is essentially insusceptible to the ionic radius and oxidation number of the cation.[34] Indeed, the NMR resonance positions of the eight compounds are practically identical within the error limits (Fig. 5), which is quite remarkable. One possible explanation is that the electron density at the N^{3-} ions is sufficiently high to mask all external influences, so that the chemical shift of the ^{14}N nucleus remains unaffected by cation substitution. However, this explanation for the invariance of the ^{14}N chemical shift needs to be further substantiated by additional experiments and possibly quantum chemical calculations.

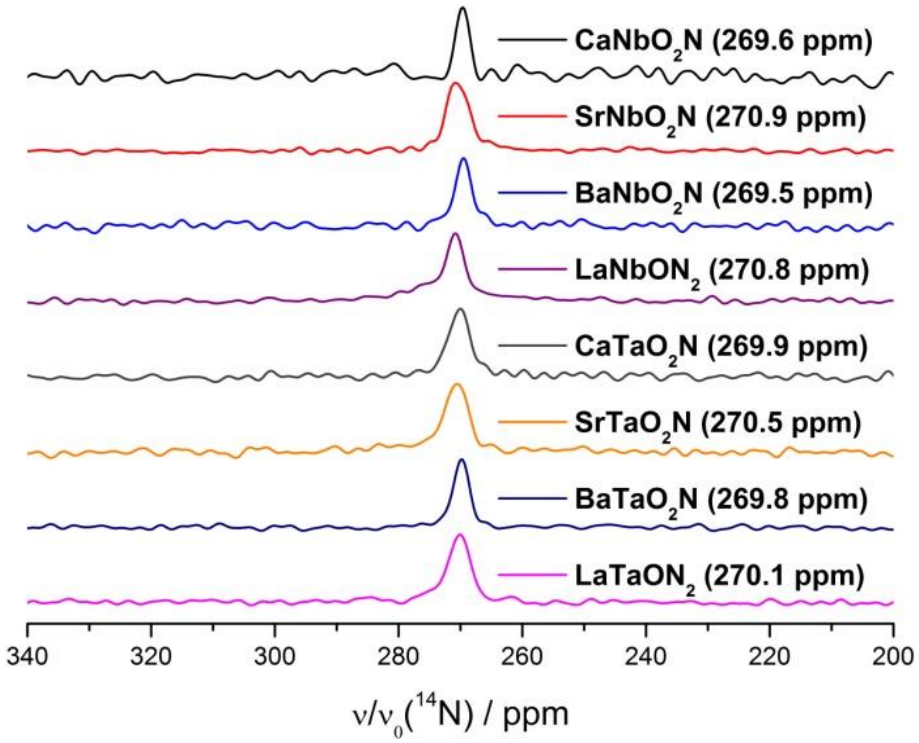

Figure 5. Solid-state NMR spectra of ^{14}N for *AM*(O,N)$_3$ with *A* = Ca, Sr, Ba, La and *M* = Nb, Ta recorded at a MAS rate of 10 kHz

Comparison of the published space groups of the eight compounds ($CaNbO_2N$: *Pnma*,[3] $SrNbO_2N$: *I*4/*mcm*,[3] $BaNbO_2N$: $Pm\bar{3}m$,[3] $LaNbO_2N$: *Pnma*,[70] $CaTaO_2N$: *Pnma*,[3] $SrTaO_2N$: *I*4/*mcm*,[3] $BaTaO_2N$: $Pm\bar{3}m$,[3] $LaTaO_2N$: *C*2*m*,[30] *Imma*[71]) illustrates the differing crystallographic symmetry of the anion substructures. By lowering the symmetry from cubic over tetragonal to orthorhombic space groups there is no marked change of the ^{14}N chemical shift of the signal (~270 ppm). Therefore, the coordination of nitrogen in all compounds seems to remain virtually unchanged in this rigid oxonitride perovskite family. Therefore, NMR results suggest nearly isotropic symmetry and similar electron density around N^{3-} for all *A* (Ca, Sr, Ba, La) and *M* (Nb, Ta) although symmetry deviations have been predicted in literature for some compounds.[56, 71-74]

Table 1. Crystallographic data of *EAM*O$_2$N (*EA* = Sr, Ba; *M* = Nb, Ta) obtained by Rietveld refinement.

Formula	$SrNbO_2N$	$BaNbO_2N$	$SrTaO_2N$	$BaTaO_2N$
Crystal system	Tetragonal	Cubic	Tetragonal	Cubic
Space group	*I*4/*mcm* (no. 140)	$Pm\bar{3}m$ (no. 221)	*I*4/*mcm* (no.140)	$Pm\bar{3}m$ (no. 221)
Lattice Parameters / Å	*a* = *b* = 5.7082(2) *c* = 8.0589(3)	*a* = *b* = c = 4.1285(1)	*a* = *b* = 5.6852(35) *c* = 8.0403(21)	*a* = *b* = c = 4.1087(6)
Cell volume / Å^3	262.588(17)	70.367(4)	259.870(323)	69.362(30)
Formula units / cell	4	1	4	1
Density / g cm^3	5.7302(4)	8.5961(6)	8.0404(100)	8.7208(38)
T / K	293(2)			
Diffractometer	STOE STADI P			
Radiation / A	Cu-Kα_1 (λ = 1.54056 Å)			
2θ range /°	5.0 ≤ 2θ ≤ 119.555			
Data points	7638			
Total number of reflections	63	22	63	22
Refined parameters	25	22	46	33
Background function	Shifted Chebyshev			
R values	R_p = 0.0738 R_{wp} = 0.0973	R_p = 0.09532 R_{wp} = 0.1231	R_p = 0.8377 R_{wp} = 0.1118	R_p = 0.1069 R_{wp} = 0.1427
Goodness of fit	0.922	0.924	0.887	1.093

2.3 Conclusions

In summary, we report about the successful synthesis of Sr/Ba-Nb/TaO_2N oxonitride perovskites employing the ammonothermal approach in custom-built high-temperature autoclaves. In this ammonothermal route NaN_3 and NaOH were used with Sr/Ba and Nb/Ta and placed in Nb/Ta liners inside the autoclave. With a temperature of 900 K the ammonia pressure rises up to a maximum value of 300 MPa. The oxonitride perovskites are crystalline and only little residual side phases occur. Amides could be

eliminated by washing with water and ethanol. NbH and TaH arise from the liner which prevents the autoclave from corrosion. For the ammonothermal reaction of oxonitrides, some intermediates can be considered. It seems most likely that intermediates with amide, imide, and hydroxide groups are a reactive species in the reaction. A gradual decomposition leads to the formation of oxonitrides. With respect to the observed cubic habitus of the crystals we assume a solution-based crystallization mechanism. The obtained crystals show different sizes in the range 1-10 µm. Chemical composition determined by EDX corresponds with an atomic ratio 1:1:2:1 (*EA*:Nb/Ta:O:N with *EA* = Sr, Ba). UV/VIS measurements reveal the band gaps (1.9 – 2.1 eV) of these compounds. Therefore, the materials could be suitable for water splitting applications. Further materials property measurements are now planned for better understanding of such oxonitride perovskites. We believe that the ammonothermal approach could be further developed for bulk crystal growth of oxonitride perovskites. Although the crystals are only a few µm in size, initial experiments show that larger crystals are possible. By increasing temperature and pressure, the synthesis of new compounds seems possible because of the better solubility at elevated conditions. The smart use of reactive precursors could lead to other oxonitride perovskites as well. We could show that the ammonothermal approach is a powerful technique to synthesize new as well as known oxonitride perovskites with an increased crystal size compared to conventional methods. Further research to achieve the preparation of larger crystals without compositional change, like in thin films and the respective substrate, will lead to a better understanding of intrinsic properties and lead towards new applications for oxonitride perovskites. The crystals obtained by this method will allow studying dielectric properties in insulating samples and also carrier transport in conducting ones. Accordingly, the ammonothermal synthesis of oxonitride perovskite crystals is very promising for the discovery of novel and innovative next generation semiconductors.

2.4 Experimental Section

2.4.1 Autoclave set up

For all manipulations an argon-filled glovebox (Unilab, MBraun, Garching, O_2 < 1 ppm, H_2O < 1 ppm) was used to avoid oxygen and water contamination. Therefore, all autoclaves (inner volume 11 mL) were loaded with starting materials and sealed in gloveboxes. Subsequently, the autoclaves were finally screwed with the required torque. For the condensation process a combined glass and steal vacuum line (≤ 0.1 Pa) was connected to the autoclaves via a peripheral equipment consisting of hand valve (SITEC), pressure transmitter (HBM P2VA1/5000 bar) and safety head with integrated bursting disc (SITEC) (Fig. 6) with a 3/8" high-pressure tubing connection. Ammonia (Air Liquide, 99.999%) was passed through upstreamed gas purification cartridges (Micro Torr, FT400-702FV, SAES Pure Gas Inc., San Luis Obispo, Ca, USA) via the line in the evacuated and cooled autoclave to provide a constant purity level of < 1 ppbV H_2O, O_2, CO_2 and metals.

Figure 6. Custom-built autoclave made from Inconel 718 with peripheral equipment.

Custom-built high-pressure autoclaves manufactured from nickel-based superalloys (Inconel 718) were used for the ammonothermal syntheses (Fig. 6). Further details of the autoclaves can be obtained from literature.[18, 19, 26-28, 75]

2.4.2 Synthesis of *EAM*O_2N (*EA* = Sr, Ba; *M* = Nb, Ta)

Sr and Ba (both 1 mmol, Sigma-Aldrich, 99.99%), Ta (0.8 mmol Sigma-Aldrich, 99.9%, -325 mesh), Nb (0.8 mmol, Sigmal-Aldrich, 99.8%, -325 mesh) NaN_3 (7 mmol, Sigmal-Aldrich, 99.5%) and NaOH (0.8 mmol, Grüssing, 99%) were placed in custom-built Nb or Ta liners (14 cm, Ø 0.6 cm, wall thickness: 0.05 cm), respectively. The Nb/Ta liners were vertically transferred into the autoclaves. To easily remove them after reaction a small Inconel 600 spring was placed under the liner in the reaction chamber of the autoclave. The autoclaves were closed under argon, evacuated and cooled with ethanol and liquid nitrogen to 200 K. Ammonia was condensed with overpressure (0.4 MPa) for 15 minutes with a regulator valve. As a result, about 5 mL liquid ammonia was condensed. After heating up to room temperature with a conventional hair dryer, the autoclave was transferred vertically into a custom built furnace (Loba, HTM Reetz, Berlin) and heated up to 900 K within three hours and held for 80 h at this temperature. The maximum pressure was 300 MPa. The autoclaves were cooled to room temperature by switching off the furnace. Products were subsequently washed with conc. HCl, H_2O and ethanol and dried at air. $SrNbO_2N$ was obtained as dark red, $BaNbO_2N$ as brown, $SrTaO_2N$ and $BaTaO_2N$ as brick-red powders, respectively. $CaNbO_2N$ and $CaTaO_2N$ could not be obtained by this route.

2.4.3 Synthesis of *A*Nb/Ta(O,N)$_3$ (with *A* = Ca, Sr, Ba, La) for ^{14}N solid-state NMR measurements

All products were synthesized by literature known synthetic procedures.[3, 5, 30, 76] Powdered ACO_3 (*A* = Ca, Sr, Ba, La) (≥ 99%, Sigma-Aldrich; 99.9%, Sigma-Aldrich; ≥ 99%, Sigma-Aldrich; 99%, Fluka) and Nb_2O_5 / Ta_2O_5 (99.9%, Fluka; 99%, Fluka) or synthesized ternary oxide precursors were ground in an agate mortar and heated in an alumina boat in a silica tube mounted in a horizontal tube furnace from 720-950 °C for different amounts of time (8-18 h) under flowing ammonia (Air Liquide, 99.999%, ~50 mL / min).

2.4.4 Powder X-ray Diffraction

The obtained products were ground to fine powder in an agate mortar and loaded into glass capillaries (0.1 mm, 0.01 mm wall thickness, Hilgenberg GmbH). XRD measurements were performed using a Stoe STADI P diffractometer. (Cu-Kα_1, λ = 1.54056 Å, Ge(111) monochromator, Mythen 1K detector) in modified Debye-Scherrer geometry. TOPAS-Academic Software was used for Rietveld refinement applying the fundamental parameters model with direct convolution of source emission profiles, axial instrument contributions, crystallite size and microstrain effects for the peak shape function.[77] Capillary absorption correction (inner diameter 0.08 mm) was performed with the calculated absorption coefficient. Further details on the crystal structure investigations may be obtained from the Fachinformationszentrum Karlsruhe, 76344 Eggenstein-Leopoldshafen, Germany (fax: +49-7247-808-666; email: crysdata@fiz-karlsruhe.de), on quoting the depository numbers CSD-434769 ($SrNbO_2N$), CSD-434770 ($BaNbO_2N$), CSD-434768 ($SrTaO_2N$), CSD-434767 ($BaTaO_2N$).

2.4.5 Scanning electron microscopy (SEM / EDX)

Crystal morphology and elemental distribution of the products were investigated using a FEI Helios G3 UC scanning electron microscope (SEM, field emission gun, acceleration voltage 30 KV). The products were placed on an adhesive carbon pad and subsequently coated with a conductive carbon film using a high-vacuum sputtercoater (BAL-TEC MED 020, Bal Tec AG).

2.4.6 UV/VIS spectroscopy

UV/VIS spectra were recorded by using a PerkinElmer Lambda 1050 spectrometer equipped with a 150 mm InGaAs integrating sphere. Diffuse reflectance spectra were collected with a Praying Mantis (Harrick) accessory and were referenced to $BaSO_4$ (Sigma-Aldrich, 99.99%) powder as white standard.

2.4.7 Solid-state MAS (magic-angle spinning) ^{14}N NMR

^{14}N solid-state NMR spectra were recorded on a Bruker Avance-III 500 spectrometer. The sample was transferred into a ZrO_2 rotor with an outer diameter of 4 mm, which was mounted in a commercial MAS probe (Bruker) and spun at a rotation frequency of 10 kHz. An echo sequence[78] was used for spectra acquisition to avoid base line problems. All spectra were referenced to the secondary standard NH_4Cl at 0 ppm, which is shifted by –342.4 ppm against the ^{14}N resonance of liquid nitromethane.[79]

2.4.8 Digital Microscope

A digital microscope (VHX-5000, Keyence) was used to record pictures of obtained samples. All sample pictures were recorded with a magnification of 200 x.

2.5 Acknowledgements

The authors gratefully acknowledge financial support by the Deutsche Forschungsgemeinschaft (DFG) within the research group “Chemistry and Technology of the Ammonothermal Synthesis of Nitrides” (FOR 1600), project SCHN377/16-2, as well as the Fonds der Chemischen Industrie (FCI). We would like to thank Christian Minke for EDX, SEM and NMR measurements, Lukas Bauer (both at Department of Chemistry of LMU Munich) for synthetic assistance.

2.6 References

[1] M. Jansen, H. P. Letschert, *Nature* **2000**, *404*, 980-982.

[2] N.-Y. Park, Y.-I. Kim, *J. Mater. Sci.* **2012**, *47*, 5333-5340.

[3] Y.-I. Kim, P. M. Woodward, K. Z. Baba-Kishi, C. W. Tai, *Chem. Mater.* **2004**, *16*, 1267-1276.

[4] A. B. Jorge, J. Oró-Solé, A. M. Bea, N. Mufti, T. T. M. Palstra, J. A. Rodgers, J. P. Attfield, A. Fuertes, *J. Am. Chem. Soc.* **2008**, *130*, 12572-12573.

[5] R. Marchand, F. Pors, Y. Laurent, *Rev. Int. Hautes Temp. Refract.* **1986**, *23*, 11-15.

[6] A. Fuertes, *Mater. Horiz.* **2015**, *2*, 453-461.

[7] J. Ahchawarattaworn, D. P. Thompson, F. Azough, R. Freer, *J. Ceram. Sci. Tech.* **2016**, *7*, 39-46.

[8] C. Le Paven-Thivet, L. Le Gendre, J. Le Castrec, F. Cheviré, F. Tessier, J. Pinel, *Prog. Solid State Chem.* **2007**, *35*, 299-308.

[9] D. Oka, Y. Hirose, T. Fukumura, T. Hasegawa, *Cryst. Growth Des.* **2014**, *14*, 87-90.

[10] M. Yang, J. A. Rodgers, L. C. Middler, J. Oró-Solé, A. B. Jorge, A. Fuertes, J. P. Attfield, *Inorg. Chem.* **2009**, *48*, 11498-11500.

[11] C. Tassel, Y. Kuno, Y. Goto, T. Yamamoto, C. M. Brown, J. Hester, K. Fujita, M. Higashi, R. Abe, K. Tanaka, Y. Kobayashi, H. Kageyama, *Angew. Chem. Int. Ed.* **2015**, *54*, 516-521.

[12] Y. Kuno, C. Tassel, K. Fujita, D. Batuk, A. M. Abakumov, K. Shitara, A. Kuwabara, H. Moriwake, D. Watabe, C. Ritter, C. M. Brown, T. Yamamoto, F. Takeiri, R. Abe, Y. Kobayashi, K. Tanaka, H. Kageyama, *J. Am. Chem. Soc.* **2016**, *138*, 15950-15955.

[13] Y. Lu, C. Le Paven, H. V. Nguyen, R. Benzerga, L. Le Gendre, S. Rioual, F. Tessier, F. Cheviré, A. Sharaiha, C. Delaveaud, X. Castel, *Cryst. Growth Des.* **2013**, *13*, 4852-4858.

[14] J. Odahara, A. Miura, N. C. Rosero-Navarro, K. Tadanaga, *Inorg. Chem.* **2018**, *57*, 24-27.

[15] T. Watanabe, K. Tajima, J. Li, N. Matsushita, M. Yoshimura, *Chem. Lett.* **2011**, *40*, 1101-1102.

[16] C. Izawa, T. Kobayashi, K. Kishida, T. Watanabe, *Adv. Mater. Sci. Eng.* **2014**, *2014*, 1-5.

[17] T. Toshima, K. Kishida, Y. Maruyama, T. Watanabe, *J. Ceram. Soc. Jpn.* **2017**, *125*, 643-647.

[18] N. Cordes, W. Schnick, *Chem. Eur. J.* **2017**, *23*, 11410-11415.

[19] J. Häusler, W. Schnick, *Chem. Eur. J.* **2018**, *24*, 11864-11879.

[20] Y.-I. Kim, *Ceram. Int.* **2014**, *40*, 5275-5281.

[21] A. Hosono, Y. Masubuchi, T. Endo, S. Kikkawa, *Dalton Trans.* **2017**, *46*, 16837-16844.

[22] M. Hojamberdiev, K. Yubuta, J. J. M. Vequizo, A. Yamakata, S. Oishi, K. Domen, K. Teshima, *Cryst. Growth Des.* **2015**, *15*, 4663-4671.

[23] M. Sano, Y. Hirose, S. Nakao, T. Hasegawa, *J. Mater. Chem. C* **2017**, *5*, 1798-1802.

[24] Y.-I. Kim, W. Si, P. M. Woodward, E. Sutter, S. Park, T. Vogt, *Chem. Mater.* **2007**, *19*, 618-623.

[25] A. David, S. Guérin, B. E. Hayden, R. Noble, J.-P. Soulié, C. Vian, I. P. Koutsaroff, S. i. Higai, N. Tanaka, T. Konoike, A. Ando, H. Takagi, T. Yamamoto, T. Fukura, H. Ieki, *Cryst. Growth Des.* **2014**, *14*, 523-532.

[26] J. Häusler, S. Schimmel, P. Wellmann, W. Schnick, *Chem. Eur. J.* **2017**, *23*, 12275-12282.

[27] J. Häusler, L. Neudert, M. Mallmann, R. Niklaus, A.-C. L. Kimmel, N. S. A. Alt, E. Schlücker, O. Oeckler, W. Schnick, *Chem. Eur. J.* **2017**, *23*, 2583-2590.

[28] J. Häusler, R. Niklaus, J. Minár, W. Schnick, *Chem. Eur. J.* **2018**, *24*, 1686-1693.

[29] J. Häusler, L. Eisenburger, O. Oeckler, W. Schnick, *Eur. J. Inorg. Chem.* **2018**, 759-764.

[30] E. Günther, R. Hagenmayer, M. Jansen, *Z. Anorg. Allg. Chem.* **2000**, *626*, 1519-1525.

[31] M. Yang, J. Oro-Sole, J. A. Rodgers, A. B. Jorge, A. Fuertes, J. P. Attfield, *Nat. Chem.* **2011**, *3*, 47-52.

[32] T. Bräuniger, T. Müller, A. Pampel, H.-P. Abicht, *Chem. Mater.* **2005**, *17*, 4114-4117.

[33] L. A. O'Dell, *Prog. Nucl. Magn. Reson. Spectrosc.* **2011**, *59*, 295-318.

[34] Y.-I. Kim, Y. Paik, *Solid State Sci.* **2012**, *14*, 580-582.

[35] T. Bräuniger, M. Jansen, *Z. Anorg. Allg. Chem.* **2013**, *639*, 857-879.

[36] R. Juza, H. Jacobs, H. Gerke, *Ber. Bunsen-Ges. Phys. Chem* **1966**, *70*, 1103-1105.

[37] H. Jacobs, C. Hadenfeldt, *Z. Anorg. Allg. Chem.* **1975**, *418*, 132-140.

[38] B. Wang, M. J. Callahan, *Cryst. Growth Des.* **2006**, *6*, 1227-1246.

[39] T. Richter, R. Niewa, *Inorganics* **2014**, *2*, 29-78.

[40] J. Li, T. Watanabe, H. Wada, T. Setoyama, M. Yoshimura, *Chem. Mater.* **2007**, *19*, 3592-3594.

[41] D. R. Modeshia, R. I. Walton, *Chem. Soc. Rev.* **2010**, *39*, 4303-25.

[42] Y. Hu, H. Gu, Z. Hu, W. Di, Y. Yuan, J. You, W. Cao, Y. Wang, H. L. W. Chan, *Cryst. Growth Des.* **2008**, *8*, 832-837.

[43] S. G. Ebbinghaus, H.-P. Abicht, R. Dronskowski, T. Müller, A. Reller, A. Weidenkaff, *Prog. Solid State Chem.* **2009**, *37*, 173-205.

[44] S. Pimputkar, S. Nakamura, *J. Supercrit. Fluids* **2016**, *107*, 17-30.

[45] J. Jander, H. Spandau, C. C. Addison, *Anorganische und allgemeine Chemie in flüssigem Ammoniak, Vol. 1*, F. Vieweg, **1966**.

[46] A. Glazer, *Acta Crystallogr. Sect. B* **1972**, *28*, 3384-3392.

[47] C. J. Howard, H. T. Stokes, *Acta Crystallogr. Sect. B* **1998**, *54*, 782-789.

[48] S. G. Ebbinghaus, A. Weidenkaff, A. Rachel, A. Reller, *Acta Crystallogr., Sect. C* **2004**, *60*, i91-i93.

[49] R. Shannon, *Acta Crystallogr., Sect. A* **1976**, *32*, 751-767.

[50] H. Johnston, A. P. Black, P. Kayser, J. Oro-Sole, D. A. Keen, A. Fuertes, J. P. Attfield, *Chem. Commun.* **2018**, *54*, 5245-5247.

[51] A. Hosono, S.-K. Sun, Y. Masubuchi, S. Kikkawa, *J. Eur. Ceram. Soc.* **2016**, *36*, 3341-3345.

[52] A. Hosono, Y. Masubuchi, Y. Nagamine, T. Shibahara, S. Kikkawa, *J. Eur. Ceram. Soc.* **2018**, *38*, 3478-3482.

[53] C. M. Fang, G. A. de Wijs, E. Orhan, G. de With, R. A. de Groot, H. T. Hintzen, R. Marchand, *J. Phys. Chem. Solids* **2003**, *64*, 281-286.

[54] B. Ravel, Y.-I. Kim, P. Woodward, C. Fang, *Phys. Rev. B* **2006**, *73*, 184121.

[55] K. Page, M. W. Stoltzfus, Y.-I. Kim, T. Proffen, P. M. Woodward, A. K. Cheetham, R. Seshadri, *Chem. Mater.* **2007**, *19*, 4037-4042.

[56] C.-H. Wang, B. J. Kennedy, A. L. Menezes de Oliveira, J. Polt, K. S. Knight, *Acta Crystallogr. Sect. B* **2017**, *73*, 389-398.

[57] K. Bettine, O. Sahnoun, M. Driz, *Chin. Phys. B* **2017**, *26*, 057101.

[58] J. Hertrampf, N. S. A. Alt, E. Schlücker, M. Knetzger, E. Meissner, R. Niewa, *J. Cryst. Growth* **2016**, *456*, 2-4.

[59] R. López, R. Gómez, *J. Sol-Gel Sci. Technol.* **2012**, *61*, 1-7.

[60] M. Ahmed, G. Xinxin, *Inorg. Chem. Front.* **2016**, *3*, 578-590.

[61] S. Balaz, S. H. Porter, P. M. Woodward, L. J. Brillson, *Chem. Mater.* **2013**, *25*, 3337-3343.

[62] H. Wolff, R. Dronskowski, *J. Comput. Chem.* **2008**, *29*, 2260-2267.

[63] I. E. Castelli, T. Olsen, S. Datta, D. D. Landis, S. Dahl, K. S. Thygesen, K. W. Jacobsen, *Energy Environ. Sci.* **2012**, *5*, 5814-5819.

[64] Y. Wu, P. Lazic, G. Hautier, K. Persson, G. Ceder, *Energy Environ. Sci.* **2013**, *6*, 157-168.

[65] A. M. Hafez, N. M. Salem, N. K. Allam, *PCCP* **2014**, *16*, 18418-18424.

[66] R. Aguiar, D. Logvinovich, A. Weidenkaff, A. Rachel, A. Reller, S. G. Ebbinghaus, *Dyes Pigm.* **2008**, *76*, 70-75.

[67] S. G. Ebbinghaus, R. Aguiar, A. Weidenkaff, S. Gsell, A. Reller, *Solid State Sci.* **2008**, *10*, 709-716.

[68] T. Matoba, K. Maeda, K. Domen, *Chem. Eur. J.* **2011**, *17*, 14731-14735.

[69] K. Maeda, *PCCP* **2013**, *15*, 10537-10548.

[70] D. Logvinovich, Stefan G. Ebbinghaus, A. Reller, I. Marozau, D. Ferri, A. Weidenkaff, *Z. Anorg. Allg. Chem.* **2010**, *636*, 905-912.

[71] S. H. Porter, Z. Huang, P. M. Woodward, *Cryst. Growth Des.* **2014**, *14*, 117-125.

[72] Y.-R. Zhang, T. Motohashi, Y. Masubuchi, S. Kikkawa, *J. Ceram. Soc. Jpn.* **2011**, *119*, 581-586.

[73] J. P. Attfield, *Cryst. Growth Des.* **2013**, *13*, 4623-4629.

[74] A. Kubo, G. Giorgi, K. Yamashita, *Chem. Mater.* **2017**, *29*, 539-545.

[75] M. Mallmann, J. Häusler, N. Cordes, W. Schnick, *Z. Anorg. Allg. Chem.* **2017**, *643*, 1956-1961.

[76] A. Rachel, S. G. Ebbinghaus, M. Güngerich, P. J. Klar, J. Hanss, A. Weidenkaff, A. Reller, *Thermochim. Acta* **2005**, *438*, 134-143.

[77] A. Coelho, *TOPAS Academic, Version 4.1*, Coelho Software, Brisbane (Australia), **2007**.

[78] A. C. Kunwar, G. L. Turner, E. Oldfield, *J. Magn. Reson. (1969-1992)* **1986**, *69*, 124-127.

[79] A. K. Khitrin, B. M. Fung, *J. Chem. Phys.* **1999**, *111*, 8963-8969.

3 Ammonothermal Synthesis of Crystalline Oxonitride Perovskites *Ln*$TaON_2$ (*Ln* = La, Ce, Pr, Nd, Sm, Gd)

Published in: *Chem. Eur. J.* **2017**, *23*, 11410–11415.

Authors: Niklas Cordes, Wolfgang Schnick

https://onlinelibrary.wiley.com/doi/abs/10.1002/chem.201702231

Keywords: Perovskite phases • Crystal growth • High-pressure chemistry • Solvothermal

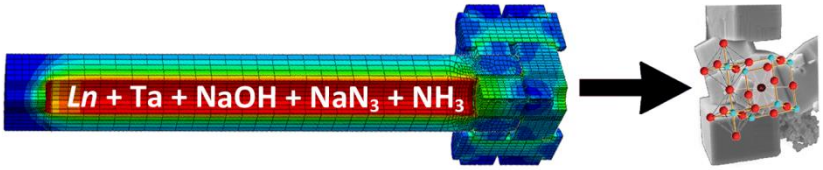

Highly crystalline oxonitride perovskite (*Ln*$TaON_2$ *Ln* = La, Ce, Pr, Nd, Sm, Gd) were synthesized by the ammonothermal approach in custom built high-pressure autoclaves at relatively low temperatures between 870–1070 K and pressures of up to 300 MPa. This more sophisticated route requires no precursor and results in cube like crystals up to 15 µm.

Abstract: The perovskite type oxonitridotantalates *Ln*$TaON_2$ with *Ln* = La, Ce, Pr, Nd, Sm and Gd were synthesized by the ammonothermal method employing custom-built autoclaves made of nickel-based superalloy. Metal powders were reacted with NaOH and NaN_3 as mineralizers under supercritical conditions with purified ammonia at temperatures of 870–1070 K and pressures in the range 150–300 MPa. Crystal structures and the space groups were determined using powder X-ray diffraction and refined by the Rietveld method. The refined lattice parameters are for $LaTaON_2$ (*a* = 5.7156(1), *b* = 8.0675(1), *c* = 5.7465(1) Å, R_{wp} = 0.0471), $CeTaON_2$ (*a* = 5.6761(11), *b* = 8.0386(16), *c* = 5.7891(12) Å, R_{wp} = 0.1834), $PrTaON_2$ (*a* = 5.6920(1), *b* = 8.0197(1), *c* = 5.6804(1) Å, R_{wp} = 0.03495), $NdTaON_2$ (*a* = 5.6884(1), *b* = 8.0037(2) , *c* = 5.6554(1) Å, R_{wp} = 0.026), $SmTaON_2$ (*a* = 5.6827(1), *b* = 7.9656(2), *c* = 5.6103(1) Å, R_{wp} = 0.042), $GdTaON_2$ (*a* = 5.6160(10), *b* = 7.9359(12), *c* = 5.5962(10) Å, R_{wp} = 0.118). $LaTaON_2$ crystallizes in space group *Imma* (no. 74) and the other compounds *Ln*$TaON_2$ with *Ln* = Pr, Nd, Sm, Gd in *Pnma* (no. 62). SEM measurements were performed to investigate the elemental composition and morphology of the oxonitride perovskites. The band gap values of the oxonitrides ($LaTaON_2$: 1.8 eV, $CeTaON_2$: 1.7 eV; $PrTaON_2$: 1.9 eV, $NdTaON_2$: 2.0 eV, $SmTaON_2$: 2.0 eV, $GdTaON_2$: 1.8 eV) were estimated using UV/VIS measurements and the Kubelka-Munk function.

3.1 Introduction

Oxonitride perovskites have attracted great interest because of their various application fields,[1] for example as magnetic materials,[2] nontoxic pigments,[3] photocatalysts,[4] energy conversion and storage materials.[5] $LaTaON_2$ for instance has been identified as a visible light absorbing pigment with extraordinary photocatalyst feature responding to visible light.[6] Some properties were discovered long after the first exploration of oxonitride perovskites by Jansen[3], Domen[7] and others. By the introduction of nitrogen into an oxidic compound the possibilities to tune their properties expand significantly. Oxonitrides may be synthesized by a number of reaction methods,[1, 5] including ammonolysis,[8] high-pressure syntheses[9] and ammonothermal approaches.[10]

Oxonitrides with general formula *AB*$(O,N)_3$ (*A* = Alkaline earth, *B* = Nb, Ta) were first synthesized by Marchand et al. in 1986.[11] Later (La, Nd, Gd)$TaON_2$ were obtained and reported as cubic, whereas $SmTaON_2$ as orthorhombic. Ternary oxides were used as starting materials, which were reacted with flowing ammonia at 1120–1270 K.[12] Subsequently, oxonitride perovskites were obtained using oxides and carbonates as starting materials. In order to enhance crystallinity of the products, NaCl or $CaCl_2$ were added as flux.[3, 8] Further synthetic approaches for oxonitride perovskites were established using amorphous precursors, which were synthesized from oxides and nitrates in diluted nitric acid. Thereby, $LaZrO_2N$, $NdTiO_2N$ and $LaTiO_2N$ were obtained in flowing ammonia at 1220–1580 K. One disadvantage of these reactions is attributed to frequent intermediate grinding.[13] The citrate route, as stated, for example, by Kikkawa for $Ca_{1-x}Eu_xTa(O,N)_3$,[14] represents a less complex and therefore faster alternative. Thereby, a transition metal halide ($TaCl_5$) was dissolved in anhydrous ethanol with an equimolar amount of citric acid as complexing agent. Generally, all ammonolysis reactions were performed at high temperatures of 970–1320 K,[15] and the type of the precursors was reported to be decisive. The precursor $Ca_2Nb_2O_7$ was used for synthesis of $CaNbO_2N$ instead of $CaCO_3$ and Nb_2O_5 in combination with salts as flux, which helped to minimize the formation of side phases like NbO_xN_y.[16]

Another interesting approach uses a combination of high temperature and high pressure. Therefore, oxonitride perovskites like *Ln*ZrO_2N (*Ln* = Pr, Nd, Sm) were obtained employing a direct solid-state reaction without a nitriding gas atmosphere. Ln_2O_3 and Zr_2ON_2 were used as starting materials, placed in a multianvil press

assembly and heated up to 1470–1770 K at a pressure of 2–3 GPa.[9] Besides, the hydrothermal approach is widely used for the preparation of oxide perovskites.[17] Due to higher dissociation energy of N_2 compared to that of O_2 and the lower bond energy of most elements to nitrogen as compared with bonds to O,[15, 18] formation of oxonitrides is unlikely under hydrothermal conditions. Instead, another approach has to be followed. Watanabe et al. used the ammonothermal method to prepare $LaTaON_2$, starting from an arc-melted binary metal precursor in a sodium amide melt under supercritical ammonia in a high-pressure autoclave.[10]

Syntheses of oxonitrides are quite challenging and often lead to mixtures of several phases and microcrystalline or amorphous powders. In order to improve crystallinity and also to facilitate syntheses, new approaches have to be developed. The ammonothermal method provides a well suited method to obtain oxonitride perovskites at relatively low temperatures compared to others routes without the need of an oxidic precursor. Generally, ammonothermal synthesis has been extensively used to manufacture GaN and AlN[19, 20]. First Jacobs et al. performed reactions in supercritical ammonia for synthesis of binary nitrides like Be_3N_2[21] and later for ternary compounds, for instance, $NaSi_2N_3$.[22] Recently, new nitrides ($CaGaSiN_3$,[23] $ZnSiN_2$ and $ZnGeN_2$)[24] became accessible by ammonothermal synthesis employing high-temperature stable, custom-built autoclaves.

In this contribution, we report on a new and more sophisticated route for synthesis of oxonitride perovskites with composition *Ln*$TaON_2$ (*Ln* = La,[10] Ce, Pr, Nd, Sm, Gd). Crystal structures were solved and refined using powder X-ray diffraction and will be described in detail. Results of UV/VIS measurements are presented. SEM pictures reveal crystal size and morphology.

3.2 Results and Discussion

3.2.1 Synthesis

The oxonitride perovskites with composition *Ln*$TaON_2$ (*Ln* = La, Ce, Pr, Nd, Sm, Gd) were obtained by an ammonothermal approach using custom-built autoclaves made of nickel-based superalloy.[23] *Ln*$TaON_2$ (*Ln* = La, Pr, Nd, Sm) were successfully synthesized at temperatures of about 870 K and pressures up to 300 MPa. Using these

reaction parameters, *Ln*$TaON_2$ with *Ln* = Ce or Gd could not be obtained. Instead, CeO_2 and Gd_2O_3 were the main products, respectively. At higher reaction temperatures (1070 K) and pressures of 150 MPa $CeTaON_2$ and $GdTaON_2$ became accessible. The as-synthesized products are dark red (*Ln*$TaON_2$ with *Ln* = La, Pr, Nd, Sm, Gd) and ocher ($CeTaON_2$), respectively, and turned out to be crystalline. The oxonitrides are chemically inert to concentrated HCl and aqua regia.[3]

Metallic Ta and respective lanthanides as well as NaN_3 and NaOH were used as starting materials. During synthesis, NaN_3 decomposes thermally at 570 K[19] to Na which reacts with NH_3 under formation of $NaNH_2$. Residual Na-mineralizers were removed by washing with water. In supercritical ammonia the latter acts as mineralizer besides NaOH,[19] which was additionally used as oxygen source. Finely ground reaction mixtures were placed in Ta liners, which were transferred into the autoclave. Powdery reactants were used for better solubility in supercritical ammonia while Ta liners were employed in order to avoid corrosion of the autoclave steel. Previously reported syntheses[10] directly started from $NaNH_2$, which is disadvantageous regarding its moisture sensitivity.

There are several considerations of reaction intermediates, which might be relevant for the formation of oxonitride perovskites in supercritical ammonia. As mentioned above, NaN_3 in ammonia forms $NaNH_2$ during heating to 770 K. $NaNH_2$ probably reacts with the lanthanide to intermediate species with assumed composition $Na_3Ln(NH_2)_6$ or $NaLn(NH_2)_4$.[25] Formation of $Ln(NH_2)_3$[26] or intermediate species like $Ta(OH)_5NH_3$, as reported for $TaF_5(NH_3)_3$.[27] Single octahedral anions $Ta(O_{1-x},N_x)_6^{(7+6x)-}$, which forms $NaTa(O_{1-x}N_x)_{3-x}$ might as well be possible.[28] The latter is also known from hydrothermal syntheses, in which a dissolution–precipitation process forms cube-like crystals of oxide perovskites.[29] These intermediates decompose to reactive species at higher temperatures.[23] Furthermore, it is also possible that starting materials may be dissolved in a $NaNH_2$ / NaOH melt at the bottom of the Ta liner,[22] resulting in druse like agglomerations. The formation of *Ln*$TaON_2$ via oxide perovskites is also possible due to the high supercritical NH_3 pressure and the dissociation products N_2 and H_2 at the conditions in the autoclaves mentioned above.

An arc-melting procedure,[10] as described for the synthesis of $LaTaON_2$ to form a reactive precursor/alloy or an amorphous oxide, was not necessary to obtain nearly phase pure products. Purification of the samples was not necessary due to the growth

of crystals on the inside wall of the liner. Powder X-ray diffraction patterns show highly crystalline products which are phase pure or have only little amounts of side phases like $NaTaN_2$ or Ln_2O_3. $NaTaN_2$ as side phase was typically observed on the outside of the Ta liner forming orange to red crystals with sizes < 30 µm. This can be ascribed to the high amount of dissolved mineralizer in the system, which seems to be necessary for the formation of reactive intermediates.

Ln$TaON_2$ with *Ln* = La, Pr, Nd, Sm and Gd was obtained nearly phase pure, whereas several side phases including CeO_2 and other unidentifiable phases were found for $CeTaON_2$ (see supplementary information, figure S2). Side phases may be due to lower solubility of Ce and therefore a possible explanation for yet unknown $Ce(NH_2)_3$. Another reason could be the electronic configuration of Ce because Ce^{+IV} likely forms the stable oxide CeO_2[30] instead of the desired oxonitride perovskite $CeTaON_2$ in supercritical ammonia with NaOH and NaN_3. Thereby, Ce would be depleted in solution giving rise to formation of Ta/N sidephases. Another reason is the preferred formation of CeN, which is apparent in the PXRD (see supplementary information, figure S2). Besides, the oxonitride perovskites *Ln*$TaON_2$ of the heavier lanthanides *Ln* = Tb – Lu could not be obtained through ammonothermal synthesis route as yet. This can be explained by the lanthanide contraction, which leads to a decrease of the ionic radii to higher atomic numbers and thereby a destabilization of the perovskite structure.[31]

The formability of oxonitride perovskites has been predicted on the basis of the tolerance and the octahedral factors. These parameters have been applied for generating structure maps that reveal the stability regions of perovskite structures. By this model the tantalum oxonitrides are not in the typical range of the tolerance factor of 0.827 – 1.042 and were therefore not assumed to be stable. According to this method the oxonitride perovskites $LaTaON_2$ and $PrTaON_2$ were predicted as stable, whereas $NdTaON_2$ and $SmTaON_2$ were expected to be unstable. No further lanthanide tantalum oxonitrides were examined by this method, but with respect to the lanthanide contraction they would be predicted unstable by this method.[31] The ammonothermal methods clearly demonstrate that these substances are accessible.

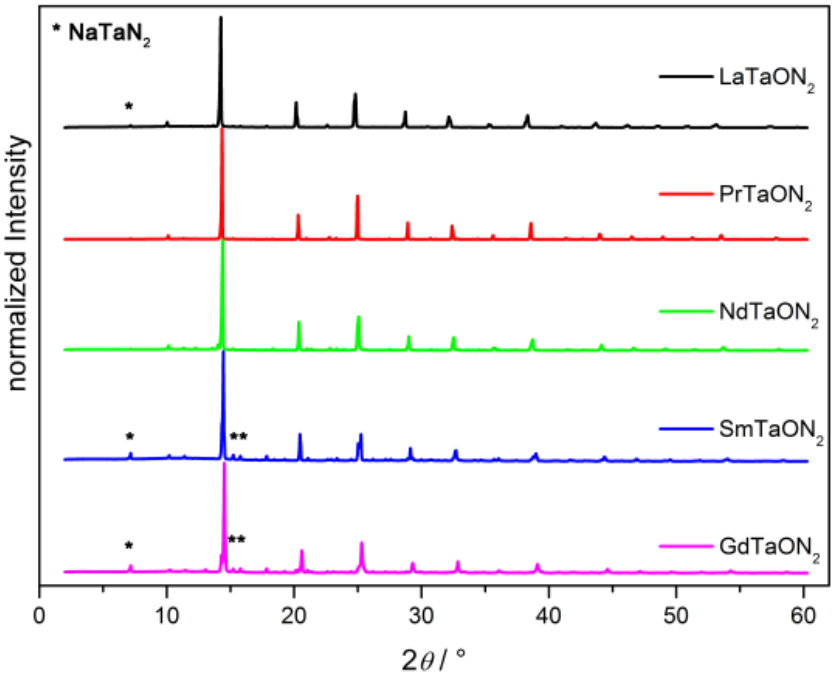

Figure 1. Powder X-ray diffraction of *Ln*TaON$_2$ (*Ln* = La, Pr, Nd, Sm, Gd). Normalized on the most intense reflection. NaTaN$_2$ is marked with stars (*).

3.2.2 Crystal Structure Analysis

Crystal structures were analyzed and refined by powder X-ray diffraction (PXRD). Wyckoff positions and coordinates of orthorhombic space groups were used to refine parameters. According to the small peak widths, the products are very crystalline. Furthermore, no remarkable background is visible in the PXRD patterns. The refinement was conducted with different space groups for each product. The space group with the lowest R_{wp} values was chosen. The powder X-ray diffraction patterns are shown in Figure 1, crystallographic data are summarized in Table 1. Detailed results of the Rietveld refinements are given in the Supplementary Information. For the compound LaTaON$_2$ the orthorhombic space group *Imma* and for *Ln*TaON$_2$ (*Ln* = Ce, Pr, Nd, Sm, Gd) the space group *Pnma* was chosen giving the best results. This is in agreement with recent neutron diffraction data from literature.[32] The refinement for LaTaON$_2$ was also performed in the space group *C2/m*. The beta angle was still 90° within between the errors of the refinement. Therefore a monoclinic distortion could not be found.[33] Lattice parameters are in good agreement with the values reported

elsewhere[34] (Table 1). The shift of the reflections to higher 2θ values is obvious due to the decrease of the Ln^{3+} radii caused by the lanthanide contraction.

3.2.3 Electron microscopy

SEM images (Fig. 2) show morphologies of *Ln*TaON$_2$ with Ln = La, Ce, Pr, Nd, Sm and Gd similar to those reported for $BaTaO_2N$,[35] $LaTaON_2$,[10] $LaNbON_2$,[36] and $LaTiO_2N$.[37] Ammonothermally synthesized crystals were obtained with diameters up to 15 µm. The atomic ratio of *Ln* (*Ln* = La, Ce, Pr, Nd, Sm, Gd), Ta, N and O was confirmed by energy dispersive X-ray spectroscopy. Several measurements were averaged to confirm the atomic ratio (see supplementary information Table S1–S6).

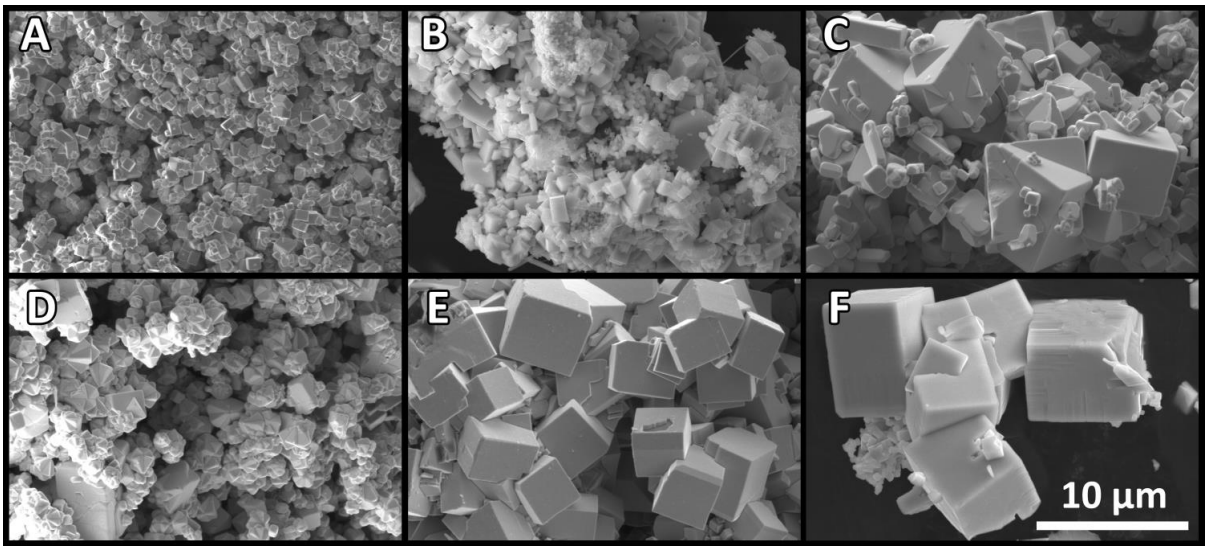

Figure 2. SEM images of crystalline oxonitrido perovskites with scale bar on the bottom right corner. All pictures were made with a magnification of 8000x. a) $LaTaON_2$, b) $CeTaON_2$, c) $PrTaON_2$, d) $NdTaON_2$, e) $SmTaON_2$, f) $GdTaON_2$.

Within the accuracy of the method, the measured atomic ratios correspond well to the stoichiometric formula *Ln*TaON$_2$. The good crystallinity is evident (Figure 2). According to the SEM pictures some oxonitride perovskites form larger crystals than others. A possible explanation could be that some of the compounds have a higher solubility in supercritical ammonia than others, since the reaction conditions (heating rate, duration, maximum pressure) were identical for all products in this investigation.

The ammonothermal approach has frequently been used to grow crystals of different chemical and structural composition.[38] Ammonothermal synthesis of $LaTaON_2$ and

$LaNbON_2$ has been described in literature with crystal sizes up to 1 µm.[10, 36] Compared to the ammonothermal approach in the ammonolysis reaction carried out in flowing ammonia there are not many examples known for large cube like crystals.[35] Possibly, the crystal size of the products is affected by the $NaNH_2$ / NaOH melt always found at the bottom of the autoclave forming agglomerates looking like druses. This assumption is supported by the observation of other authors that the ammonolysis reaction leads to better crystallinity with the use of flux.[35, 37] Another possible mechanism could be a dissolution-precipitation process as known from hydrothermal syntheses.[28, 29] The ammonothermal growth mechanism of oxonitride perovskite crystals has scarcely been investigated so far.

3.2.4 UV/VIS

UV/VIS measurements were used to determine the optical properties and band gap values of the products. Therefore, the obtained product was finely ground and mixed with $BaSO_4$. The UV/VIS diffuse reflectance (R) spectra were measured and converted to absorption spectra using Kubelka-Munk function ($F(R) = (1 - R)^2 / 2R$).[39]

Subsequently, Tauc plots were employed to determine the optical band gap, by drawing a tangent at the inflection points.[40] The measured band gaps of the oxonitride perovskites are between 1.7–2.0 eV ($LaTaON_2$: 1.8 eV, $CeTaON_2$: 1.7 eV; $PrTaON_2$: 1.9 eV, $NdTaON_2$: 2.0 eV, $SmTaON_2$: 2.0 eV, $GdTaON_2$: 1.8 eV). These values are similar to those of other oxonitridotantalate perovskites that have been reported in literature ($LaTaON_2$: 1.93 – 2.07 eV,[6] $CeTaON_2$: 1.9 eV[32] and $PrTaON_2$: 2.0 eV).[32,

[41] These small discrepancies can be ascribed to different approximation methods, different synthesis conditions, measuring methods, defect and impurity concentrations and to a varying degree of ordering. Band gap values determined by UV/VIS depend on the type of reaction and are altered by ammothermal synthesis.[42] In summary, this leads to a considerable under- or overestimation of the band gaps. The colors of the compounds giving on the other hand a good estimation of the band gap as well. All product products are red (*Ln*TaON$_2$ with La, Pr, Nd, Sm, Gd) or occer (CeTaON$_2$).

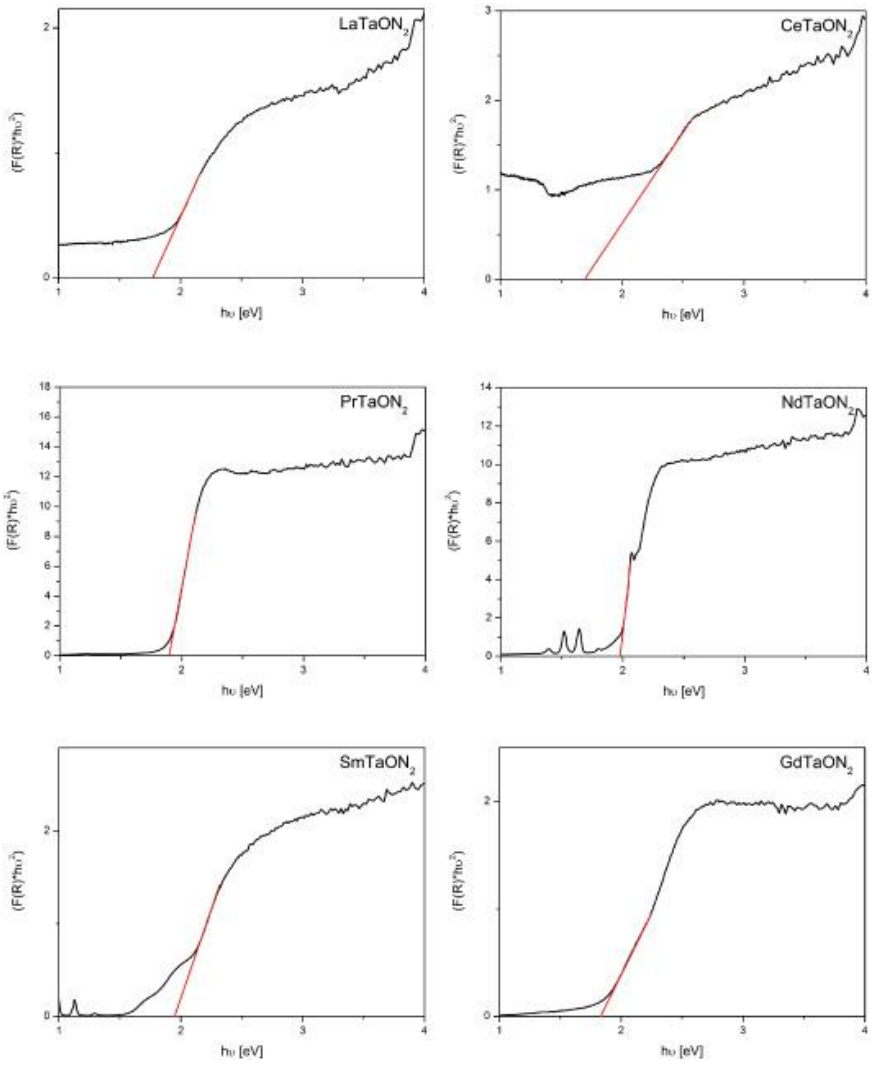

Figure 3. Tauc plots of crystalline oxonitride perovskites (LaTaON$_2$, CeTaON$_2$, PrTaON$_2$, NdTaON$_2$, SmTaON$_2$, GdTaON$_2$).

However, the measured band gaps of the ammonothermally synthesized oxonitridotantalate perovskites are in the range as the other referred experimental band gaps. The features visible in the UV/VIS reflectance (Figure 4) measurements can be explained by f-f-transitions. LaTaON$_2$ has no f-f-transition due to the empty f-

shell of La. *Ln*TaON$_2$ (*Ln* = Pr, Nd, Sm) show common transitions in the visible to near infrared part of the spectra. A comparison of the optical absorption spectra of the presented oxonitridoperovskite series with the Dieke diagram,[43] results in the identification of spectroscopic transitions for PrTaON$_2$ ($^1D_2$, $^1G_4$, $^3F_4$, $^3F_3$, $^3F_2 \leftarrow {}^3H_4$), NdTaON$_2$ ($^4G_{7/2}$, $^4G_{5/2}$, $^4F_{9/2}$, $^4F_{7/2}$ $^4F_{5/2}$, $^4F_{3/2}$, $^4I_{15/2} \leftarrow {}^4I_{9/2}$) and SmTaON$_2$ ($^4F_{3/2}$, $^6F_{11/2}$, $^6F_{9/2}$, $^6F_{7/2}$, $^6F_{5/2}$, $^6H_{15/2}$, $^6F_{1/2}$, $^6H_{13/2} \leftarrow {}^6H_{5/2}$) shown in Figure 4.

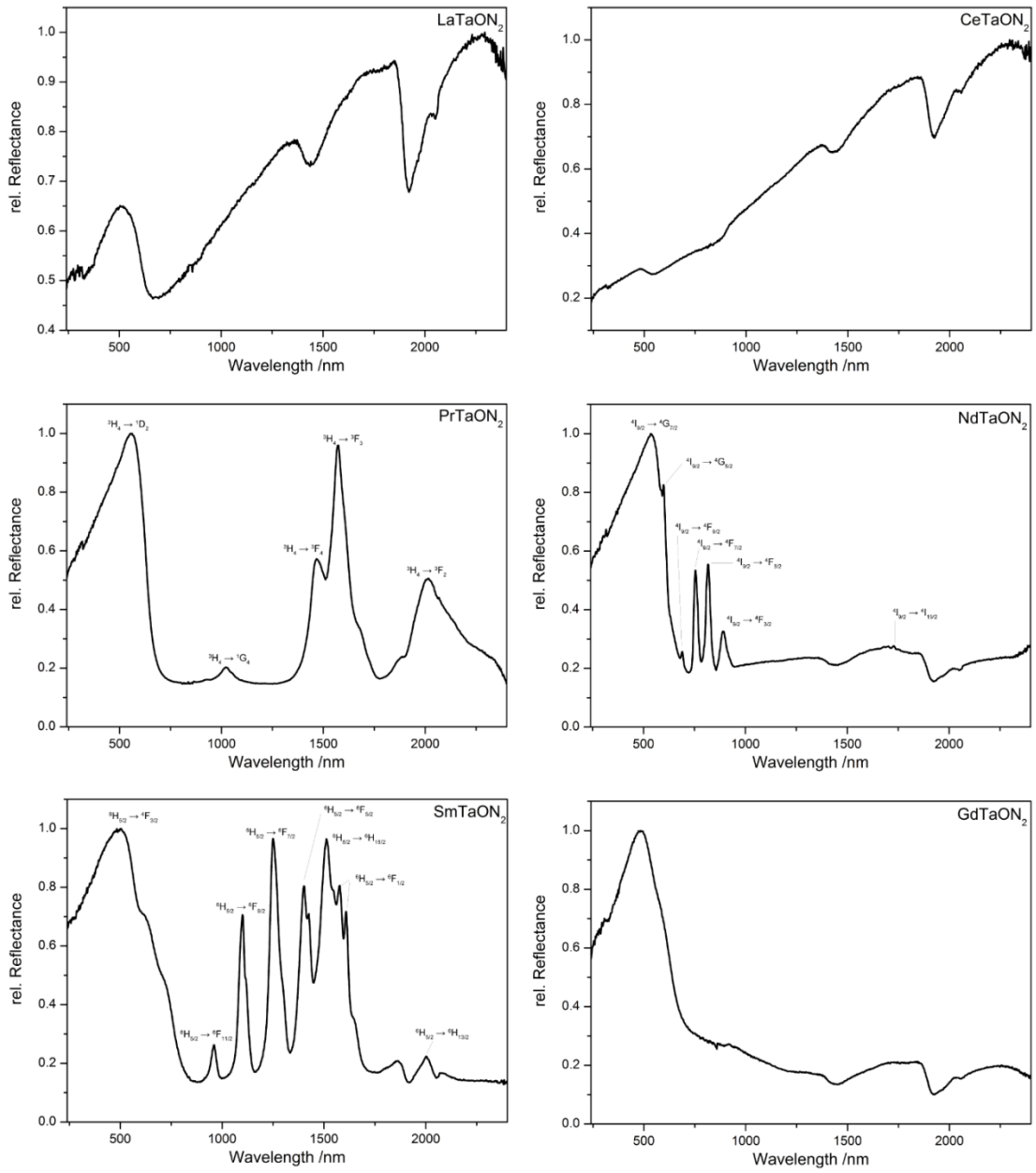

Figure 4. UV/Vis measurements of LaTaON$_2$, CeTaON$_2$, PrTaON$_2$, NdTaON$_2$, SmTaON$_2$, GdTaON$_2$ with assignment of f–f transitions.

Table 1. Crystallographic data of LnTaON$_2$ obtained by Rietveld refinement.

Formula	**LaTaON$_2$**	**CeTaO$_2$N**	**PrTaON$_2$**	**NdTaON$_2$**	**SmTaON$_2$**	**GdTaON$_2$**
Crystal system	orthorhombic					
Space group	*Imma (74)*			*Pnma (62)*		
Lattice Parameters / Å	5.7156(1) 8.0675(1) 5.7465(1)	5.6761(11) 8.0386(16) 5.7891(12)	5.6920(1) 8.0197(1) 5.6804(1)	5.6884(1) 8.0037(2) 5.6554(1)	5.6827(1) 7.9656(2) 5.6103(1)	5.6160(10) 7.9359(13) 5.5962(10)
Cell volume / Å^3	264.964(7)	264.143(93)	259.310(7)	257.477(8)	253.955(8)	249.410(79)
Formula units / cell	4					
Density / g cm^3	9.1215(2)	9.1802(32)	9.3717(2)	9.5244(3)	9.8165(3)	10.1789(32)
T / K	293(2)					
Diffractometer	STOE STADI P					
Radiation / A	Mo-Kα_1 (λ = 0.70930 Å)					
2θ range /°	2.0 ≤ 2θ ≤ 60.2					
Data points	3886					
Total number of reflections	226	429	410	400	396	392
Refined parameters	27	44	27	33	36	44
Background function	Shifted Chebyshev					
***R* values / %**	R_p = 2.96 R_{wp} = 4.71	R_p = 12.86 R_{wp} = 18.36	R_p = 2.21 R_{wp} = 3.49	R_p = 1.93 R_{wp} = 2.60	R_p = 3.12 R_{wp} = 4.22	R_p = 7.83 R_{wp} = 11.86
Goodness of fit	3.623	5.966	2.116	1.670	2.037	3.420

3.3 Conclusion

The oxonitridotantalate perovskites *Ln*TaON$_2$ with *Ln* = La, Ce, Pr, Nd, Sm and Gd were successfully synthesized by the ammonothermal approach in custom-built high-temperature autoclaves. The oxonitride perovskites crystallize in space group *Imma* (for LaTaON$_2$) or *Pnma* (for Ln = Ce, Pr, Nd, Sm, GdTaON$_2$), respectively. This synthesis route uses pure metals instead of intermetallic arc melted precursors and NaN_3 and NaOH as mineralizers placed in a tantalum liner. Rietveld refinement revealed phase purity or only little amounts of side phases like $NaTaN_2$ besides the products. Nevertheless, the reactive intermediate is still unknown. Sodium amidolanthanides are eligible which decompose at higher temperatures. On the bottom of the tantalum liner an agglomerate of salt druses were formed. This suggests that a kind of a $NaNH_2$ / NaOH salt melt reacts at the bottom where the product is formed or deposited through crystallization from solution. It is possible that in this melt ammonia, nitrogen and oxygen are soluble.

Interestingly, SEM pictures and PXRD pattern indicate (very) crystalline products. The crystals are up to 15 µm in length with sharp edges. This are by far the largest crystals of oxonitridotantalate perovskites *Ln*$TaON_2$ reported in literature. UV/VIS measurements reveal band gap values similar to already known compounds like $LaTiO_2N$ or $BaNbO_2N$. With regard to the properties of crystals of oxonitridotantalate perovskites new applications in watersplitting and bulk crystals for semiconductor devices are possible. Therefore we believe that the ammonothermal approach for synthesis of oxonitride perovskites offers benefits for bulk crystals for electronic and semiconducting applications.

In summary, we could show that the ammonothermal route is a powerful and useful method to synthesize oxonitride perovskites. Furthermore, better crystallinity and improved morphology of crystals can be achieved. Thus, the ammonothermal synthesis approach emerges as a powerful synthetic tool which is well suited for the preparation and crystal growth not only of binary GaN or AlN but for ternary and higher nitrides and oxonitrides as well.

3.4 Experimental Section

All manipulations were carried out in flame-dried Schlenk-type glassware connected to a vacuum line (≤ 0.1 Pa) or in Ar-filled glove boxes (Unilab, MBraun, Garching, O_2 < 1 ppm, H_2O < 1ppm) to rigorously exclude oxygen and moisture during preparation and syntheses. Ammonia (Air Liquide, 99.999%) was purified through a gas purification cartridge (Micro Torr MC400-702FV, SAES Pure Gas Inc. San Luis Obispo, Ca, USA) to obtain a purity level of < 1ppbV H_2O, O_2 and CO_2.

3.4.1 Ammonothermal Synthesis

All syntheses were performed in supercritical ammonia with custom-built autoclaves made of nickel-based superalloy (718 Inconel, Haynes 282) sustaining a maximum pressure of 300 MPa at 870 K (*Ln*$TaON_2$ *Ln* = La, Pr, Nd, Sm) and 170 MPa at 1070 K (*Ln*$TaON_2$ *Ln* = Ce, Gd). The peripheral devices consist of the hand valve (SITEC), pressure transmitter (HBM P2VA1/5000bar) and a safety head with an integrated rupture disc (SITEC). To seal the autoclaves silver coated C-rings (GFD seals) made of Inconel 718 were used. The autoclaves were placed vertically in custom-built

furnaces (Loba, HTM Reetz) and connected to a pressure display unit (HBM). The pressure was recorded by an AD-converter connected to a PC. The signal was recorded as average values every 20 s.

Ta (1 mmol, Sigma-Aldrich, -325 mesh, 99.9%) and rare earth elements (La, Ce, Pr (Sigma-Aldrich, 99.9%), Nd (smart-elements, 99.9%), Sm (selteneerden.de, 99.999%), Gd (Sigma-Aldrich, 99.9%, 1 mmol) were powderized in a glove box, NaOH (Grüssing, 99%, 1 mmol,) and NaN_3 (Sigma-Aldrich, 99.99%, 4 mmol) were crushed to a powder in an agate mortar and then placed in custom-built tantalum liners (WHS Sondermetalle) (length 140 mm, diameter 6 mm) which were placed vertically in the autoclaves. Purified ammonia was then condensed in the evacuated and cooled (193 K) autoclave with 0.1 MPa overpressure with a combined glass-steel-line. After warming up to room temperature the autoclave was placed in a vertical tube furnace. Subsequently, the autoclave was heated to the respective reaction temperature in 3 or 6 h and kept at this temperature for 110 h. The pressure slowly decreased over time because of hydrogen loss of the autoclave.

3.4.2 Powder X-ray Diffraction

The powder XRD measurements were performed in glass capillaries (0.2 mm diameter, Hilgenberg GmbH) with a Stoe STADI P diffractometer (Mo-$K\alpha_1$ radiation, Ge(111) monochromator, Mythen 1K detector) in modified Debye-Scherrer geometry. TOPAS package was used for Rietveld refinement.[44]

Further details on the crystal structure investigations may be obtained from the Fachinformationszentrum Karlsruhe, 76344 Eggenstein- Leopoldshafen, Germany (fax: +49–7247-808-666; e-mail: crysdata@fiz-karlsruhe.de, http://www.fiz-karlsruhe.de/request for deposited data.html), on quoting the depository number CSD-433036, -433037, -433038, -433039, -433040, -433041 (*Ln*$TaON_2$ with *Ln* = La, Ce, Pr, Nd, Sm, Gd).

3.4.3 UV/VIS Spectroscopy

UV/VIS spectra were recorded using a Perkin-Elmer Lambda 1050 spectrometer equipped with a 150 mm InGaAs integrating sphere. Diffuse reflectance spectra were

collected with a Praying Mantis (Harrick) accessory and were referenced to $BaSO_4$ (Sigma-Aldrich, 99,99%) powder as white standard.

3.4.4 SEM / EDX

The atomic ratio was confirmed by energy-dispersive X-ray spectroscopy (EDX). SEM measurements were taken with a Dualbeam Helios Nanolab G3 UC (FEI) with X-Max 80 SDD Detector (Oxford Instruments). The software AzTec was used for EDX analysis and pictures.

3.5 Acknowledgements

The authors gratefully acknowledge financial support by the Deutsche Forschungsgemeinschaft (DFG) within the research group “Chemistry and Technology of the Ammonothermal Synthesis of Nitrides” (FOR 1600), project SCHN377/16. We also thank Christian Minke for SEM/EDX measurements and Laura Ascherl for UV/VIS measurements (both at LMU Munich), Thomas Steigerwald and Anna Kimmel (FAU Erlangen) for development and maintenance of the autoclaves.

3.6 References

[1] M. Ahmed, G. Xinxin, *Inorg. Chem. Front.* **2016**, *3*, 578-590.

[2] M. Yang, J. Oró-Solé, A. Kusmartseva, A. Fuertes, J. P. Attfield, *J. Am. Chem. Soc.* **2010**, *132*, 4822-4829.

[3] M. Jansen, H. P. Letschert, *Nature* **2000**, *404*, 980-982.

[4] F. Oehler, R. Naumann, R. Köferstein, D. Hesse, S. G. Ebbinghaus, *Mater. Res. Bull.* **2016**, *73*, 276-283.

[5] A. Fuertes, *Mater. Horiz.* **2015**, *2*, 453-461.

[6] N.-Y. Park, Y.-I. Kim, *J. Mater. Sci.* **2012**, *47*, 5333-5340.

[7] A. Kasahara, K. Nukumizu, G. Hitoki, T. Takata, J. N. Kondo, M. Hara, H. Kobayashi, K. Domen, *J. Phys. Chem. A* **2002**, *106*, 6750-6753.

[8] E. Günther, R. Hagenmayer, M. Jansen, *Z. Anorg. Allg. Chem.* **2000**, *626*, 1519-1525.

[9] M. Yang, J. A. Rodgers, L. C. Middler, J. Oró-Solé, A. B. Jorge, A. Fuertes, J. P. Attfield, *Inorg. Chem.* **2009**, *48*, 11498-11500.

[10] T. Watanabe, K. Tajima, J. Li, N. Matsushita, M. Yoshimura, *Chem. Lett.* **2011**, *40*, 1101-1102.

[11] R. Marchand, F. Pors, Y. Laurent, *Rev. Int. Hautes Temp. Refract.* **1986**, *23*, 11-15.

[12] R. Marchand, F. Pors, Y. Laurent, *Ann. Chim. - Sci. Mat.* **1991**, *16*, 553-560.

[13] S. J. Clarke, B. P. Guinot, C. W. Michie, M. J. C. Calmont, M. J. Rosseinsky, *Chem. Mater.* **2002**, *14*, 288-294.

[14] T. Motohashi, Y. Hamade, Y. Masubuchi, T. Takeda, K.-i. Murai, A. Yoshiasa, S. Kikkawa, *Mater. Res. Bull.* **2009**, *44*, 1899-1905.

[15] S. G. Ebbinghaus, H.-P. Abicht, R. Dronskowski, T. Müller, A. Reller, A. Weidenkaff, *Prog. Solid State Chem.* **2009**, *37*, 173-205.

[16] Y.-I. Kim, P. M. Woodward, K. Z. Baba-Kishi, C. W. Tai, *Chem. Mater.* **2004**, *16*, 1267-1276.

[17] D. R. Modeshia, R. I. Walton, *Chem. Soc. Rev.* **2010**, *39*, 4303-25.

[18] W. Schnick, *Angew. Chem. Int. Ed. Engl.* **1993**, *32*, 806-818; *Angew. Chem.* **1993**, *105*, 846-858.

[19] B. Wang, M. J. Callahan, *Cryst. Growth Des.* **2006**, *6*, 1227-1246.

[20] D. Ehrentraut, E. Meissner, M. Bockowski, *Technology of Gallium Nitride Crystal Growth*, Springer-Verlag GmbH Heidelberg, **2010**.

[21] R. Juza, H. Jacobs, H. Gerke, *Ber. Bunsen-Ges. Phys. Chem* **1966**, *70*, 1103-1105.

[22] H. Jacobs, H. Mengis, *Eur. J. Solid State Inorg. Chem.* **1993**, *30*, 45-53.

[23] J. Häusler, L. Neudert, M. Mallmann, R. Niklaus, A.-C. L. Kimmel, N. S. A. Alt, E. Schlücker, O. Oeckler, W. Schnick, *Chem. Eur. J.* **2017**, *23*, 2583-2590.

[24] J. Häusler, S. Schimmel, P. Wellmann, W. Schnick, *Chem. Eur. J.* **2017**, 10.1002/chem.201701081.

[25] V. H. Jacobs, H. Scholze, *Z. Anorg. Allg. Chem.* **1976**, *427*, 8-16.

[26] B. Gieger, H. Jacobs, C. Hadenfeldt, *Z. Anorg. Allg. Chem.* **1974**, *410*, 104-112.

[27] S. A. Baer, M. Lozinšek, F. Kraus, *Z. Anorg. Allg. Chem.* **2013**, *639*, 2586-2588.

[28] Y. Hu, H. Gu, Z. Hu, W. Di, Y. Yuan, J. You, W. Cao, Y. Wang, H. L. W. Chan, *Cryst. Growth Des.* **2008**, *8*, 832-837.

[29] H. Liu, C. Hu, Z. L. Wang, *Nano Lett.* **2006**, *6*, 1535-1540.

[30] H. Jacobs, D. Kablitz, *Z. Anorg. Allg. Chem.* **1979**, *454*, 35-42.

[31] W. Li, E. Ionescu, R. Riedel, A. Gurlo, *J. Mater. Chem.* **2013**, *1*, 12239-12245.

[32] S. H. Porter, Z. Huang, P. M. Woodward, *Cryst. Growth Des.* **2014**, *14*, 117-125.

[33] L. Clark, J. Oró-Solé, K. S. Knight, A. Fuertes, J. P. Attfield, *Chem. Mater.* **2013**, *25*, 5004-5011.

[34] P. Maillard, F. Tessier, E. Orhan, F. Cheviré, R. Marchand, *Chem. Mater.* **2005**, *17*, 152-156.

[35] M. Hojamberdiev, K. Yubuta, J. J. M. Vequizo, A. Yamakata, S. Oishi, K. Domen, K. Teshima, *Cryst. Growth Des.* **2015**, *15*, 4663-4671.

[36] C. Izawa, T. Kobayashi, K. Kishida, T. Watanabe, *Adv. Mater. Sci. Eng.* **2014**, *2014*, 1-5.

[37] K. Kawashima, M. Hojamberdiev, H. Wagata, K. Yubuta, S. Oishi, K. Teshima, *Cryst. Growth Des.* **2015**, *15*, 333-339.

[38] T. Richter, R. Niewa, *Inorganics* **2014**, *2*, 29-78.

[39] R. López, R. Gómez, *J. Sol-Gel Sci. Technol.* **2012**, *61*, 1-7.

[40] J. Tauc, R. Grigorovici, A. Vancu, *Phys. Status Solidi B* **1966**, *15*, 627-637.

[41] S. Balaz, S. H. Porter, P. M. Woodward, L. J. Brillson, *Chem. Mater.* **2013**, *25*, 3337-3343.

[42] K. Kishida, T. Watanabe, *J. Solid State Chem.* **2012**, *191*, 15-18.

[43] G. H. Dieke, *Spectra and Energy Levels of Rare Earth Ions in Crystals*, Interscience, New York, **1968**.

[44] A. Coelho, *TOPAS Academic, Version 4.1*, Coelho Software, Brisbane (Australia), **2007**.

4 Ammonothermal Synthesis of the Mixed-Valence Nitrogen-Rich Europium Tantalum Ruddlesden-Popper Phase $Eu^{II}Eu^{III}_2Ta_2N_4O_3$

Published in: *Chem. Eur. J.* **2019**, *2019*, 2304–2311.

Authors: Niklas Cordes, Markus Nentwig, Lucien Eisenburger, Oliver Oeckler, Wolfgang Schnick

https://doi.org/10.1002/ejic.201900245

Keywords: Nitride oxide • Ruddlesden-Popper phases • Ammonothermal synthesis • Crystal Structure Elucidation • High pressure

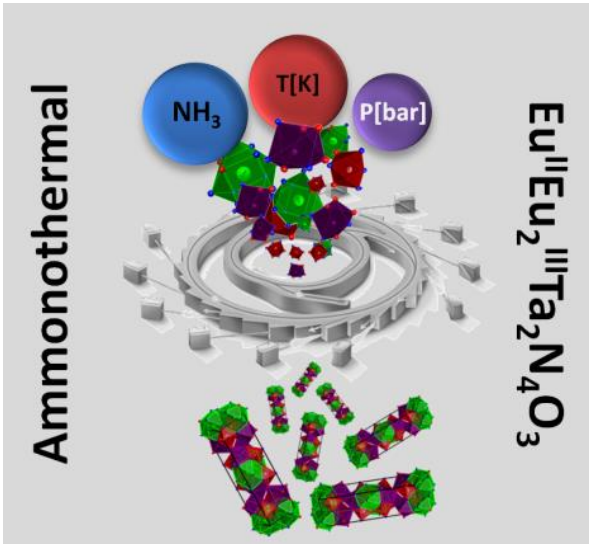

The first nitrogen rich Ruddlesden-Popper phase with mixed valence europium, namely $Eu_3Ta_2N_4O_3$ was synthesized under ammonothermal reaction conditions using custom-built high-pressure autoclaves. X-ray diffraction using microfocused synchrotron radiation and EDX analyses are consistent with crystal-chemical calculations with respect to $Eu^{II/III}$ and N/O ordering. According to diffuse reflectance spectra, the band gap amounts to 0.6 eV.

Abstract: The mixed-valence europium tantalum nitride oxide $Eu^{II}Eu^{III}_2Ta_2N_4O_3$ was synthesized with the ammonothermal approach in high-pressure custom-built autoclaves. The reaction was performed at 1070 K and a maximum pressure of 170 MPa in an ammonobasic environment with NaN_3 and NaOH as mineralizers. $Eu^{II}Eu^{III}_2Ta_2N_4O_3$ was obtained as a black microcrystalline powder. Single-crystal synchrotron diffraction data revealed a Ruddlesden-Popper phase crystallizing in space group $P4_2/mnm$ (no. 136) with a = 5.7278(1), c = 19.8149(5) Å and Z = 4. The crystallographic results from single-crystal diffraction data have been confirmed by powder diffraction and TEM measurements. Anion positions were assigned to O and N based on bond-valence (BVS), lattice energy (MAPLE) and charge distribution calculations (CHARDI). Eu^{II} and Eu^{III} are crystallographically ordered. The band gap was estimated from UV/VIS measurements employing the Kubelka-Munk function to be 0.6 eV, which supports the black color and the mixed-valence of europium.

4.1 Introduction

Since the pioneering work of Jacobs and Juza in the 1960s, the ammonothermal method has emerged as a versatile synthetic approach for a broad spectrum of compounds, e.g. amides, imides, nitrides, hydroxides and chalcogenides.[1-3] Despite this synthetic potential, synthesis in supercritical ammonia has been predominantly employed for crystal growth of GaN targeting appropriate substrate crystals for homoepitaxial growth of this important wide band gap semiconductor.[4] Recently, the ammonothermal approach has again been utilized for explorative synthetic solid-state chemistry of novel complex nitrides, e. g. $CaGaSiN_3$, $ZnSiN_2$, $ZnGeN_2$, Zn_2PN_3 as well as nitride oxide perovskites such as *Ln*TaN_2O with *Ln* = La, Ce, Pr, Nd, Sm and Gd and *EAM*NO_2 with *EA* = Sr, Ba and *M* = Nb, Ta.[3, 5-8] Novel materials with mixed anions such as nitride oxides came into research focus in the last decade. Oxygen and nitrogen have differences in polarizability, electronegativity and anion charge. Anion substitution further increases the diversity of applications of these materials. However, such substitutions are by far less investigated than e.g. cation doping. With the exchange of oxygen by nitrogen, these compounds gain more varied materials properties compared to analogous oxides. This variation is due to the change of covalence of the metal-nitrogen bond and also the energy changes of electronic levels. For example, in an insulating oxide the band gap typically decreases with nitride substitution and the optical absorption properties may change drastically from UV to the visible part of the spectrum. The nitride anion has a higher charge than oxides and may possibly allow higher oxidation states of the corresponding metal. This leads to versatile compounds with different properties compared to oxides.[9-11]

An extensively investigated class of compounds are nitride oxide perovskites (formerly denominated oxynitrides), which exhibit intriguing features. In particular, different tantalum, niobium and titanium nitride oxide perovskites have suitable band gaps for photocatalytic water splitting.[12] Furthermore, these materials have been discussed as non-hazardous inorganic pigments.[13] The study of $EuNbNO_2$ and $EuTaNO_2$ was motivated by the possibility of discovering new multiferroic materials, in which ferromagnetic and ferroelectric polarizations are coupled.[14, 15] Combining Eu^{II} with spin of S = 7/2 and transition metals like Nb, Ta and W results in interesting properties like low-temperature ferromagnetism[16] and colossal magnetoresistance[17] in nitride oxide perovskites.

Some Eu-containing nitride oxide perovskites, such as $Ca_{1-x}EuTa(N,O)_3$,[15] $EuWN_{2-x}O_{1+x}$ (x = −0.16 – 0.46),[18] $EuWN_{1.42}O_{1.58}$[19] and $EuMNO_2$ (M = Nb, Ta)[14-16] can be synthesized by ammonolysis of oxide precursors, obtained by ceramic or citrate routes in flowing gaseous NH_3 at elevated temperatures between 870 – 1173 K. At other temperatures, either decomposition of respective nitride oxides or no formation of these compounds was observed. For example, the formation of scheelite-type phases can be suppressed by thermal treatment.[19] Therefore, different temperatures, precursors and intermediate grinding steps have been necessary for successful synthesis of nitride oxide perovskites.[9]

The unequivocal distinction of N and O atoms is difficult with X-ray diffraction due to their similar X-ray scattering factors. Marchand *et al*. suggested a cubic structure for $EuTa(N,O)_3$.[20] However, the precise anion composition and details of the structure were not elucidated at that time. Europium can occur in oxidation states Eu^{II} and Eu^{III} and therefore the N/O distribution is variable. The Eu valence state can be probed with different analytical techniques like Mößbauer spectroscopy and susceptibility measurements.[21]

Perovskite-like compounds offer a wide variety of substitution possibilities for anions and cations. Thus, the combination of different structure types is possible. A well known structural variation of the perovskite structure type is represented by the Ruddlesden-Popper phases $A'_2A_{(n-1)}B_nX_{(3n+1)}$ with n = 1 – 3, consisting of a perovskite structure intergrown with NaCl-type oxide blocks.[22, 23] Structural and dimensional similarity between the two structures is a key requirement. The general structure of the n = 2 Ruddlesden-Popper phases are double perovskite layers and an intergrowth of half a NaCl-type layer. The A cations are located in the large cuboctahedron sites in the perovskite layer. The A' cations have a ninefold coordination and are situated at the boundary between perovskite and rocksalt-type layer.[24]

While most research efforts concerning oxides have focused on modifications of the cation composition, a less-explored approach concerns the investigation of modifications of the anion composition in Ruddlesden-Popper phases. Accordingly, a number of oxides are known in this structure type and well examined.[25-27] From oxides to nitride oxides, the anionic substitution of oxygen by nitrogen causes an increase in covalency of the metal-ligand bonds, giving rise to a marked variation of the structural, optical and magnetic properties.[19] In recent years, some nitrogen-containing

representatives of the Ruddlesden-Popper phases, e.g. A_2TaNO_3 (A = Ca, Sr, Ba),[28, 29] Sr_2NbNO_{3-x} (n = 1), $Sr_3Nb_2N_2O_{5-x}$ (n = 2)[30-32] and $Rb_{1+x}Ca_2Nb_3N_xO_{10-x} \cdot yH_2O$ (x = 0.7 – 0.8, y = 0.4 – 0.6)[33] have been reported and attracted significant attention.[34] DFT calculations revealed that layered structures like Sr_2TaNO_3 could exhibit promising photocatalytic activities.[35] As with the perovskites,[36] there are inverse representatives of Ruddlesden-Popper phases like $Ca_7(Li_{1-x}Fe_x)Te_2N_2$[37] and $(A_{3n+1}N_{n-1}O)Bi_{n+1}$ with A = Sr, Ba and n = 1, 3.[38] However, these compounds have relatively low nitrogen content.

Herein, we report on the ammonothermal synthesis of the new mixed-valence nitrogen-rich Ruddlesden-Popper phase $Eu^{II}Eu^{III}_2Ta_2N_4O_3$.

4.2 Results and Discussion

4.2.1 Synthesis

$Eu^{II}Eu^{III}_2Ta_2N_4O_3$ was synthesized by an ammonothermal approach using custom-built high-temperature autoclaves made of nickel-based superalloy.[3, 5-7] Metallic Ta and Eu were used as powders. Eu was rasped from compact pieces in a glovebox. NaN_3 and NaOH were added as mineralizers and oxygen source, respectively. All starting materials were crushed to a powder and placed in a custom-built tantalum liner (length 14 cm, Ø 6 mm), which subsequently was transferred vertically into the autoclave. Since side phases occur during ammonothermal synthesis of nitride oxide perovskites,[7] NaOH and Ta were used in substoichiometric amounts to reduce the formation of $NaTaN_2$ and Eu_2O_3 and promote synthesis of soluble side phases like amides. The maximum reaction temperature of 1070 K and a maximum pressure of 170 MPa resulted in a black crystalline product (Figure 1). The product was washed with aqua regia to remove potential residual side phases like $NaNH_2$, NaOH and Eu_2O_3. In contrast, at lower temperatures of 870 K only $NaEuO_2$ was obtained as large colorless crystals of up to 100 µm. Still, besides the Ruddlesden-Popper phase $Eu_3Ta_2N_4O_3$, the nitride oxide perovskite $EuTa(N,O)_3$ (SI Figure 2) was obtained as a side phase.

A possible intermediate is $NaEuO_2$, since it occurs at the reaction temperature of 870 K with the above mentioned reaction conditions. Presumably, it decomposes at higher

temperatures and reacts to the desired product $Eu_3Ta_2N_4O_3$ in supercritical ammonia. Non-condensed octahedral anions $Ta(N_x,O_{1-x})_6^{(7+6\cdot x)-}$, which react to $NaTa(O_{1-x}N_x)_{3-x}$, might form as well.[39] However, the intermediates / reactive species are still a matter of debate.[7, 8, 40] Compared to other ammonothermal reactions with lanthanides and tantalum, only the Ruddlesden-Popper phase $Eu^{II}Eu^{III}_2Ta_2N_4O_3$ (see *crystal structure determination*) could be synthesized. Despite the similar radii of Ta and Nb,[41] the analogous nitride oxide with Eu and Nb could not be obtained under similar conditions employing Nb-liners in the temperature range up to 1070 K. Our recent investigations have shown that stable inorganic compounds with wurtzite-type or perovskite-type structures are thermodynamically preferred reactions products in ammonothermal syntheses.[3, 7, 8] Unfortunately, we were not able to obtain the perovskite phase $EuTa(N,O)_3$[15, 20] in reasonable yield like it was possible in other studies on lanthanide tantalum perovskites ($LnTaN_2O$ with *Ln* = La, Ce, Pr, Nd, Sm, Gd).[7]

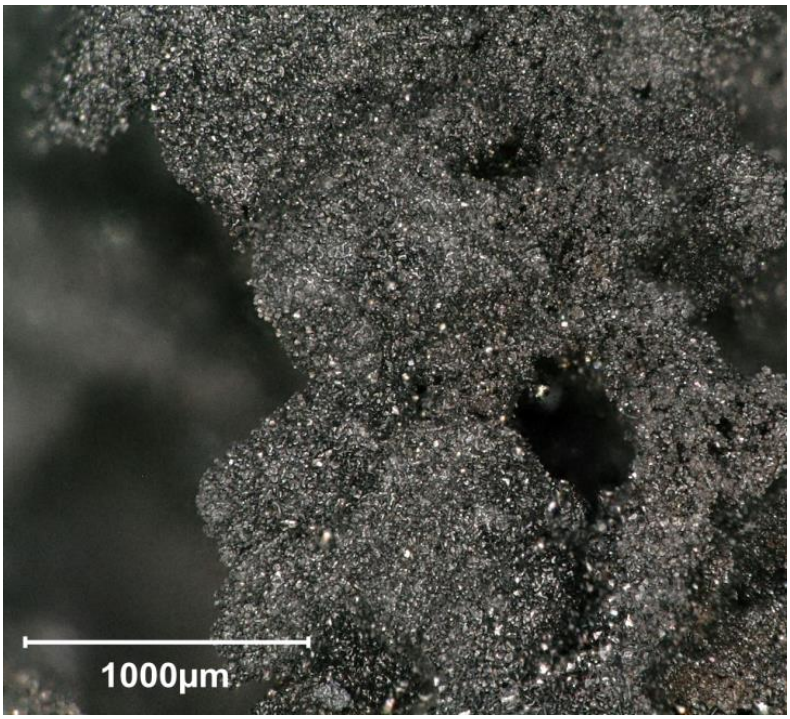

Figure 1. Optical micrograph of the black crystalline product.

4.2.2 Crystal structure determination

According to single crystal X-ray diffraction with microfocused synchrotron radiation, $Eu_3Ta_2N_4O_3$ crystallizes in tetragonal space group $P4_2/mnm$ (no. 136). Crystallographic data are summarized in Table 1. Atomic coordinates and isotropic displacement parameters are given in Table 2. Bond lengths and angles are given in Table 3, anisotropic displacement parameters (ADPs) of $Eu_3Ta_2N_4O_3$ in Table SI 2.

Table 1. Crystallographic data and structure refinement of $Eu_3Ta_2N_4O_3$.

Formula mass / g · mol^{-1}	921.81
Space group	$P4_2/mnm$ (no. 136)
Lattice parameters / Å	a = 5.7278(1), c = 19.8149(5)
Cell volume / Å^3	650.08(3)
formula units per unit cell Z	4
X-ray density / g · cm^{-1}	9.419
Linear absorption coefficient / cm^{-1}	33.147
F(000)	1548
Crystal dimensions / µm^3	2 x 3 x 5
Radiation / Å	0.30996 (synchrotron, ESRF, ID11)
Temperature / K	296
Abs. correction	semiempirical
θ range / °	1.61 – 13.78
Measured reflections	6736
Independent reflections	697
Refined parameters	41
GOF	1.195
R indices ($F_o^2 \geq 2\sigma(F_o^2)$)	$R1$ = 0.0249, $wR2$ = 0.0564
R indices (all data)	$R1$ = 0.0254, $wR2$ = 0.0570
min / max residual electron density / eÅ^{-3}	2.892 / -4.715

Table 2. Atomic coordinates, equivalent isotropic displacement parameters, of $Eu_3Ta_2N_4O_3$ (all sites are fully occupied).

Atom	Wyckoff pos.	*x*	*y*	*z*	U_{eq} (in A^2)
Ta1	8*j*	0.26377(3)	0.26377(3)	0.09890(2)	0.00842(10)
Eu2	4*g*	0.23507(5)	0.76493(5)	0	0.01066(13)
Eu3	8*j*	0.27615(4)	0.27615(4)	0.31573(2)	0.00744(11)
O1	4*e*	0	0	0.0918(2)	0.0116(7)
O2	8*j*	0.1860(4)	0.1860(4)	0.20828(13)	0.0114(5)
N3	4*e*	0	0	0.3707(2)	0.0088(7)
N4	4*f*	0.2898(5)	0.2898(5)	0	0.0087(7)
N5	8*h*	0	1/2	0.11167(15)	0.0082(5)

Table 3. Bond lengths and selected angles in $Eu_3Ta_2N_4O_3$ with standard deviations in parentheses.

	O1	**O2**	**N3**	**N4**	**N5**
$Eu2^{II}$	2.632(3)	-	-	2.738(3) / 3.024(3)	3.000(2)
$Eu3^{III}$	2.579(3)	2.252(3) / 2.405(2)	2.489(2)	-	2.4941(2)
Ta1	2.1213(4)	2.256(3)	2.0055(2)	1.9710(6)	2.0436(4)
N3-**Ta1**-O1	166.41(16)	O1-**Eu2**-O1	87.32(13)	O2-**Eu3**-N5	133.37(6)
N5-**Ta1**-N5	164.55(16)	O1-**Eu2**-N5	122.53(4)	O2-**Eu3**-O1	154.24(10)
O2-**Ta1**-N4	170.00(14)	N4-**Eu2**-N5	112.80(5)	N3-**Eu3**-N5	70.76(5)

4.2.3 Powder X-ray diffraction and Rietveld analysis

The products were analyzed by powder X-ray diffraction to determine the phase composition and identify side phases. (SI Figure 2). Wyckoff positions and atomic coordinates for Rietveld refinement were based on the structure model obtained from single-crystal X-ray data. The obtained crystallographic data are listed in SI Table 1.

4.2.4 TEM measurements

Unit cell metrics were initially determined from SAED tilt series with *a* = 5.84 and *c* = 20.1 Å (Figure 2), which indicated a new phase. Suitable single crystals for microfocused X-ray diffraction were prepared on TEM copper grids with continuous carbon support film. SI Fig. 1 shows the crystal used for data collection.

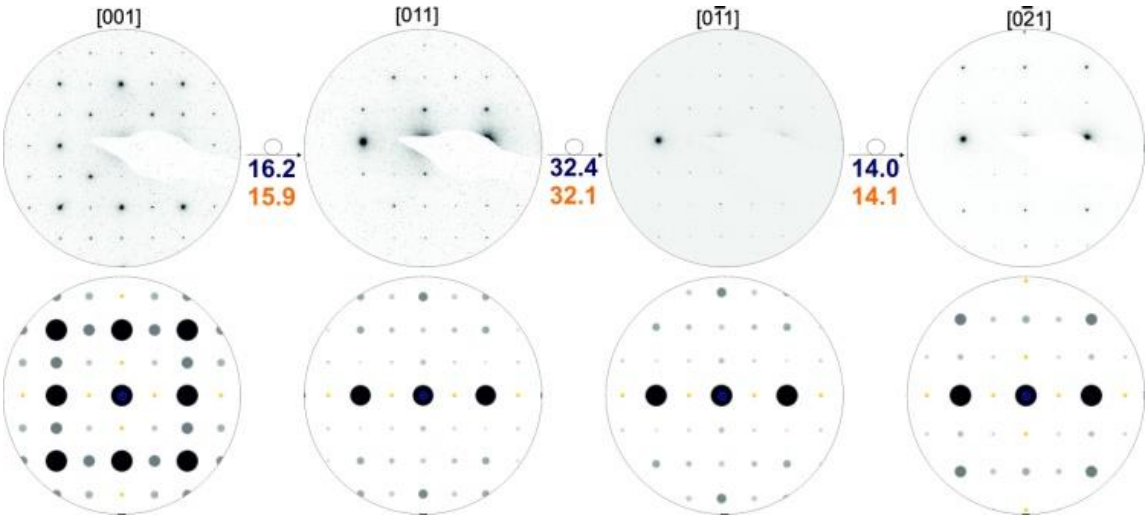

Figure 2. SAED-tilt series with experimental (blue) and theoretical (red) angles between the zone axes (top). Corresponding simulations based on the structure model obtained from single crystal data (bottom).

4.2.5 Crystal structure description

$Eu^{II}Eu^{III}_2Ta_2N_4O_3$ crystallizes in the $SrTb_2Fe_2O_7$ (Sr^{II} ≙ Eu^{II}, Tb^{III} ≙ Eu^{III}, Fe^{III} ≙ Ta^{V}, O^{-II} ≙ N^{-III} / O^{-II}) structure type[42] and corresponds to a Ruddlesden-Popper phase[22, 23] with general formula $A'_2A_{(n-1)}B_nX_{(3n+1)}$ with n = 2; A' = Eu^{III}, A = Eu^{II}, B = Ta^{V} and X = N^{-III} / O^{-II}. The structure, displayed in Figure 3, can be interpreted as an intergrowth of perovskite-type and rocksalt-type slabs.

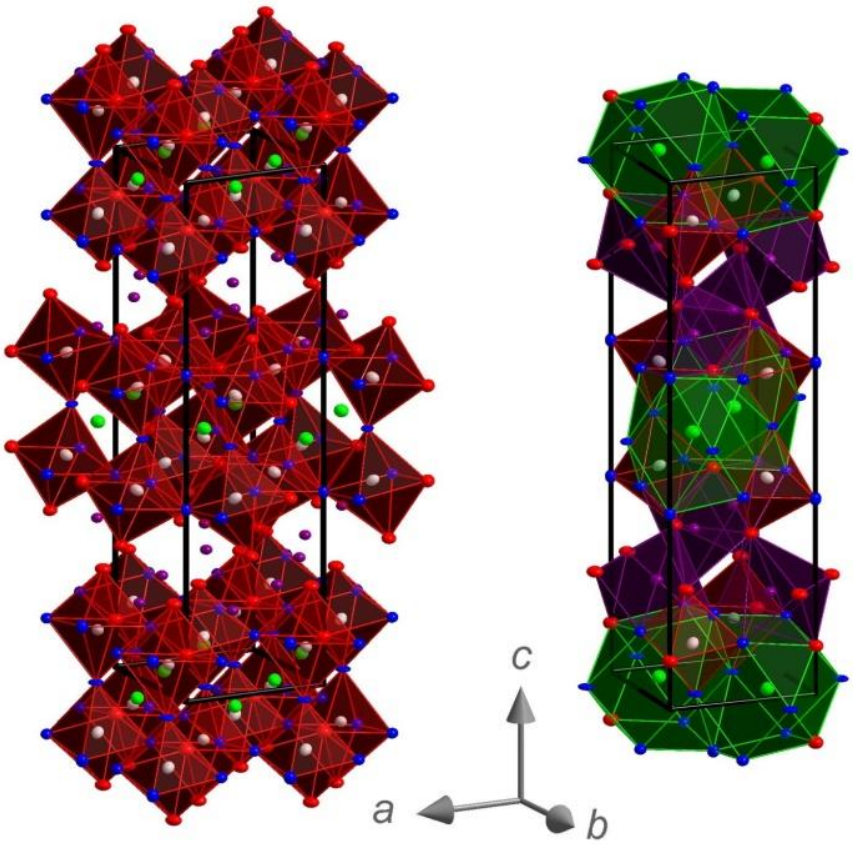

Figure 3. Unit cell of $Eu_3Ta_2N_4O_3$ (left) with Eu^{II} green, Eu^{III} purple, Ta grey, O red and N blue. Distorted $Ta(N,O)_6$ octahedrons are highlighted in red; right: with $Eu^{II}(N,O)_{12}$ cuboctahedrons highlighted in green, $Eu^{III}(N,O)_7$ trigonal capped prism highlighted in purple, $Ta(N,O)_6$ octahedrons highlighted in red, O red and N blue.

Two distorted $Ta(N,O)_6$ octahedrons (cf. angles in Table 3) are interconnected by common vertices to form double layers extending parallel (001). The coordination sphere of $Eu^{II}(N,O)_{12}$ (Eu2: 4*g*) is a distorted cuboctahedron (cf. angles in Table 3). The cuboctahedrons are interconnected with common square faces and also form layers parallel (001). These are part of the $Ta(N,O)_6$ double layer. Consecutive layers of cuboctahedrons are rotated by 180°. Coordination polyhedrons $Eu^{III}(N,O)_7$ (Eu3: 8*j*) are smaller and can be described as single-capped trigonal prisms. These prisms share common trapezium faces with $Eu^{II}(N,O)_{12}$ (Eu2) cuboctahedrons and triangular faces of the $Ta(N,O)_6$ octahedrons and form layers between layers of the $Eu^{II}(N,O)_{12}$ cuboctahedrons and $Ta(N,O)_6$ octahedrons, respectively. Between two $Eu^{II}(N,O)_{12}$ layers, there is one layer of octahedrons missing. The coordination polyhedrons and the corresponding interatomic distances are displayed in Figure 4. Ta-N distances are 1.970(6) – 2.0436(4) Å and Ta-O distances are 2.1413(4) – 2.256(3) Å (Table 3).

These values are in good agreement with known compounds such as TaNO,[43] Ta_3N_5,[44] Ta_2O_5[45] and $EuTa(N,O)_3$.[15] Eu^{II} has an ionic radius of 1.35 Å[41] and is coordinated by 12 anions forming a distorted cuboctahedron, similar to the nitride oxide perovskite $EuTa(N,O)_3$,[15] whereas the smaller Eu^{III} has a radius of 1.01 Å[41] and is coordinated by seven anions resulting in a single-capped trigonal prism, which is similar to the coordination of Eu^{III} in Eu_2O_3.[41, 46] The distances between Eu^{II} and the associated 12 N/O ligands are between 2.632(3) – 3.024(3) Å. With exception of the longest distance of the cuboctahedron (3.342(1) Å), these values are in good agreement with literature.[15, 47, 48] The distances between the smaller Eu^{III} and the seven anions are 2.252(3) – 2.579(3) Å and can be compared to the europium compounds Eu_3O_4[48] and EuN.[49] The presence of two different valence states of europium in one compound has been reported e.g. for Eu_2SiN_3[50] or $Eu_3F_4S_2$.[51] Nevertheless, to the best of our knowledge, $Eu^{II}Eu^{III}_2Ta_2N_4O_3$ is the first mixed-valence Ruddlesden-Popper phase with $Eu^{II/III}$.

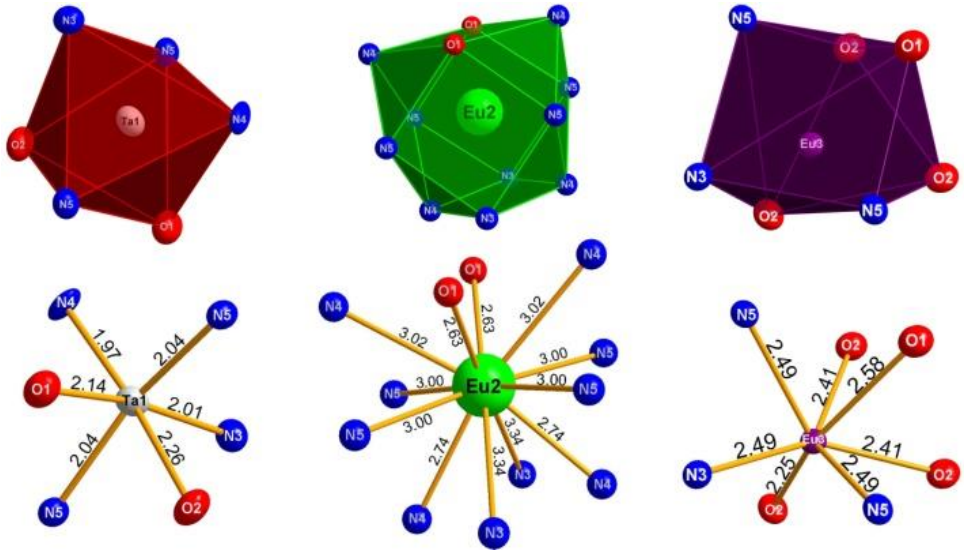

Figure 4. Coordination polyhedrons of TaV (Ta1), Eu^{II} (Eu2) and Eu^{III} (Eu3) with interatomic distances in Å (error >0.001) of Ta1, Eu2 (Eu^{II}) and Eu3 (Eu^{III}) to the respective anions.

The corresponding tilt system for space group $P4_2/mnm$ (no. 136) by Aleksandrov and Bartolome is (ϕ00)(0ϕ0)[52] and by Glazer $(a^-b^0c^0)(b^0a^-c^0)$[53, 54] for the Ruddlesden-Popper phase $Eu^{II}Eu^{III}_2Ta_2N_4O_3$.

4.2.6 Scanning electron microscopy and EDX

EDX data confirm the composition of $Eu_3Ta_2N_4O_3$ (calculated values of the atomic composition in atom% in parenthesis): Eu: 23.3±2.1 (25), Ta: 18.0±1.3 (16.6), N: 32.4±2.1 (33.4), O: 26.3±1.4 (25); see SI Table 3. Residual mineralizer was almost completely removed from the product by washing with aqua regia. SEM images of the purified product predominantly show platelets and, in addition, cube- and cuboid-like crystals (Figure 5). Based on the PXRD (SI Figure 2) and EDX results (SI Table 3), the platelets can be assigned to $Eu_3Ta_2N_4O_3$. The other crystals are attributed to $EuTa(N,O)_3$.[15] Such a platelet morphology has not yet been observed in other ammonothermal reactions, but could be found in the ammonolysis product of $LaTiNO_2$.[55, 56] The morphology of cuboid crystals were already observed in other ammonothermal reactions of nitride oxide perovskites.[7, 8, 40, 57, 58] SEM images show that there are more cuboid-shaped crystals in the centre of the liner and platelets were found almost exclusively at the bottom of the liner. This observation could be due to local concentration maxima during synthesis inside the autoclave.

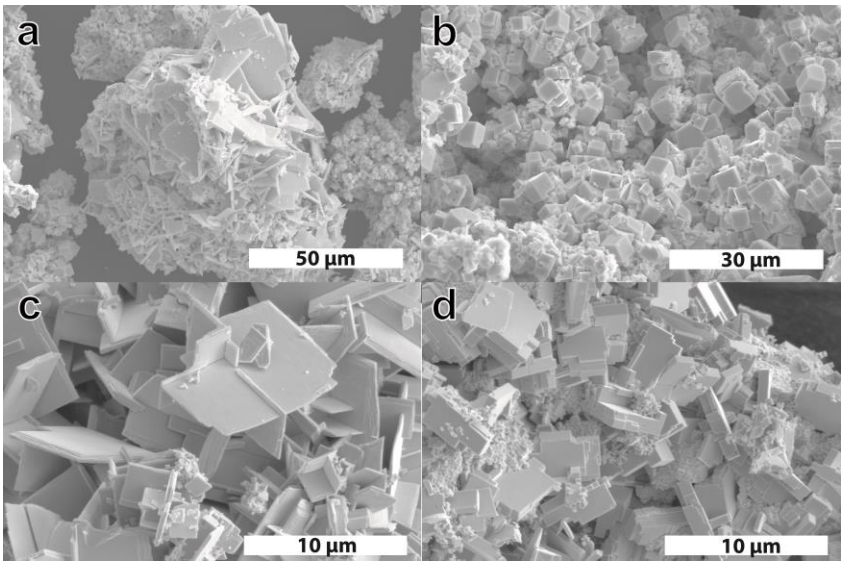

Figure 5. SEM images of different crystals from the ammonothermal synthesis at 1070 K: a) an overview of the sample with different crystal morphologies (platelets in the centre of the image and cubes around them), b) cube-shaped crystals of $EuTa(N,O)_3$, c) platelets of $Eu_3Ta_2N_4O_3$ and d) cuboid crystals of $EuTa(N,O)_3$.

4.2.7 N/O assignment, BVS and MAPLE

Due to the presence of heavy atoms, the N/O assignment is problematic. Still, the N/O assignment was indicated by R-values and displacement parameters. Assuming charge neutrality, BVS calculations[59, 60] were performed in order to reasonably assign sites to N or O and Eu^{II} or Eu^{III}, respectively, despite their very similar X-ray scattering factors. On the basis of the assumed N/O distribution, the BVS of the cations and anions were determined (SI Table 4). This leads to a charge neutral formula, which is corroborated by EDX measurements, Madelung part of the lattice energy (MAPLE, Table 4) and CHARDI calculations (SI Table 5). MAPLE calculations confirm the electrostatic consistency of the crystal structure of $Eu^{II}Eu^{III}_2Ta_2N_4O_3$. MAPLE values were calculated[61] for each ion type and for the entire structure. The sum formula was formally separated into the binary compounds Ta_3N_5,[44] TaNO,[62] EuO,[47] Eu_2O_3.[46] Compared to the sum of total MAPLE values, the deviation of total lattice energies of $Eu^{II}Eu^{III}_2Ta_2N_4O_3$ is 0.6% (Table 4). The partial MAPLE value of $Eu2^{II}$ (1931 kJ/mol) (coordination by 12 anions) is significantly smaller than that of $Eu3^{III}$ (4388 kJ/mol) (coordination by 7 anions) according to the oxidation states $Eu2^{II}$ and $Eu3^{III}$, and the larger distances of 2.6329 – 3.3417 Å to the corresponding 12 anions compared to 2.2506 – 2.5783 Å to the 7 anions. All MAPLE values for N3 – N5 are in the range of 4876 – 4937 kJ/mol. The O1 value (2421 kJ/mol) is larger compared to O2 (2121 kJ/mol) (Table 4). The MAPLE calculations thus suggest that N and O are not significantly disordered. Charge distribution (CHARDI) calculations were performed with VESTA[63] (SI Table 5), following the theory of Hoppe et al.[63, 64] The CHARDI values for each cation are: Ta^{V} (Ta1) = 5.037, $Eu2^{II}$ = 1.915 and $Eu3^{III}$ = 3.006.

Table 4. Results of the MAPLE calculations for $Eu_3Ta_2N_4O_3$ with increment calculations and comparative values in parentheses in kJ/mol.

MAPLE Values.[65-70]								
Ta1	$Eu2^{II}$	$Eu3^{III}$	O1	O2	N3	N4	N5	$Eu_3Ta_2N_4O_3$
13181	1931	4388	2421	2121	4897	4876	4937	63367
-	(1700-2100)	(3500-5100 (RE^{3+}))	(2000-2800)	(2000-2800)	(4300-6200)	(4300-6200)	(4300-6200)	-

MAPLE	MAPLE
$Eu_2O_3 + EuO + Ta_3N_5$ - TaNO	$Eu^{II}Eu^{III}_2Ta_2N_4O_3$
13948 kJ/mol + 3775 kJ/mol + 66027 kJ/mol – 20774 kJ/mol	
= 62976 kJ/mol	63367 kJ/mol
Δ = −0.6%	

4.2.8 UV/VIS

UV/VIS measurements reveal optical properties and band gap values of the product. After mixing with $BaSO_4$, diffuse reflectance R spectra were measured and converted to absorption spectra using the Kubelka-Munk function $F(R) = (1 - R)^2 / 2R$ assuming a direct band gap.[71] Tauc plots determine the optical band gap (Figure 6) by a tangent at the inflection points.[72] The measured band gap is 0.6 eV. This value is significantly smaller than that of other *Ln*TaN_2O nitride oxide perovskites, which possess varying body-colors and have larger band gaps.[7]

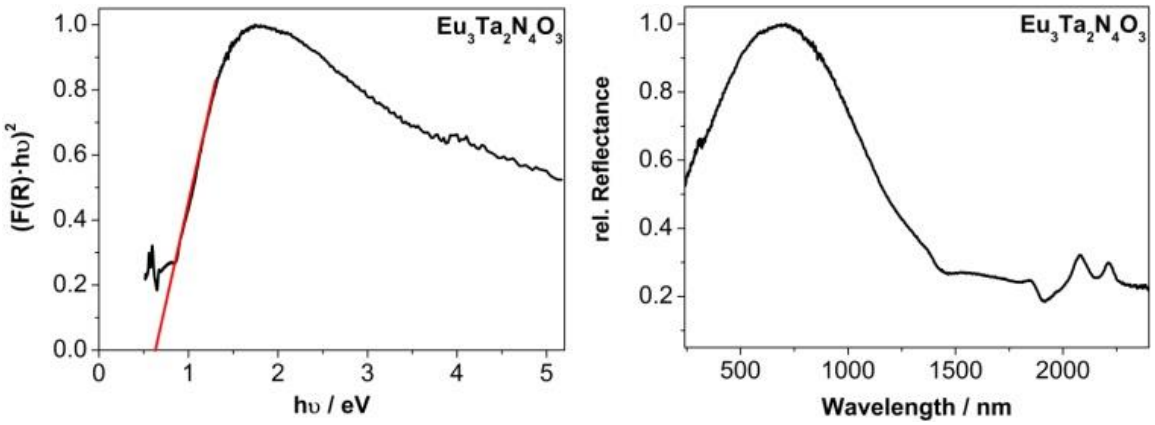

Figure 6. Tauc plot of $Eu_3Ta_2N_4O_3$ and diffuse reflectance measurements.

The relative reflectance shows a broad maximum at about 690 nm, which can be explained by a superposition of 4f–4f transitions.[73]

The black color of the obtained product (Figure 1) is in good agreement with the corresponding band gap.[50] Although structural ordering of europium atoms with different oxidation states has been refined (see *crystal structure description*), a certain amount of charge delocalization with some polaron activity is assumed, as supported by the black color of $Eu_3Ta_2N_4O_3$.[51] Apparently, both Eu^{II} and Eu^{III} ions occur simultaneously during synthesis in a reducing reaction atmosphere (see *synthesis*).

4.3 Conclusions

A new Ruddlesden-Popper phase (n = 2) $Eu^{II}Eu^{III}_2Ta_2N_4O_3$ was obtained by ammonothermal synthesis. Single-crystal data recorded with microfocused synchrotron diffraction revealed the atomic structure and Rietveld refinements corroborate the results. $Eu^{II}Eu^{III}_2Ta_2N_4O_3$ crystallizes in $P4_2/mnm$ with lattice constants a = 5.7278(1) and c = 19.8149(5) Å. $Ta(N,O)_6$ octahedrons are connected *via* common vertices to double layers, where cuboctahedrally coordinated Eu^{II} is located within these layers. Between the layers, there are Eu^{III} atoms, which have a capped trigonal prismatic coordination and are linked by common faces with the $Ta(N,O)_6$ octahedrons. MAPLE, BVS and CHARDI calculations confirm electrostatic consistency. Nitrogen and oxygen could be tentatively assigned in single crystal structure refinements and their distribution was confirmed by the computational methods mentioned.

$Eu^{II}Eu^{III}_2Ta_2N_4O_3$ is the first mixed-valence europium-containing Ruddlesden-Popper phase. Through the use of Ta^{V}, which is highly charged, nitride anions can be incorporated into the compound. This principle should enable manifold substitution of Eu and Ta towards other new compounds. Thus, the ammonothermal method is most likely a promising approach to new perovskite-related materials. In addition, the synthesis of crystals in µm range shows that the solution based ammonothermal synthesis with supercritical ammonia is superior to other methods such as gas flow ammonolysis in terms of crystal growth.

The ammonothermal synthesis of $Eu_3Ta_2N_4O_3$ shows that the intergrowth of a distorted NaCl-like slab in nitride oxide perovskites is possible despite the lower thermodynamic stability of nitrides. The further development of new explorative methods is imperative in order to synthesize larger single crystals for the investigation of physical properties of nitride oxides.

4.4 Experimental Section

All manipulations were carried out in flame-dried Schlenk-type glassware connected to a vacuum line (≤ 0.1 Pa) or in Ar-filled gloveboxes (Unilab, MBraun, Garching, O_2 < 1 ppm, H_2O < 1 ppm) to rigorously exclude oxygen and moisture during preparation and syntheses. Ammonia (Air Liquide, 99.999%) was purified through a gas purification cartridge (Micro Torr MC400-702FV, SAES Pure Gas Inc. San Luis Obispo, Ca, USA) to obtain a purity level of < 1 ppbV H_2O, O_2 and CO_2.

4.4.1 Ammonothermal Synthesis

All syntheses were performed in supercritical ammonia with custom-built autoclaves made of nickel based superalloy (Haynes 282) sustaining a maximum pressure of 170 MPa at 1070 K.[74, 75] The peripheral devices consist of the hand valve (SITEC), pressure transmitter (HBM P2VA1/5000 bar) and a safety head with an integrated rupture disc (SITEC). To seal the autoclave, silver coated C-rings (GFD seals) made of Inconel 718 were used. The autoclaves were placed vertically in custom-built three-zone furnaces (Loba, HTM Reetz) and connected to a pressure display unit (HBM). The pressure was recorded by an AD-converter. The signal was recorded with an average value of each 20 s.

Ta (1 mmol, Sigma-Aldrich, -325 mesh, 99.9%) and Eu (smart-elements 99.9%), 1 mmol) were powdered with a file in a glovebox, NaOH (0.8 mmol, Grüssing) and NaN_3 (99.99% Sigma-Aldrich, 4 mmol) were crushed to a powder in an agate mortar and then placed in custom-built tantalum liners (WHS Sondermetalle; length 140 mm, diameter 6 mm), which were placed vertically in the autoclave and sealed in gloveboxes. Subsequently, the autoclaves were finally screwed. Purified ammonia was then condensed into the evacuated and cooled (193 K) autoclave with 1 bar overpressure with a combined glass-steel-line. After warming up to room temperature, the autoclave was placed vertically in a tube furnace. Subsequently, the autoclave was heated to the respective reaction temperature within 6 h and kept at this temperature for 110 h. The pressure slowly decreased over time because of hydrogen loss of the autoclave. Further details of the used autoclaves can be found in literature.[2, 3, 5-7, 36, 76-84]

4.4.2 Single-Crystal X-ray Diffraction

X-ray diffraction data of a $Eu_3Ta_2N_4O_3$ were obtained by microfocus synchrotron diffraction (beamline ID11, ESRF, Grenoble)[85] on a Huber diffractometer (λ = 0.30996 Å) with a FReLoN2K CCD detector.[86] A crystallite that had been pre-characterized by TEM methods (see below) was used.[87] Integration and empirical absorption correction was done with CrysAlis Pro.[88] Incomplete absorption in the CCD phosphor was taken into account.[89] Solution and refinement of the structure was conducted with SHELX-2014.[90] Further details on the crystal structure analysis can be obtained from the Cambridge Crystallographic Data Centre on quoting the depository no. CCDC 1890993. The crystal structure was visualized with Diamond.[91]

4.4.3 Powder X-ray Diffraction

PXRD measurements were performed in glass capillaries (0.2 mm diameter, Hilgenberg GmbH) with a Stoe STADI P diffractometer (Mo-$K_{\alpha1}$ radiation, Ge(111) monochromator, Mythen 1K detector) in modified Debye-Scherrer geometry. The TOPAS package was used for Rietveld refinement.[92]

4.4.4 UV/VIS Spectroscopy

UV/VIS spectra were recorded using a Perkin-Elmer Lambda 1050 spectrometer equipped with a 150 mm InGaAs integrating sphere. Diffuse reflectance spectra were collected with a Praying Mantis (Harrick) accessory and were referenced to $BaSO_4$ (Sigma-Aldrich, 99.99%) powder as white standard.

4.4.5 SEM / EDX

The atomic ratio of $Eu_3Ta_2N_4O_3$ was confirmed by energy-dispersive X-ray spectroscopy (EDX). SEM images were taken with a Dualbeam Helios Nanolab G3 UC (FEI) with X-Max 80 SDD Detector (Oxford Instruments). The software AzTec was used for EDX analysis.

4.4.6 TEM

For sample preparation, crystals of $Eu_3Ta_2N_4O_3$ were ground in absolute ethanol and drop-cast on copper grids with holey carbon film (Plano GmbH, Germany). The grids were mounted on a double-tilt holder and transferred into a FEI Tecnai G2 20 S-TWIN. TEM images were recorded on a TVIPS camera (TemCam F216, Tietz). The microscope was operated at 200 kV accelerating voltage. For evaluation of the TEM data, the following software was used: Digital Micrograph (measurement of d-values from SAEDs), ProcessDiffraction7 (geometric calculations for SAED) and jEMS (SAED-Simulations).[87, 93-95]

4.5 Acknowledgements

The authors gratefully acknowledge financial support by the Deutsche Forschungsgemeinschaft (DFG) within the research group “Chemistry and Technology of the Ammonothermal Synthesis of Nitrides” (FOR 1600), project SCHN377/16. We thank Dr. Thomas Steigerwald and Anna Kimmel (FAU Erlangen) for development and maintenance of the autoclaves, Christian Minke for SEM measurements, Laura Ascherl for UV/VIS spectra (both at LMU Munich). The authors thank Dr. Jonathan Wright (ESRF, Grenoble), Dr. Christopher Benndorf and Christina Fraunhofer (both at Leipzig University) for their support during measurements at ID11 and the ESRF for granting beamtime (project CH-5140).

4.6 References

[1] R. Juza, H. Jacobs, H. Gerke, *Ber. Bunsen-Ges. Phys. Chem* **1966**, *70*, 1103-1105.

[2] T. Richter, R. Niewa, *Inorganics* **2014**, *2*, 29-78.

[3] J. Häusler, W. Schnick, *Chem. Eur. J.* **2018**, *24*, 11864-11879.

[4] B. Wang, M. J. Callahan, *Cryst. Growth Des.* **2006**, *6*, 1227-1246.

[5] J. Häusler, L. Neudert, M. Mallmann, R. Niklaus, A.-C. L. Kimmel, N. S. A. Alt, E. Schlücker, O. Oeckler, W. Schnick, *Chem. Eur. J.* **2017**, *23*, 2583-2590.

[6] J. Häusler, S. Schimmel, P. Wellmann, W. Schnick, *Chem. Eur. J.* **2017**, *23*, 12275-12282.

[7] N. Cordes, W. Schnick, *Chem. Eur. J.* **2017**, *23*, 11410-11415.

[8] N. Cordes, T. Bräuniger, W. Schnick, *Eur. J. Inorg. Chem.* **2018**, *2018*, 5019-5026.

[9] A. Fuertes, *Prog. Solid State Chem.* **2018**, *51*, 63-70.

[10] A. Fuertes, *Mater. Horiz.* **2015**, *2*, 453-461.

[11] R.-J. Xie, H. T. Hintzen, *J. Am. Ceram. Soc.* **2013**, *96*, 665-687.

[12] A. Kasahara, K. Nukumizu, G. Hitoki, T. Takata, J. N. Kondo, M. Hara, H. Kobayashi, K. Domen, *J. Phys. Chem. A* **2002**, *106*, 6750-6753.

[13] M. Jansen, H. P. Letschert, *Nature* **2000**, *404*, 980-982.

[14] A. B. Jorge, J. Oró-Solé, A. M. Bea, N. Mufti, T. T. M. Palstra, J. A. Rodgers, J. P. Attfield, A. Fuertes, *J. Am. Chem. Soc.* **2008**, *130*, 12572-12573.

[15] T. Motohashi, Y. Hamade, Y. Masubuchi, T. Takeda, K.-i. Murai, A. Yoshiasa, S. Kikkawa, *Mater. Res. Bull.* **2009**, *44*, 1899-1905.

[16] E. C. Pascual, V. B. Gutierrez, M. Subda, R. Sáez Puche, *Solid State Sci.* **2008**, *10*, 1905-1909.

[17] A. Kusmartseva, M. Yang, J. Oró-Solé, A. M. Bea, A. Fuertes, J. P. Attfield, *Appl. Phys. Lett.* **2009**, *95*, 022110.

[18] M. Yang, J. Oró-Solé, A. Kusmartseva, A. Fuertes, J. P. Attfield, *J. Am. Chem. Soc.* **2010**, *132*, 4822-4829.

[19] R. Pastrana-Fábregas, J. Isasi-Marín, C. Cascales, R. Sáez-Puche, *J. Solid State Chem.* **2007**, *180*, 92-97.

[20] R. Marchand, F. Pors, Y. Laurent, *Ann. Chim. - Sci. Mat.* **1991**, *16*, 553-560.

[21] R. Mikita, T. Aharen, T. Yamamoto, F. Takeiri, T. Ya, W. Yoshimune, K. Fujita, S. Yoshida, K. Tanaka, D. Batuk, A. M. Abakumov, C. M. Brown, Y. Kobayashi, H. Kageyama, *J. Am. Chem. Soc.* **2016**, *138*, 3211-3217.

[22] S. N. Ruddlesden, P. Popper, *Acta Crystallogr.* **1957**, *10*, 538-539.

[23] S. N. Ruddlesden, P. Popper, *Acta Crystallogr.* **1958**, *11*, 54-55.

[24] R. Dronskowski, S. Kikkawa, A. Stein, *Handbook of Solid State Chemistry*, Wiley-VCH, Weinheim, **2017**.

[25] J. A. Rodgers, A. J. Williams, J. P. Attfield, *Z. Naturforsch. B: Chem. Sci.* **2006**, *61*, 1515-1526.

[26] I. B. Sharma, D. Singh, *Bull. Mater. Sci.* **1998**, *21*, 363-374.

[27] X. Sun, Y. Mi, F. Jiao, X. Xu, *ACS Catal.* **2018**, *8*, 3209-3221.

[28] N. Diot, R. Marchand, J. Haines, J. M. Léger, P. Macaudière, S. Hull, *J. Solid State Chem.* **1999**, *146*, 390-393.

[29] S. J. Clarke, K. A. Hardstone, C. W. Michie, M. J. Rosseinsky, *Chem. Mater.* **2002**, *14*, 2664-2669.

[30] G. Tobias, J. Oro-Sole, D. Beltran-Porter, A. Fuertes, *Inorg. Chem.* **2001**, *40*, 6867-6869.

[31] G. Tobías, J. Oró-Solé, D. Beltrán-Porter, A. Fuertes, *Cryst. Eng.* **2002**, *5*, 479-485.

[32] G. Tobías, D. Beltrán-Porter, O. I. Lebedev, G. Van Tendeloo, J. Rodríguez-Carvajal, A. Fuertes, *Inorg. Chem.* **2004**, *43*, 8010-8017.

[33] J. A. Schottenfeld, A. J. Benesi, P. W. Stephens, G. Chen, P. C. Eklund, T. E. Mallouk, *J. Solid State Chem.* **2005**, *178*, 2313-2321.

[34] S. Wei, X. Xu, *Appl. Catal., B* **2018**, *228*, 10-18.

[35] M. Bouri, U. Aschauer, *PCCP* **2018**, *20*, 2771-2776.

[36] R. Niewa, *Z. Anorg. Allg. Chem.* **2013**, *639*, 1699-1715.

[37] G. Wang, S. Manni, Q. Lin, P. McVey, R. S. Houk, L. Wu, S. L. Bud'ko, P. C. Canfield, *Philos. Mag. Lett.* **2018**, *98*, 118-125.

[38] F. Gäbler, Y. Prots, R. Niewa, *Z. Anorg. Allg. Chem.* **2007**, *633*, 93-97.

[39] Y. Hu, H. Gu, Z. Hu, W. Di, Y. Yuan, J. You, W. Cao, Y. Wang, H. L. W. Chan, *Cryst. Growth Des.* **2008**, *8*, 832-837.

[40] T. Toshima, K. Kishida, Y. Maruyama, T. Watanabe, *J. Ceram. Soc. Jpn.* **2017**, *125*, 643-647.

[41] R. Shannon, *Acta Crystallogr., Sect. A* **1976**, *32*, 751-767.

[42] D. Samaras, A. Collomb, J. C. Joubert, *J. Solid State Chem.* **1973**, *7*, 337-348.

[43] M. Weishaupt, J. Strähle, *Z. Anorg. Allg. Chem.* **1977**, *429*, 261-269.

[44] J. Strähle, *Z. Anorg. Allg. Chem.* **1973**, *402*, 47-57.

[45] K. Lehovec, *J. Less-Common Met.* **1964**, *7*, 397-410.

[46] H. Kohlmann, C. Hein, R. Kautenburger, C. Hansen Thomas, C. Ritter, S. Doyle, *Z. Kristallogr. - Cryst. Mater.* **2016**, *231*, 517-523.

[47] H. A. Eick, N. C. Baenziger, L. Eyring, *J. Am. Chem. Soc.* **1956**, *78*, 5147-5149.

[48] R. Rau, *Acta Crystallogr.* **1966**, *20*, 716-723.

[49] W. Klemm, G. Winkelmann, *Z. Anorg. Allg. Chem.* **1956**, *288*, 87-90.

[50] M. Zeuner, S. Pagano, P. Matthes, D. Bichler, D. Johrendt, T. Harmening, R. Pöttgen, W. Schnick, *J. Am. Chem. Soc.* **2009**, *131*, 11242-11248.

[51] H. Grossholz, I. Hartenbach, G. Kotzyba, R. Pöttgen, H. Trill, B. D. Mosel, T. Schleid, *J. Solid State Chem.* **2009**, *182*, 3071-3075.

[52] K. S. Aleksandrov, J. Bartolome, *J. Phys.: Condens. Matter* **1994**, *6*, 8219-8235.

[53] A. Glazer, *Acta Crystallogr. Sect. B* **1972**, *28*, 3384-3392.

[54] M. J. Pitcher, P. Mandal, M. S. Dyer, J. Alaria, P. Borisov, H. Niu, J. B. Claridge, M. J. Rosseinsky, *Science* **2015**, *347*, 420-424.

[55] M. Hojamberdiev, A. Yamaguchi, K. Yubuta, S. Oishi, K. Teshima, *Inorg. Chem.* **2015**, *54*, 3237-3244.

[56] K. Kawashima, M. Hojamberdiev, H. Wagata, K. Yubuta, S. Oishi, K. Teshima, *Cryst. Growth Des.* **2015**, *15*, 333-339.

[57] T. Watanabe, K. Tajima, J. Li, N. Matsushita, M. Yoshimura, *Chem. Lett.* **2011**, *40*, 1101-1102.

[58] C. Izawa, T. Kobayashi, K. Kishida, T. Watanabe, *Adv. Mater. Sci. Eng.* **2014**, *2014*, 1-5.

[59] N. E. Brese, M. O'Keeffe, *Acta Crystallogr. Sect. B* **1991**, *47*, 192-197.

[60] I. D. Brown, D. Altermatt, *Acta Crystallogr. Sect. B* **1985**, *41*, 244-247.

[61] R. Hübenthal, *MAPLE, Programm zur Berechnung des Madelunganteils der Gitterenergie, Version 4*, Universität Giessen, **1993**.

[62] H. Schilling, A. Stork, E. Irran, H. Wolff, T. Bredow, R. Dronskowski, M. Lerch, *Angew. Chem. Int. Ed. Engl.* **2007**, *46*, 2931-2934; *Angew. Chem.* **2007**, *119*, 2989-2992.

[63] K. Momma, F. Izumi, *J. Appl. Crystallogr.* **2011**, *44*, 1272-1276.

[64] R. Hoppe, S. Voigt, H. Glaum, J. Kissel, H. P. Müller, K. Bernet, *J. Less-Common Met.* **1989**, *156*, 105-122.

[65] R. Hoppe, *Angew. Chem. Int. Ed. Engl.* **1966**, *5*, 95-106; *Angew. Chem.* **1966**, *78*, 52-63;.

[66] R. Hoppe, *Angew. Chem. Int. Ed. Engl.* **1970**, *9*, 25-34; R. Hoppe, *Angew. Chem*. **1970**, *82*, 7-16.

[67] R. Lauterbach, *Doctoral Thesis - Synthese, Strukturen und Materialeigenschaften neuartiger Oxonitridosilicate (Sione) und Oxonitridoalumosilicate (Sialone)*, University of Bayreuth, **1999**.

[68] H. A. Höppe, *Doctoral Thesis - Optische, magnetische und strukturelle Eigenschaften von Nitridosilicaten, Oxonitridosilicaten und Carbidonitridosilicaten*, University of Munich (LMU), **2001**.

[69] K. Köllisch, *Doctoral Thesis - Neue Beiträge zur Strukturchemie der Sione und Sialone*, University of Munich (LMU), **2001**.

[70] M. Zeuner, S. Pagano, W. Schnick, *Angew. Chem. Int. Ed.* **2011**, *50*, 7754-7775; *Angew. Chem*. **2011**, *123*, 7898-7920.

[71] R. López, R. Gómez, *J. Sol-Gel Sci. Technol.* **2012**, *61*, 1-7.

[72] J. Tauc, R. Grigorovici, A. Vancu, *Phys. Status Solidi B* **1966**, *15*, 627-637.

[73] G. H. Dieke, *Spectra and Energy Levels of Rare Earth Ions in Crystals*, Interscience, New York, **1968**.

[74] B. Hertweck, A.-C. L. Kimmel, T. G. Steigerwald, N. S. A. Alt, E. Schlücker, *Chem. Eng. Technol.* **2018**, *41*, 994-1002.

[75] A. C. L. Kimmel, T. F. Malkowski, S. Griffiths, B. Hertweck, T. G. Steigerwald, L. P. Freund, S. Neumeier, M. Göken, J. S. Speck, E. Schluecker, *J. Cryst. Growth* **2018**, *498*, 289-300.

[76] M. Mallmann, J. Häusler, N. Cordes, W. Schnick, *Z. Anorg. Allg. Chem.* **2017**, *643*, 1956-1961.

[77] J. Häusler, R. Niklaus, J. Minár, W. Schnick, *Chem. Eur. J.* **2018**, *24*, 1686-1693.

[78] J. Häusler, L. Eisenburger, O. Oeckler, W. Schnick, *Eur. J. Inorg. Chem.* **2018**, 759-764.

[79] M. Mallmann, C. Maak, R. Niklaus, W. Schnick, *Chem. Eur. J.* **2018**, *24*, 13963-13970.

[80] S. Zhang, F. Hintze, W. Schnick, R. Niewa, *Eur. J. Inorg. Chem.* **2013**, *2013*, 5387-5399.

[81] J. Hertrampf, N. S. A. Alt, E. Schlücker, M. Knetzger, E. Meissner, R. Niewa, *J. Cryst. Growth* **2016**, *456*, 2-4.

[82] J. Hertrampf, P. Becker, M. Widenmeyer, A. Weidenkaff, E. Schluecker, R. Niewa, *Cryst. Growth Des.* **2018**, *18*, 2365-2369.

[83] S. Schimmel, P. Duchstein, T. G. Steigerwald, A. C. L. Kimmel, E. Schlücker, D. Zahn, R. Niewa, P. Wellmann, *J. Cryst. Growth* **2018**, *498*, 214-223.

[84] S. Schimmel, M. Koch, P. Macher, A.-C. L. Kimmel, T. G. Steigerwald, N. S. A. Alt, E. Schlücker, P. Wellmann, *J. Cryst. Growth* **2017**, *479*, 59-66.

[85] G. B. M. Vaughan, J. P. Wright, A. Bytchkov, C. Curfs, C. Grundlach, M. Orlova, H. G. L. Erra, T. Buslaps, A. Götz, G. Suchet, S. Petitdemange, M. Rossat, L. Margulies, W. Ludwig, A. Snigirey, I. Snigireva, H. O. Sorensen, E. M. Lauridsen, U. L. Olsen, J. Oddershede, H. F. Poulsen, *Proceedings of the 31st Risø International Symposium on Materials Science, Vol. 457*, Technical University of Denmark, **2010**.

[86] J. C. Labiche, O. Mathon, S. Pascarelli, M. A. Newton, G. G. Ferre, C. Curfs, G. Vaughan, A. Homs, D. F. Carreiras, *Rev. Sci. Instrum.* **2007**, *78*, 091301.

[87] F. Fahrnbauer, T. Rosenthal, T. Schmutzler, G. Wagner, G. B. M. Vaughan, J. P. Wright, O. Oeckler, *Angew. Chem. Int. Ed.* **2015**, *54*, 10020-10023; *Angew. Chem.* **2015**, *54*, 10158-10161.

[88] A. Technologies, *CrysAlis Pro 171.38.41*, Yarnton, Oxfordshire, England, **2015**.

[89] G. Wu, B. L. Rodrigues, P. Coppens, *J. Appl. Crystallogr.* **2002**, *35*, 356-359.

[90] G. M. Sheldrick, *Acta Crystallogr. Sect. C: Cryst. Struct. Commun.* **2015**, *71*, 3-8.

[91] K. Brandenburg, *Diamond 3*, Crystal Impact GbR, Bonn, Germany, **2014**.

[92] A. Coelho, *TOPAS Academic, Version 4.1*, Coelho Software, Brisbane (Australia), **2007**.

[93] I. Gatan, Digital Micrograph, Pleasanton, California, USA, **1999**.

[94] J. L. Lábár, *Ultramicroscopy* **2005**, *103*, 237-249.

[95] J. P. A. Stadelmann, CIME-EPFL, Saas-Fee, Switzerland, 2008.

5 Ammonothermal Crystal Growth of $ATaN_2$ with A = Na, K, Rb, Cs and their Optical and Electronic Properties

Published in: *Cryst. Growth Des*. **2019**, *19*, 3484–3490.

Authors: Niklas Cordes, Robin Niklaus, Wolfgang Schnick

https://pubs.acs.org/doi/10.1021/acs.cgd.9b00357

Keywords: Ammonothermal Synthesis • Nitride • Crystal Growth • DFT Calculations • Band gap • Electronic Structure

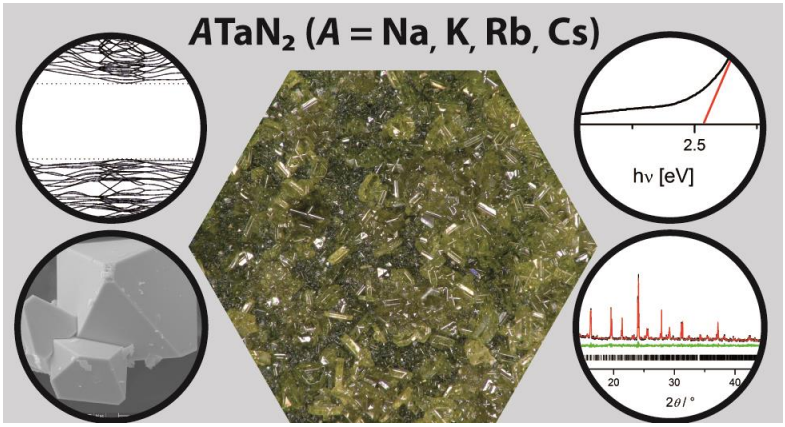

Crystals of alkali nitridotantalates $ATaN_2$ with A = Na, K, Rb, Cs with well developed shape were grown by ammonothermal syntheses at temperatures of up to 1070 K and an internal pressure of up to 170 MPa. The syntheses have been performed in custom-built high-pressure autoclaves made of the nickel-based super alloy Haynes 282 employing tantalum liners.

Abstract: Crystals of alkali nitridotantalates ATaN$_2$ (A = Na, K, Rb, Cs) with well developed shape were grown from corresponding alkali amides or azides and elementary Ta in supercritical ammonia. The aforementioned alkali mineralizers provide an ammonobasic environment for crystal growth. Temperatures of up to 1070 K resulted in an internal pressure of up to 170 MPa in high-pressure custom-built autoclaves. For successful crystal growth, a custom-built Ta liner was used as substrate. The obtained ATaN$_2$ crystals vary in size depending on the used alkali metal (Na: 50 µm; K: 40 µm; Rb: 200 µm; Cs: 50 µm). In addition, a second temperature step at the decomposition temperature of the respective mineralizer is required for the successful synthesis of crystals, due to formation of intermediates at lower temperatures. The obtained products were examined by PXRD, SEM and UV-Vis spectroscopy. The electronic properties were investigated by DFT calculations.

5.1 Introduction

Nitrides are one of the increasingly studied materials, due to their structural versatility along with promising electronic and optical properties, useful in a variety of applications.[1-3] While binary nitrides like Ta_3N_5 (an n-type semiconductor with d^0 configuration) are for example studied as favorable solar energy conversion materials, ternary nitrides have likewise shifted into the focus.[3] It has been demonstrated, that e.g. TaON is an effective photoanode under visible light irradiation.[4] However, multinary nitrides are still relatively unexplored.[3, 5]

In view of the current technological requirements, significant and substantial developments in key applications like electronics have been made in a short time.[6] Whereas research on binary transition metal nitrides is mostly driven by technical and industrial interest, the investigation of ternary and higher nitrides primarily focuses on exploration with respect to the development of new synthetic strategies, the design of new materials and further investigation of materials properties.[7] Ternary nitridometalates, e.g. ATaN$_2$ with A = alkali or transition metals have been synthesized but not yet further investigated.[8, 9] CuTaN$_2$ for example is an interesting candidate for thin film photovoltaics. Analogous ternary nitrides CuNbN$_2$ and AgTaN$_2$ can be synthesized by ion exchange reactions and show promising optical and electronic properties, relevant for solar energy conversion applications.[10-12]

Binary nitrides are accessible by conventional high-temperature solid-state methods, where oxide precursors are transformed into nitrides via reaction with reactive gases like ammonia or mixtures of H_2/N_2 (gas flow ammonolysis). The binary Ta^{+V} nitride Ta_3N_5, for example, can thus be obtained by ammonolysis of Ta_2O_5.[13] Interestingly, the corresponding niobium compound "Nb_3N_5" is yet to be known,[14] whereas the existent Nb_4N_5 shows fair electronic conductivity with chemical stability and might serve as a desirable candidate for supercapacitors.[15] A common challenge in the synthesis of multinary nitrides lies within the high thermodynamic stability of the binary nitride phases. Hence, reactive nitrogen containing species like amides or azides are utilized with metals under extreme reducing conditions in order to prepare multinary nitridometalates. Employment of azides instead of amides e.g. in sealed ampules, provides metal, flux and mineralizer after decomposition without hydrogen as possible impurity. Excessive metal can be removed from the reaction products by extraction with liquid ammonia or sublimation.[6, 16]

Device applications and the efficiency of nitride semiconductors strongly depend on the crystal quality of the stacked layers grown by epitaxial growth on foreign substrates. Therefore, the development of new growth methods is nowadays one key issue in semiconductor chemistry, but still encounters challenges.[1]

Hydrothermal synthesis has proven successful for single crystal growth of oxide materials.[17, 18] In close analogy ammonothermal synthesis, using a medium of liquid or supercritical ammonia, in autoclaves works against decomposition and towards crystallization of nitride materials unstable towards hydrolysis. Explorations of single crystal growth were conducted on some key representatives of important nitrides[1, 19, 20] such as GaN,[1] InN[21] and more recently Grimm-Sommerfeld analogous wurtzite derivatives like ZnSiN$_2$, ZnGeN$_2$[22] or Zn$_2$PN$_3$.[23] Consequently, the ammonothermal process could be identified as a suitable method for crystal growth and explorative synthesis. This re-established method provides a sophisticated approach to synthesize crystals with acceptable sizes and simultaneously high quality in terms of impurities, adhesions and imperfections.[1, 19, 24-26]

However, in many cases it is still difficult to find the critical synthesis conditions to grow nitride crystals. The alkali nitridotantalates ATaN$_2$ (A = Na, K, Rb, Cs) have only been obtained as microcrystalline powders so far.[9, 27] NaTaN$_2$ and KaTaN$_2$ are accessible in a tube furnace starting from sodium or potassium metal, respectively, and Ta$_3$N$_5$ with flowing ammonia operating under normal pressure. This gas flow ammonolysis reaction can also be employed for the corresponding Nb containing compound NaNbN$_2$.[16] The niobium compounds, NaNbN$_2$ and CsNbN$_2$, on the other hand, were synthesized as crystals by reaction at 1070 K in salt melts in high-pressure vessels starting from NbN and the respective amides.[28-30] Sodium compounds of corresponding niobium and tantalum nitrides can be further used to perform ion exchange reactions. Utilizing CuI, Na^+ can be exchanged by Cu^+ in NaTaN$_2$ forming CuTaN$_2$ crystallizing in the layered delafossite structure type.[8, 31] So far it was however not possible to obtain suitable single crystals from ion exchange reactions.[3, 5, 11, 31]

As such until now no µm-sized crystals of ATaN$_2$ with A = Na, K, Rb, Cs could be synthesized, neither in ammonolysis[16] nor under ammonothermal conditions.[9, 27] In the past, NaTaN$_2$ occurred as residual side phase growing on the tantalum liner in the process of ammonobasic ammonothermal reactions utilizing NaN$_3$ or NaNH$_2$ as a mineralizer.[25]

In this contribution, we report on the first synthesis of crystals in the several tens to hundred µm range of alkali nitridotantalates (Na-, K-, Rb- and $CsTaN_2$) by use of ammonothermal synthesis. Structural investigation of the ternary tantalum nitrides was performed by powder X-ray diffraction methods, whereas the morphology was investigated by scanning electron microscopy (SEM). Furthermore, the optical and electronic properties of these compounds were examined by UV-Vis spectroscopy and DFT calculations. Our work showcases the principal feasibility to obtain crystals of ternary nitride materials of several tens of micrometers that may be advantageous for the investigation of fundamental materials properties.

5.2 Experimental Section

5.2.1 Synthesis

Due to oxygen and moisture sensitivity of the starting materials all handlings were performed in an argon-filled glovebox (MBraun, Garching, Germany). Reactions were carried out in customized 11 mL autoclaves made of the nickel-based super alloy Haynes 282[1] with tantalum liners. Further details about the autoclaves can be found in literature.[1, 25] The autoclave was placed vertically in a tube furnace (HTM Reetz GmbH, Berlin, Germany) designed in order to heat it completely (without peripherical devices) and guarantee uniform heat distribution in the reaction chamber. Small temperature differences between the furnace and the inner reactor of the autoclave are expected due to heat loss between heat source and inner wall of the autoclave. The pressure was monitored using a digital pressure transmitter (P2VA1/5000 bar, HBM GmbH, Ismaning, Germany) and logged with a conventional computer. Gaseous ammonia (Air Liquide, 99.999%) used for the reaction was purified with a gas purification cartridge (MicroTorr MC400-702FV, SAES Pure Gas Inc., San Luis Obispo, Ca, USA) to obtain a low impurity level of <1 ppbV of H_2O, O_2 and CO_2. The amount of ammonia condensed into the autoclave was determined using a flow meter (MASS-STREAM D-6320-DR, Bronkhorst, Ruurlo, Netherlands).

The following chemicals were used as delivered: NaN_3 (Sigma-Aldrich, 99.9%), KN_3 (Sigma-Aldrich, 99.9%), $RbNH_2$ (synthesized from Rb (Sigma-Aldrich 99.99%) in liquid ammonia),[14] CsN_3 (Sigma-Aldrich, 99.99%), Ta (Sigma-Aldrich, -325 mesh, 99.9%). The starting materials were mixed and placed in the Ta-liner, which was then

transferred into the autoclave. The autoclave was shut in the glovebox. Subsequently, the autoclave screws were tightened with the required torque outside the glovebox. Then, the autoclave was evacuated, cooled and ammonia was condensed into the autoclave with a combined glass and steel vacuum line (≤ 0.1Pa). After heating to room temperature the autoclave was placed in a vertically orientated furnace, heated with different rates for each compound and maintained for several hours, reaching a maximum pressure of 170 MPa before the oven was cooled to room temperature by a final cooling step. (**NaTaN$_2$**: 1.6 K/min → 673 K, hold for 35 h, 1.6°K/min → 1073 K, hold for 90 h, cool to RT; **KTaN$_2$**: 2.2 K/min → 673 K, hold for 20 h, 0.1 K/min → 1073 K, hold for 96 h, 0.1 K/min → RT; **RbTaN$_2$**: 2.1 K/min → 653 K, hold for 24 h, 1.4 K/min → 900 K, hold for 24 h, 0.4 K/min → RT; **CsTaN$_2$**: 2 K/min → 623 K, hold for 48 h, 2.5 K/min → 1073 K, hold for 48 h, 0.4 K/min → RT). The residual pressure after the reaction was drained through an oil bubbler. The products were analyzed by powder X-ray diffraction (PXRD), using a powder diffraction system STADI-P (Stoe & Cie) equipped with a Mythen 1K detector and Mo $K_{\alpha1}$ radiation (λ = 0.71093 Å). Scanning electron microscopy (SEM) images were captured using a Dualbeam Helios Nanolab G3 UC (FEI) microscope with X-Max 80 SDD Detector (Oxford Instruments). The software AzTec was used for processing of pictures. Diffuse reflectance spectroscopy measurements were conducted using a Jasco V-650 UV-Vis spectrophotometer equipped with Czerny-Turner mount, photomultiplier tube detector and deuterium (190 – 350 nm) / halogen (330 – 900 nm) lamps as light sources.

5.2.2 Computational Details

Structural relaxations for ATaN$_2$ (A = Na, K, Rb, Cs) were performed with the Vienna ab initio simulation package (Vasp)[32-35] until total energies were converged to 10^{-7} eV/atom with total residual atomic forces below 1×10^{-2} eV/Å. The generalized gradient approximation (GGA) of Perdew, Burke and Ernzerhof[36, 37] was used to treat exchange correlation along with the projector-augmented-wave (PAW) method.[38, 39] Brillouin zone sampling was done on a Γ-centered k-mesh (NaTaN$_2$: 16 x 18 x 4; KTaN$_2$ 10 x 6 x 5; RbTaN$_2$: 10 x 6 x 5; CsTaN$_2$: 6 x 6 x 6) produced from the method of Monkhorst and Pack.[40]

5.3 Results and Discussion

5.3.1 Synthesis

Variation of reaction conditions including different heating rates, second temperature steps for formation of intermediates, particularly alkali amides, and the amount of mineralizer were carried out to screen the optimum crystallization conditions. The best results for crystal growth of ternary alkali nitridotantalates were obtained using a molar ratio of Ta : alkali mineralizer of 1 : 7. Lower amounts of the mineralizer also resulted in the desired product, first recognizable by a coloration of the outside wall of the liner or on the liner substrate, but no recognizable growth of crystals was observed. Crystal growth was possibly unsuccessful due to lacking oversaturation of the medium or the lack of a necessary melt at the bottom inside of the liner. The crystal growth in melts is known from other solid-state reactions in ampules.[6, 16] Formation of NaTaN$_2$ crystals was observed at the bottom inside the liner and those of KTaN$_2$ on the liner wall. Thus, crystallization seems to depend on the respective alkali metal and consequently their solubility. In contrast, an even larger excess of the required mineralizer has no impact on crystal size and quantity of the desired product and merely increases residual amides. The reactions were conducted in two steps, owing to the preferential formation of amides at lower temperatures,[19] the significant decomposition of ammonia beyond 850 K as well as the resulting reductive atmosphere.[41] A first necessary constant temperature step in the range of the decomposition temperature of the respective mineralizers was chosen. During a first holding phase, the mineralizer dissolves in liquid / supercritical ammonia. At elevated temperatures azides decompose to nitrogen (detectable by a pressure increase) and the respective metal, which subsequently forms the corresponding amide.[19] The reactive amides are less soluble than the azides in ammonia and could form a melt at the bottom of the liner, further reacting with Ta.[42] Apart from azide decomposition, nitrogen also results from decomposition of ammonia at elevated temperatures. It is likely that nitrogen could dissolve in this melt of the respective amides at the bottom of the liner in the autoclave.[6] Previous ammonothermal syntheses showed evidence of the presence of a melt at the bottom of the liner as well.[25, 26] We assume, that this melt could, to a certain degree, chemically corrode parts of the liner's surface area and promote the crystallization process on the liner as a substrate. Initially, some amount of alkali mineralizer is

dissolved in the supercritical ammonia[43] and is available for reaction. After a second heating phase to the final temperature of 900 – 1070 K, formed intermediates, primarily alkali amides, gradually decompose to form the desired nitrides.[22] The crystal growth might also be supported by the higher reactivity of supercritical ammonia of ammonothermal synthesis compared to gas flow ammonolysis reactions due to the increased solubility and relative permittivity.[41, 43, 44] This may contribute to the fact that so far no crystals could be obtained from gas flow ammonolysis reactions. Another reason could be due to a missing solvent in such reaction systems.

In a final cooling step, supersaturation of the solution takes place, leading to µm-sized crystals. On the one hand, the liner offers a barrier between the reaction and the autoclave wall to prevent corrosion and on the other hand, it provides a mandatory substrate for the growth of the desired products as crystals. The liner can easily be removed from the inside of the autoclave and the product can finally be extracted and collected. The products with body colors orange ($NaTaN_2$), green ($KTaN_2$), orange-yellow ($RbTaN_2$) and orange-yellow ($CsTaN_2$) were extracted from the autoclave inside a glovebox. The obtained products are depicted in Figure 1.

5.3.2 Optical appearance, SEM measurements and Rietveld analysis

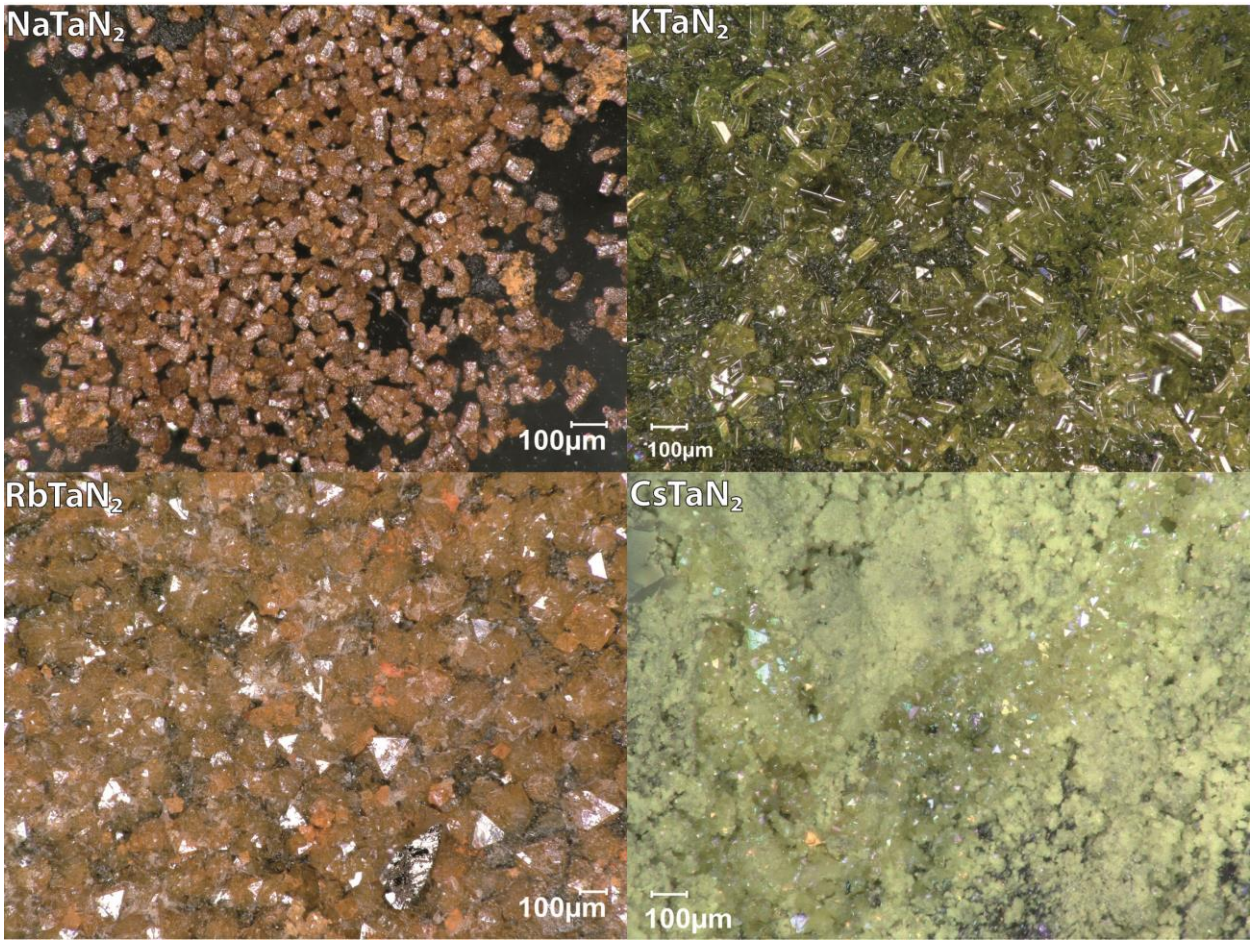

Figure 1: Optical pictures of the synthesized alkali nitridotantalates ($NaTaN_2$ orange, $KTaN_2$ green, $RbTaN_2$ orange-yellow, $CsTaN_2$ yellow-green).

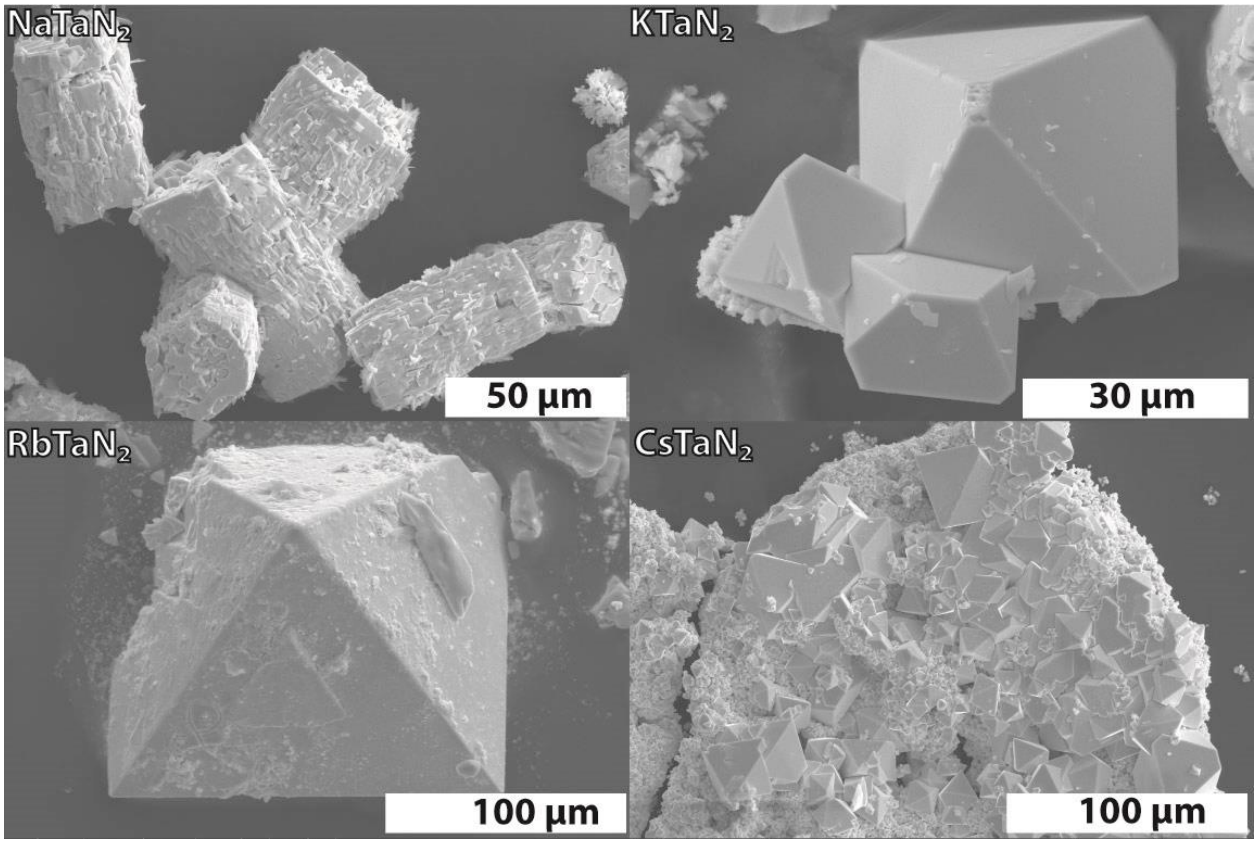

Figure 2. SEM images of the obtained crystals of ATaN$_2$ (with A = Na, K, Rb, Cs) at 1070 K with different scale bars.

The resulting crystals exhibit well developed crystal faces (Figure 2). Unfortunately, all crystals are prone to strong intergrowth and twinning. NaTaN$_2$ appears in form of fused hexagonal rods of up to 60 – 70 µm. K-, Rb- and CsTaN$_2$ crystallize in octahedral shape of different sizes. For RbTaN$_2$ the largest crystals were obtained with sizes up to 200 µm, whereas KTaN$_2$ and CsTaN$_2$ form crystals of about 50 – 60 µm. All crystals were found to grow on the inner wall of the liner.

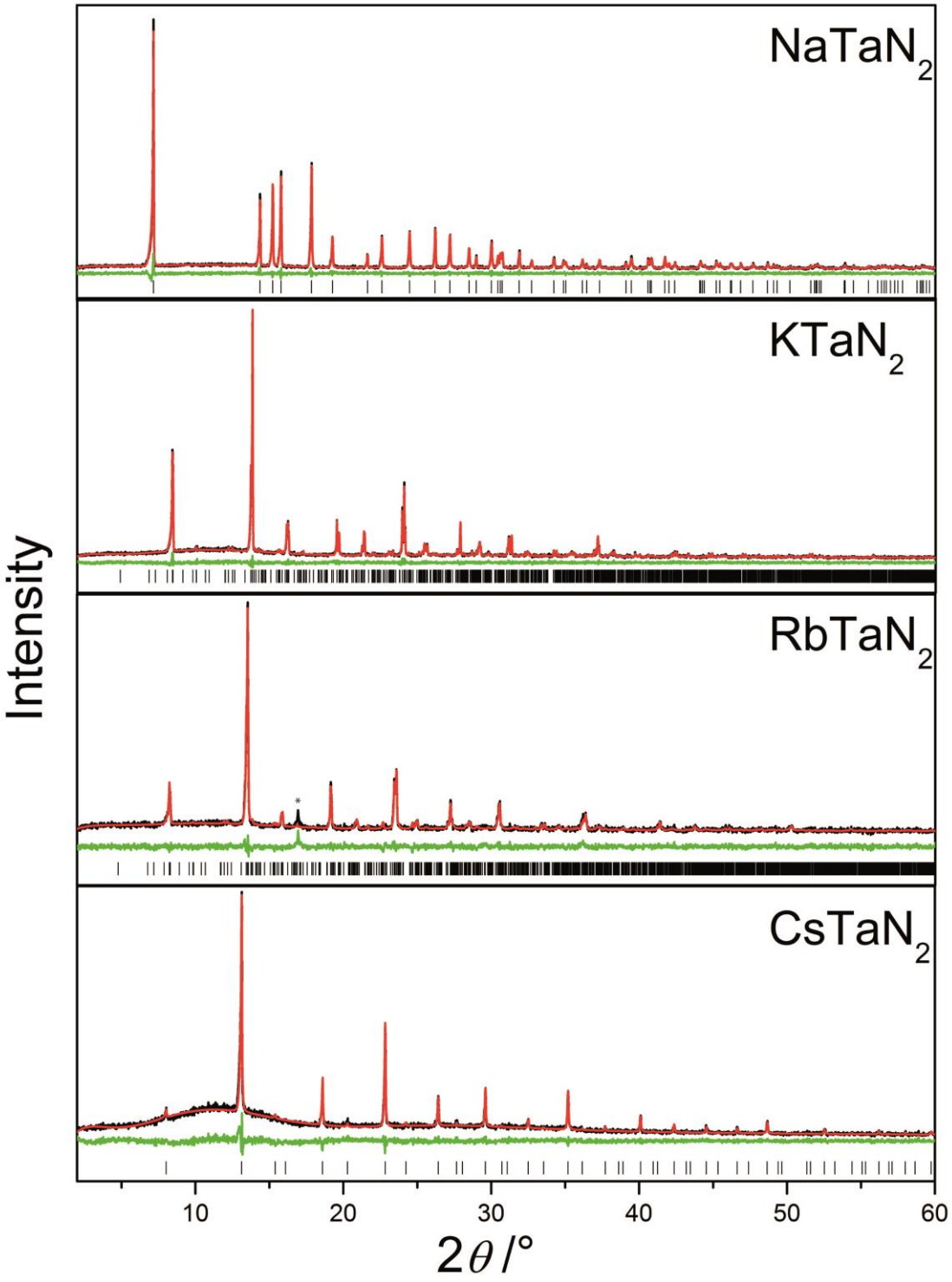

Figure 3. Rietveld refinements of NaTaN$_2$ ($R\bar{3}m$, no. 166), KTaN$_2$, RbTaN$_2$ (both *Pbca*, no. 61) and CsTaN$_2$ ($Fd\bar{3}m$, no. 227) with experimental data (black lines Mo-Kα_1, λ = 0.70930 Å), calculated patterns (red lines), difference plot (green lines) and positions of Bragg reflections (black bars). Reflection marked with asterisk (*) corresponds with TaH.

Crystal structures were analyzed and refined by powder X-ray diffraction (PXRD) data based on structural data reported in literature. NaTaN$_2$ ($R\bar{3}m$, no 166) crystallizes in the α-NaFeO$_2$ structure type, KTaN$_2$ and RbTaN$_2$ (*Pbca*, no 61) crystallize in the KGaO$_2$ structure type and CsTaN$_2$ $Fd\bar{3}m$ (no 227) in the filled β-cristobalite type.[9] Lattice parameters, atomic coordinates and displacement parameters were refined by Rietveld methods (see supporting information, crystallographic information). The small peak widths in Rietveld refinements indicate highly crystalline product formation as evidenced by SEM analysis free from additional side phases as almost no remarkable amorphous background was present. The small increase in the background of CsTaN$_2$ is due to absorption. The powder X-ray diffraction patterns are shown in Figure 3, crystallographic data are summarized in Table 1. Lattice parameters are in good agreement with the values reported in literature.[9, 27]

Table 1. Crystallographic data of ATaN$_2$ with A = Na, K, Ta, Cs obtained by Rietveld refinement.

	NaTaN$_2$	**KTaN$_2$**	**RbTaN$_2$**	**CsTaN$_2$**
Crystal system	trigonal	orthorhombic		cubic
Space group (no.)	$R\bar{3}m$ (166)	*Pbca* (61)		$Fd\bar{3}m$ (227)
***a, b, c* /Å**	a = 3.1300(3)	a = 5.8884(1)	a = 6.0632(4)	a = 8.7790(3)
	c = 17.013(5)	b = 11.866(3)	b = 12.006(7)	
		c = 16.592(3)	c = 17.020(1)	
Cell volume /Å^3	144.34 (5)	1159.27(5)	1238.90(13)	676.61(8)
Formula units per cell	3	16	16	24
Density /g·cm^{-3}	8.005(3)	5.685(2)	6.314(7)	6.712 (7)
Diffractometer	STOE STADI P			
T /K	293(2)			
Radiation	Mo-Kα_1 (λ = 0.70930 Å)			
2θ range /°	2.0 ≤ 2θ ≤ 60.2			
Data points	3886			
Total number of reflections	79	1766	1886	69
Refined parameters	53	44	37	23
Background function	Shifted Chebyshev			
***R* values**	R_P = 0.0632	R_P = 0.0604	R_P = 0.0523	R_P = 0.0717
	R_{wp} = 0.0801	R_{wp} = 0.0764	R_{wp} = 0.0683	R_{wp} = 0.09
Goodness of fit	0.894	0.838	0.930	0.96

5.3.3 UV/Vis measurements with Tauc plots

Diffuse reflectance spectra of the thoroughly powderized samples were measured to investigate the optical properties of the materials. Pseudo-absorption spectra were calculated employing the Kubelka-Munk function.[45] The optical band gaps were determined using the Tauc method.[46] All compounds absorb in the visible spectral range (see Figure 4). These are the first band gap investigations of the ternary alkali metal nitridotantalates and therefore no comparable values or calculations are known

yet. The optical band gaps obtained from diffuse reflectance of the compounds are ≈ 1.5 eV for NaTaN$_2$, ≈ 2.5 eV for KTaN$_2$, ≈ 2.5 eV for RbTaN$_2$ and ≈ 2.2 eV for CsTaN$_2$. The body colors of the compounds are in good agreement with the experimental UV-Vis measurements. NaTaN$_2$ crystals show a morphology of inferior quality compared to the those of the other ternary nitrides. This could possibly lead to defects (see Figure 2) and contribute to a narrowing of the band gap. We assume the first step in the UV-Vis measurement of CsTaN$_2$ stems from possible defects due to discontinuous crystal growth (significant differences in growth rates; see inhomogeneous crystal size fractions in Figures 1 and 2.).

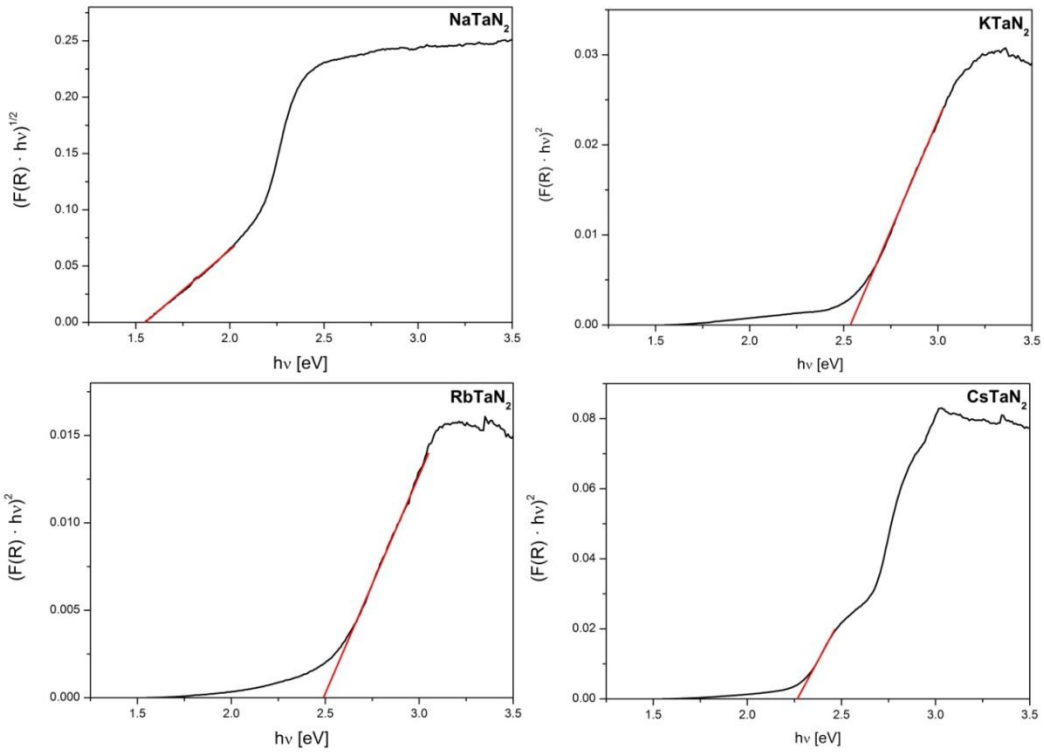

Figure 4. Tauc plots with estimation of indirect (NaTaN$_2$) and direct band gaps (K-, Rb-, CsTaN$_2$) for crystalline alkali tantalum nitrides.

5.3.4 Electronic Structure

In order to validate the experimentally determined band gaps of the compounds ATaN$_2$ (A = Na, K, Rb, Cs) we performed subsidiary DFT calculations. The resulting band structures are depicted in Figure 5.

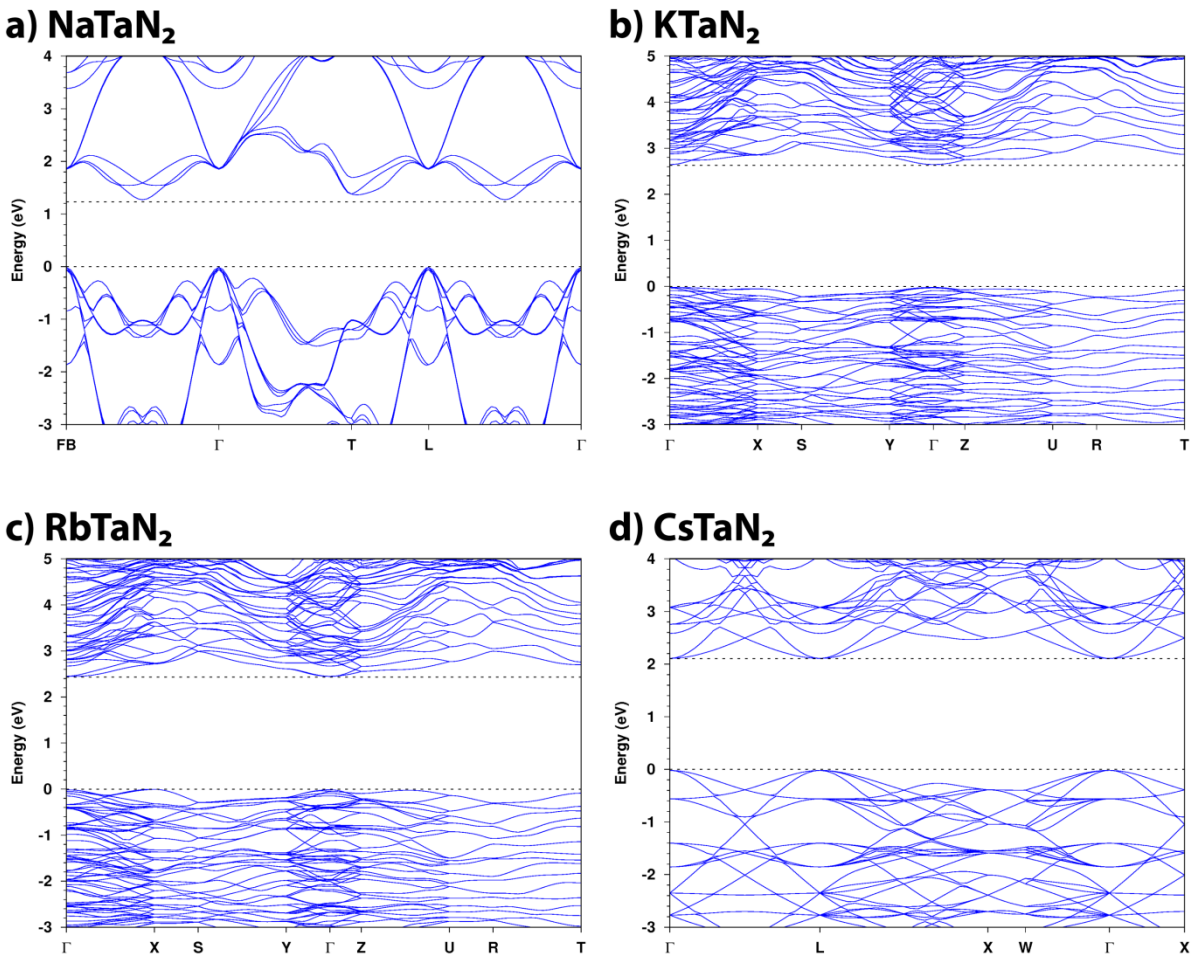

Figure 5: Band structures for a) NaTaN$_2$ (*R*$\bar{3}$*m*, no. 166), b) KTaN$_2$ (*Pbca*, no. 61) c) RbTaN$_2$ (*Pbca*, no. 61) d) CsTaN2 (*Fd*$\bar{3}$*m*, no. 227) along high symmetry directions in the first Brillouin zone.

DFT reveals an indirect electronic band gap ($(F(R)\cdot hv)^{1/2}$) for NaTaN$_2$ (1.2 eV) and direct band gaps ($(F(R)\cdot hv)^2$) in reasonable agreement, to the experimentally deduced band gaps by the chosen Kubelka Munk formalism[45, 46], with KTaN$_2$ (2.6 eV), RbTaN$_2$ (2.6 eV) and CsTaN$_2$ (2.1 eV). Apart from the slight underestimation observed for NaTaN$_2$ as often seen from standard DFT calculations, the chosen GGA-PBE functional appears sufficient for these types of small band gap semiconductors. It appears likely that, judging from the observed reddish color of the NaTaN$_2$ crystallites, in comparison to DFT calculations, the optical transitions observed from experimental reflectance spectra show only direct electronic transitions at Γ equating to 1.8 eV.

5.4 Conclusion

The alkali metal amides and azides were used in custom-built autoclaves in order to prepare ternary alkali metal nitridotantalates. The formed intermediates decompose at elevated temperatures resulting in the targeted alkali nitridotantalates ATaN$_2$ (A = Na, K, Rb, Cs). The obtained crystals of several tens of micrometers were examined by PXRD, SEM, UV-Vis and DFT calculations in order to determine their optical and electronic properties. Thus, the presented study demonstrates that the ammonothermal approach is suitable for crystal growth of ternary nitrides, which were hitherto only available as powders. The crystal size of up to 200 µm is to our knowledge one of the largest sizes observed for ternary nitrides in ammonothermal synthesis so far.

Although, research on nitrides has made a steady progress regarding structure property relationships in recent years, the synthesis of nitrides remains challenging.[7] Many precursors and products are usually unstable against air and moisture. Moreover, the synthesis of nitrides is experimentally complicated and often requires laborious explorative synthesis techniques.[6, 16] The ammonothermal approach provides an explorative way to synthesize nitridotantalates, metastable against decomposition into the binary nitrides and elements.[3, 5, 31] Therefore, only a few of these compounds obtained by the ammonothermal approach have been synthesized so far.[1, 22, 23, 47, 48] The presented results emphasize that many nitrides, which are already accessible by gas flow ammonolysis, can be synthesized as crystals with the ammonothermal method as a solution based method. One problem of this particular synthesis in a supercritical medium is the uncontrolled oversaturation of the solution during cooling which leads to the preferred formation of seeds and as a result mostly twinned crystals have been obtained. By *in situ* investigations, the dissolution temperature could be determined and optimized.[49] This will allow the determination of the optimum growing temperature to synthesize larger single crystals.[22]

Besides the synthetic challenge, ternary nitrides are an exciting field of materials, which is relatively unexplored compared to binary nitrides. They are promising candidates for thin film photovoltaics because of their interesting optical properties.[31] CuTaN$_2$ for example crystallizes in layered delafossite structure and has a strong absorption onset. Calculations indicate that the absorption coefficient is very large, what makes it suitable for solar energy conversion applications.[3] Our latest outcome should therefore

consequently be transferred to other ternary and multinary nitrides which are fundamental semiconductors, but could not previously be synthesized as crystals but only as microcrystalline powders. Furthermore, a number of ternary and multinary nitrides with promising properties are predicted by theoretical calculations.[5] The ammonothermal approach offers a sophisticated method that could expand the compositional space of nitride semiconductors in the future.

5.5 Acknowledgements

We would like to thank Christian Minke for SEM measurements and the Deutsche Forschungsgemeinschaft DFG for financial support within the research group “FOR 1600: Chemie und Technologie der Ammonothermal-Synthese von Nitriden” (SCHN 377/16).

5.6 References

[1] J. Häusler, W. Schnick, *Chem. Eur. J.* **2018**, *24*, 11864-11879.

[2] W. Schnick, *Angew. Chem. Int. Ed. Engl.* **1993**, *32*, 806-818; *Angew. Chem.* **1993**, *105*, 846-858.

[3] A. Zakutayev, *J. Mater. Chem.* **2016**, *4*, 6742-6754.

[4] M. Higashi, K. Domen, R. Abe, *J. Am. Chem. Soc.* **2012**, *134*, 6968-6971.

[5] N. J. Szymanski, L. N. Walters, O. Hellman, D. Gall, S. V. Khare, *J. Mater. Chem.* **2018**, *6*, 20852-20860.

[6] H. Yamane, F. J. DiSalvo, *Prog. Solid State Chem.* **2018**, *51*, 27-40.

[7] M. Zeuner, S. Pagano, W. Schnick, *Angew. Chem. Int. Ed.* **2011**, *50*, 7754-7775; *Angew. Chem*. **2011**, *123*, 7898-7920.

[8] U. Zachwieja, H. Jacobs, *Eur. J. Solid State Inorg. Chem.* **1991**, *28*, 1055-1062.

[9] H. Jacobs, E. von Pinkowski, *J. Less-Common Met.* **1989**, *146*, 147-160.

[10] A. Miura, M. Wessel, R. Dronskowski, *J. Ceram. Soc. Jpn.* **2011**, *119*, 663-666.

[11] A. Miura, M. Lowe, B. M. Leonard, C. V. Subban, Y. Masubuchi, S. Kikkawa, R. Dronskowski, R. G. Hennig, H. D. Abruña, F. J. DiSalvo, *J. Solid State Chem.* **2011**, *184*, 7-11.

[12] A. Zakutayev, A. J. Allen, X. Zhang, J. Vidal, Z. Cui, S. Lany, M. Yang, F. J. DiSalvo, D. S. Ginley, *Chem. Mater.* **2014**, *26*, 4970-4977.

[13] R. Dronskowski, S. Kikkawa, A. Stein, *Handbook of Solid State Chemistry*, Wiley-VCH, Weinheim, **2017**.

[14] P. W. Schenk, *Handbook of Preparative Inorganic Chemistry (Second Edition)*, Academic Press, New York, **1963**.

[15] H. Cui, G. Zhu, X. Liu, F. Liu, Y. Xie, C. Yang, T. Lin, H. Gu, F. Huang, *Adv. Sci. (Weinheim, Ger.)* **2015**, *2*, 1500126.

[16] P. E. Rauch, F. J. DiSalvo, *J. Solid State Chem.* **1992**, *100*, 160-165.

[17] A. Rabenau, *Angew. Chem.* **1985**, *97*, 1017-1032; *Angew. Chem. Int. Ed. Engl.*, **1985**, *24*, 1026-1040.

[18] D. R. Modeshia, R. I. Walton, *Chem. Soc. Rev.* **2010**, *39*, 4303-25.

[19] T. Richter, R. Niewa, *Inorganics* **2014**, *2*, 29-78.

[20] B. Wang, M. J. Callahan, *Cryst. Growth Des.* **2006**, *6*, 1227-1246.

[21] J. Hertrampf, P. Becker, M. Widenmeyer, A. Weidenkaff, E. Schluecker, R. Niewa, *Cryst. Growth Des.* **2018**, *18*, 2365-2369.

[22] J. Häusler, S. Schimmel, P. Wellmann, W. Schnick, *Chem. Eur. J.* **2017**, *23*, 12275-12282.

[23] M. Mallmann, C. Maak, R. Niklaus, W. Schnick, *Chem. Eur. J.* **2018**, *24*, 13963-13970.

[24] D. Ehrentraut, E. Meissner, M. Bockowski, *Technology of Gallium Nitride Crystal Growth*, Springer-Verlag GmbH Heidelberg, **2010**.

[25] N. Cordes, W. Schnick, *Chem. Eur. J.* **2017**, *23*, 11410-11415.

[26] N. Cordes, T. Bräuniger, W. Schnick, *Eur. J. Inorg. Chem.* **2018**, *2018*, 5019-5026.

[27] E. v. Pinkowski, *Doctoral Thesis* **1988**.

[28] H. Jacobs, B. Hellmann, *J. Alloys Compd.* **1993**, *191*, 277-278.

[29] H. Jacobs, B. Hellmann, *J. Alloys Compd.* **1993**, *191*, 51-52.

[30] L. Wang, Y. Zhu, L. Shi, L. Si, Q. Li, Y. Qian, *NbN and $NaNbN_2$ Particles: Selective Solid State Synthesis and Conduction Performance, Vol. 12*, **2012**.

[31] M. Yang, A. Zakutayev, J. Vidal, X. Zhang, D. S. Ginley, F. J. DiSalvo, *Energy Environ. Sci.* **2013**, *6*, 2994-2999.

[32] G. Kresse, J. Hafner, *Phys. Rev. B* **1993**, *47*, 558-561.

[33] G. Kresse, J. Hafner, *Phys. Rev. B* **1994**, *49*, 14251-14269.

[34] G. Kresse, J. Furthmüller, *Comput. Mater. Sci.* **1996**, *6*, 15-50.

[35] G. Kresse, J. Furthmüller, *Phys. Rev. B* **1996**, *54*, 11169-11186.

[36] J. P. Perdew, K. Burke, M. Ernzerhof, *Phys. Rev. Lett.* **1996**, *77*, 3865-3868.

[37] J. P. Perdew, K. Burke, M. Ernzerhof, *Phys. Rev. Lett.* **1997**, *78*, 1396-1396.

[38] P. E. Blöchl, *Phys. Rev. B* **1994**, *50*, 17953-17979.

[39] G. Kresse, D. Joubert, *Phys. Rev. B* **1999**, *59*, 1758-1775.

[40] H. J. Monkhorst, J. D. Pack, *Phys. Rev. B* **1976**, *13*, 5188-5192.

[41] S. Pimputkar, S. Nakamura, *J. Supercrit. Fluids* **2016**, *107*, 17-30.

[42] H. Baser, W. Schwieger, D. Freitag, T. G. Steigerwald, E. Schluecker, *Chem. Eng. Technol.* **2017**, *40*, 1101-1106.

[43] R. Juza, *Angew. Chem. Int. Ed. Engl.* **1964**, *3*, 471-481.

[44] S. Pimputkar, T. F. Malkowski, S. Griffiths, A. Espenlaub, S. Suihkonen, J. S. Speck, S. Nakamura, *J. Supercrit. Fluids* **2016**, *110*, 193-229.

[45] R. López, R. Gómez, *J. Sol-Gel Sci. Technol.* **2012**, *61*, 1-7.

[46] J. Tauc, R. Grigorovici, A. Vancu, *Phys. Status Solidi B* **1966**, *15*, 627-637.

[47] J. Häusler, L. Neudert, M. Mallmann, R. Niklaus, A.-C. L. Kimmel, N. S. A. Alt, E. Schlücker, O. Oeckler, W. Schnick, *Chem. Eur. J.* **2017**, *23*, 2583-2590.

[48] J. Häusler, R. Niklaus, J. Minár, W. Schnick, *Chem. Eur. J.* **2018**, *24*, 1686-1693.

[49] T. G. Steigerwald, J. Balouschek, B. Hertweck, A.-C. L. Kimmel, N. S. A. Alt, E. Schluecker, *J. Supercrit. Fluids* **2018**, *134*, 96-105.

6 Ammonothermal Synthesis of $PrNbN_2O$ and Evaluation of the Mineralizer Conditions for $PrTaN_2O$

Nitride oxide perovskites are accessible by many different synthetic approaches.[1, 2] Besides, typical solid-state reactions like ammonolysis, the ammonothermal approach offers a solution-based method for crystals of nitride oxide perovskites and other related compounds.[3-5]

6.1 Ammonothermal Synthesis of $PrNbN_2O$

6.1.1 Experimental

Powdery metals Pr (Sigma-Aldrich, 99.9%, 1 mmol,) Nb (Sigma-Aldrich, 99.9%, 0.8 mmol, -325 mesh) and NaN_3 (Sigma-Aldrich, 99.99%, 7 mmol) NaOH (Grüssing, 99%, 0.8 mmol,) used as mineralizer, were placed in a custom build Nb-liner (WHS Sondermetalle) inside the glove box. The liner was put inside the reaction chamber of a high-temperature autoclave. The autoclave was shut outside the glove box with the required torque, evacuated, cool and filled with 4 ml ammonia (Air Liquide, 5.0). The autoclave was heated up to room temperature with a conventional hair dryer and transferred vertically in a custom-build three zone furnace. The autoclave was heated up to 800°C in 6h. The internal maximum pressure was 1700 bar. After cooling down, the remained pressure was drained through an oil bubbler. The autoclave was opened and the product was collected. The product was washed with aqua regia and dried at 60°C. A yellow / grey powder was obtained.

6.1.2 Results and Discussion

Powder X-ray diffraction indicates the presents of $PrNb(N,O)_3$ besides Pr_2O_3. The Rietfeld refinement shows that 85.6% of the product contains $PrNb(N,O)_3$ and 14.4% of Pr_2O_3 (Figure 1). $PrNb(N,O)_3$ crystallizes in the orthorhombic space group *Pnma* (no. 62). The lattice parameters a = 5.7067(8), b = 8.0358(9) and c = 5.6884(7) are in good agreement with the literature.[6] The gas flow ammonolysis reaction of $PrNbO_4$, originating from Pr_6O_{11} and Nb_2O_5, was performed for 16h at 950°C. Since crystals are

rarely observed in ammonolysis reaction, it could be assumed that in this particular reaction no µm-range crystals could be observed. However, the ammonothermal approach is known, as a solution-based reaction, to synthesize crystals of up to 50µm sized crystals.[5]

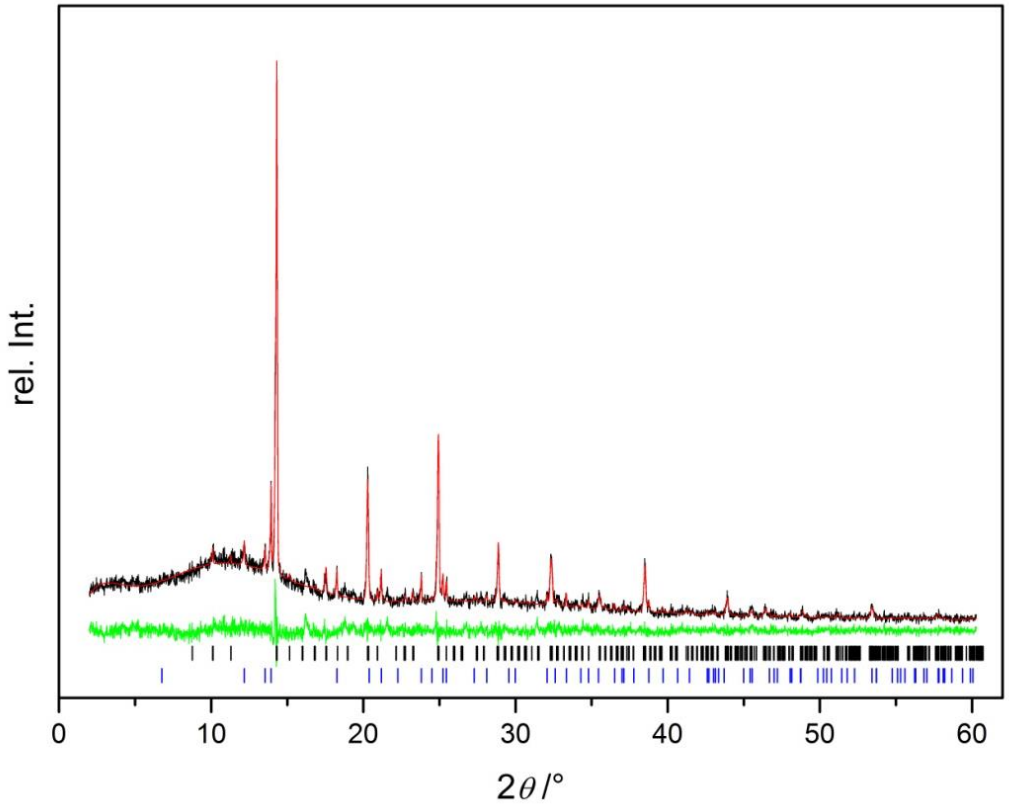

Figure 1: Powder x-ray diffraction with Rietfeld refinement of NC-A-140. Measure diffraction pattern (black) with Mo $k_{\alpha 1}$ (λ =) and difference line (green). Positions of Bragg reflections are depicted in black for $PrNb(N,O)_3$ and in blue for Pr_2O_3.

Cube-like crystals were observed in SEM measurements (Figure 2). The twinned and fused crystals have edge lengths of up to 10 µm. SEM with EDX measurements indicate a Pr : Nb distribution of 1 : 1 (see Table 1). The oxygen value is slightly increased due Pr_2O_3 and NaOH residual phases and the handling in the air. Furthermore, nitrogen and oxygen amounts are often deficient in these nitride oxide perovskites.[6]

Table 1: EDX measurements of $PrNb(N,O)_3$.

Pr	Nb	N	O
18.8	15.8	27.5	37.8
24.3	20.6	35.1	20.0
21.5	19.1	32.3	27.2
14.4	13.4	30.6	40.4
14.6	13.5	30.9	41.0
13.5	11.5	27.9	47.1
19.7	18.2	35.6	26.2
13.6	13.4	39.4	33.5
18.7	17.1	34.4	29.8
15.4	14.5	33.6	36.5
18.0	17.1	37.7	27.1
19.1	16.3	38.4	26.2
19.3	17.2	38.4	24.8
17,8	**16**	**34**	**32.1 Ø**

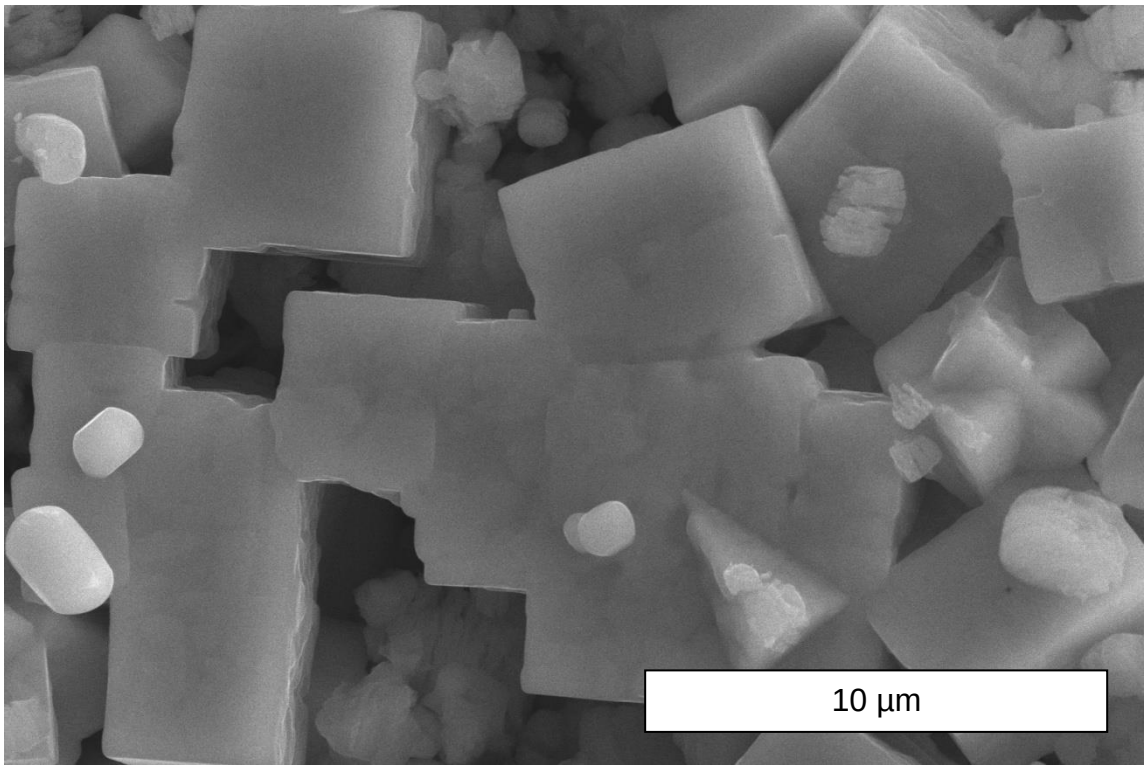

Figure 2: SEM picture of $PrNb(N,O)_3$.

6.2 Evaluation of the mineralizer conditions for $PrTaN_2O$

6.2.1 Experimental Part

In order to evaluate the crystal growth conditions of nitride oxide perovskites via the ammonothermal approach, different alkali mineralizer have been employed for the synthesis of $PrTaN_2O$. Powdery metals of Ta (0.8 mmol) and Pr (1 mmol) with NaOH (0.8 mmol) and ANH_2[7] (7 mmol) with *A* = Li, Na, K, Rb and Cs were used. The respective amides were synthesized in liquid ammonia.[7] The starting materials were handled under argon in a glove box and transferred with a Ta-liner in an autoclave. The autoclave was shut, cooled and filled with ammonia (7 mL). Afterwards the autoclave was heated to 625°C within 3 h and this temperature was hold for 80 h. After cooling down, the product was collected and washed with aqua regia, water and ethanol. Finally, the obtained product was dried at air.

6.2.2 Results and Discussion

The alkaline mineralizers ANH_2 with *A* = K, Na and Rb are suitable for the synthesis of $PrTaN_2O$ (Figure 2, 3 and 4) whereas Li- and $CsNH_2$ did not lead to the desired nitride oxide perovskite. The ammonothermal synthesis with Li- and $CsNH_2$ as mineralizers enabled to produce Pr_2O_3. It is possible, that the solubility of $LiNH_2$ is too low compared to the other alkaline mineralizers.[8]

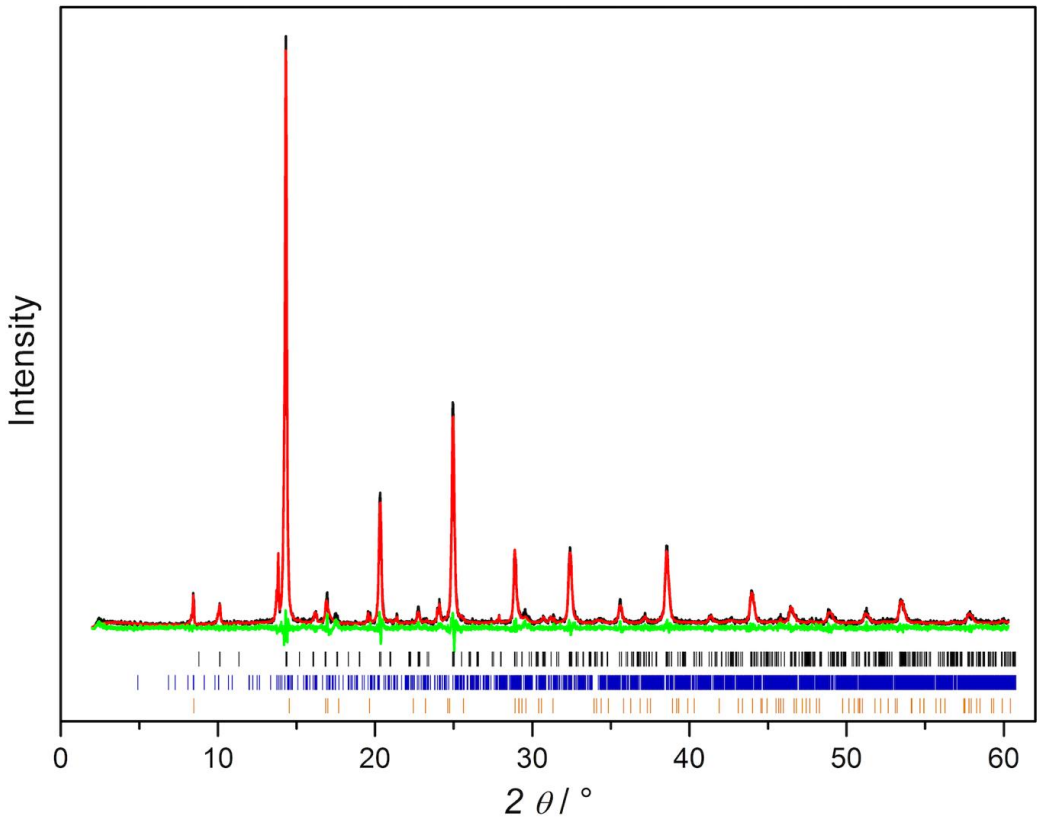

Figure 3. Powder diffractogram (Mo-$K_{\alpha 1}$, λ = 0.71073 Å) with Rietveld refinement of NC-A-110. Simulated powder diffractogram (red) compared to the measured (black) generate the difference plot (green) with marked reflections positions of 85.79 % $PrTaON_2$ (black), 9.44 % $KTaN_2$ (blue) and 4.77 % $Ta_{0.93}H$ (brown).

Though, only $NaNH_2$ lead to the crystal growth of $PrTaN_2O$. It seems, that only sodium azide respective amide used as mineralizer produces highly crystalline cube-like crystals of $PrTaN_2O$ (Figure 3 and 4). $NaNH_2$ provides an essential mineralizer for the synthesis of nitride oxide perovskites crystals.[3, 4, 9-12] It is still unclear if a melt at the bottom of the liner provides a necessary medium for the crystal growth or if the reaction is solution-based and reactive intermediates decompose to the desired product.

It is appropriate to repeat the described reactions with $NaNH_2$ in combination with *in-situ* measurements in order to adjust the perfect growth parameters like temperature and pressure.

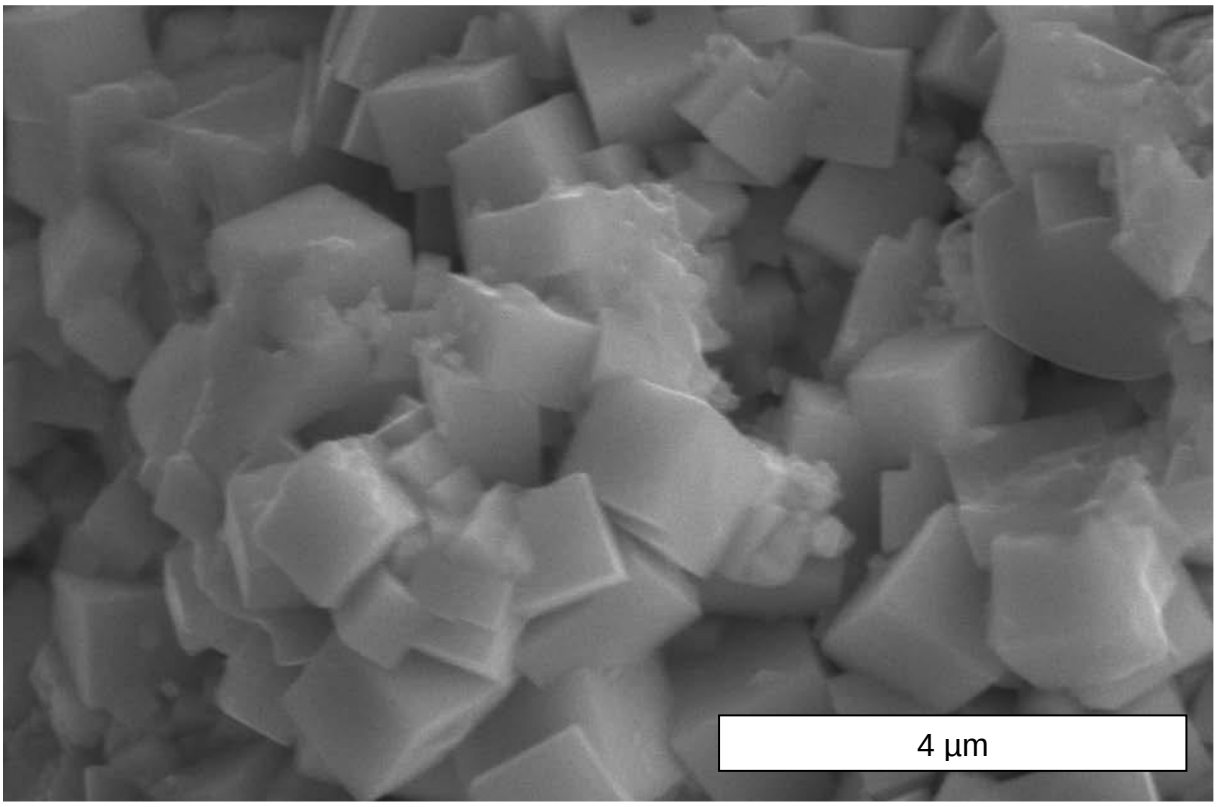

Figure 4: Scanning electron microscope recording of $PrTaN_2O$ cube-like crystals.

6.3 References

[1] A. Fuertes, *J. Mater. Chem.* **2012**, *22*, 3293-3299.

[2] A. Fuertes, *Prog. Solid State Chem.* **2018**, *51*, 63-70.

[3] N. Cordes, W. Schnick, *Chem. Eur. J.* **2017**, *23*, 11410-11415.

[4] N. Cordes, T. Bräuniger, W. Schnick, *Eur. J. Inorg. Chem.* **2018**, *2018*, 5019-5026.

[5] N. Cordes, M. Nentwig, L. Eisenburger, O. Oeckler, W. Schnick, *Eur. J. Inorg. Chem.* **2019**, *2019*, 2304-2311.

[6] N. Kumar, A. Sundaresan, C. N. R. Rao, *Mater. Res. Bull.* **2011**, *46*, 2021-2024.

[7] P. W. Schenk, *Handbook of Preparative Inorganic Chemistry (Second Edition)*, Academic Press, New York, **1963**.

[8] J. Jander, H. Spandau, C. C. Addison, *Anorganische und allgemeine Chemie in flüssigem Ammoniak, Vol. 1*, F. Vieweg, **1966**.

[9] T. Watanabe, K. Tajima, J. Li, N. Matsushita, M. Yoshimura, *Chem. Lett.* **2011**, *40*, 1101-1102.

[10] C. Izawa, T. Kobayashi, K. Kishida, T. Watanabe, *Adv. Mater. Sci. Eng.* **2014**, *2014*, 1-5.

[11] T. Toshima, K. Kishida, Y. Maruyama, T. Watanabe, *J. Ceram. Soc. Jpn.* **2017**, *125*, 643-647.

[12] Y. Setsuda, Y. Maruyama, C. Izawa, T. Watanabe, *Chem. Lett.* **2017**, *46*, 987-989.

7 Conclusion and Outlook

Conventional solid-state reactions containing oxygen and nitrogen as anions are often performed under high temperature and pressure.[1] In these reactions ammonia gas or mixtures of N_2/H_2 are typically used as nitriding agents. The obtained products are microcrystalline powders rather than crystals in the micrometer range because of the poor diffusion of starting materials in the reaction medium. The question raises how to overcome these synthetic challenges. That is why the development of new synthesis routes is a crucial step to achieve a synthetic breakthrough to obtain new compounds or crystals of known materials. In contrast to this, the solution-based ammonothermal synthesis provides a method at rather moderate temperatures and pressures.[2]

Starting materials are dissolved in supercritical ammonia in order to enhance solubility of reactive intermediates and diffusion to synthesize crystals and novel inorganic substances. Hydrothermal synthesis has already demonstrated great potential of solution-based reactions in terms of crystal growth of e.g. oxides[3] and scalability in industrial level. Whereas, the ammonothermal synthesis is at its early stage in relation to the industrial hydrothermal synthesis of for example quartz.[4-6] The hydrothermal approach provides an elemental understanding of solvothermal methods, yet these findings cannot be equally transferred to the ammonothermal approach. The ammonothermal synthesis is largely used to synthesize GaN and several amide, imides and ammoniates. The explorative potential of the ammonothermal synthesis for multinary nitrides and nitride oxides is still relatively unexplored.[7]

Comparing hydrothermal and ammonothermal synthesis, both approaches have their distinguished differences. One particular challenge of this thesis was the concurrent introduction of oxygen and nitrogen into inorganic compounds in supercritical ammonia. Nitrogen and oxygen have similarities in chemical behavior, but most elements have a larger affinity for oxygen because of their higher bond energy. That is why the formation of oxygen compounds under supercritical ammonia is an important side reaction.[8-10] This requires a strict control of the oxygen amount inside the autoclave to avoid the formation of oxides. Because of the moderate temperature during the synthesis the diffusion is only ensured by a solution based system. Based on the enormous variation possibilities concerning the starting materials, as well as the thermal treatment of the samples in supercritical ammonia in combination with the

inside pressure, the development of this approach might also enable the synthesis of further new nitride oxides.

Prior to this thesis, a lot of nitride oxides were synthesized with many different solid-state techniques, like the high-pressure multi anvil technique,[8] ammonolysis,[9, 10] explosive reaction[11] and MOCVD film techniques,[12-15] but only a few resulted in µm-range crystals.[16, 17] This presented work aimed to synthesize crystals of several nitride oxide perovskites, related structures and nitrides. Moreover, the synthesis of a new compound related to the perovskite structure has been explored. Therefore the ammonothermal approach provides a powerful and sophisticated explorative synthetic tool for the synthesis of crystals and new compounds of nitride oxides. The mentioned materials possess band gaps of suitable size and location. They have promising optical properties for solar energy conversion like photocatalytic watersplitting and photovoltaics.[18-20] The challenge though is that most of these materials are at the infancy of their optical investigations and detailed experimental and theoretical information of crystals are still to be unexplored.[21] Based on the presented results in this thesis, further investigations of the obtained semiconductor crystals could be performed in order to examine defect concentrations and impurities as well as charge carrier mobilities, electron and hole lifetimes. Furthermore, solid solutions of alkaline earth and lanthanide transition metal nitride oxide perovskites will be of great interest as harmless pigments and the photocatalytic properties can be controlled by substitution[22] Some solid solutions are already examined but no bulk crystals could be obtained.[23, 24] In this regard, the perovskite structure provides a very versatile modular set and numerous opportunities to implement dopants in solid solutions illustrated by the general formula $A_{1-x}B_xCO_{2-x}N_x$ with e.g. *A* and *B* = *EA*, *Ln* and *C* = *TM*.

The ammonothermal synthesis of $EAMO_2N$ with *EA* = Sr, Ba and *M* = Nb and Ta was performed under supercritical ammonia employing *EA* and *M* metals, using NaN_3 and NaOH as mineralizers. Commonly, the synthesis of alkaline earth nitride oxide perovskites requires flowing ammonia and several regrinding steps.[25] Unfortunately, the obtained products rarely contain µm-range crystals. Using the ammonothermal approach as a solution-based reaction method the obtained crystals were up to 10 µm. Therefore, conventional gas flow high-temperature ammonolysis is not applicable to obtain crystals. Apart from the synthetic challenge, $EAMO_2N$ compounds possess distinctive color features and could be used as inorganic harmless pigments.[26] Above

that, they have interesting band gap values for solar water splitting applications examined by UV/VIS measurements and subsequent employment of the Tauc method.[9, 27]

Ln$TaON_2$ with *Ln* = La, Ce, Pr, Nd, Sm, Eu, Gd[28] was successfully obtained by the ammonothermal approach in order to employ powdery metals and above mentioned mineralizers. Some of the nitride oxide perovskites e.g. *Ln*$TaON_2$ with *Ln* = Nd, Sm, Eu, Gd are according to the Goldschmidt tolerance factor predicted to be unstable. The Goldschmidt tolerance factor and octahedral factors give a rough but reasonable estimation of the formability on the basis of radii.[29] But nitride oxide perovskites are do not have a complete ionic structure and consist covalent content.[30] The synthetic formability by means of the sophisticated ammonothermal approach impressively demostrates the limitations of this predictive model. Therefore, new compounds and solid solutions of nitride oxide perovskites could be forecasted. The investigated band gaps of the perovskite compounds are suitable for water splitting[31, 32] and have values between 1.9 – 2.1 eV. Above that, f-f transition of lanthanide perovskites were observed with UV/VIS measurements for the first time. These two publications clearly show the feasibility of nitride oxide perovskite crystals using the ammonothermal approach. Nevertheless, the size of the crystals could be improved by determination of optimized crystallization parameters like temperature, pressure and mineralizer. The obtained products sometimes have residual side phases like TaH because of the tantalum liners employed for the reaction. Because of these ferromagnetic side phases NMR spectroscopy is complicated. Gas flow ammonolysis was used for the products to investigate ^{14}N solid-state NMR spectroscopy. Interestingly, all eight compounds have nearly the same shift of ~270 ppm. Apparently, these compounds have a very rigid network so that the exchange of cations do not influence the NMR shift of various nitride oxide perovskites and this is essentially insusceptible to the ionic radius and oxidation number of the cation. More compounds like *EATM*$(O,N)_3$ with *EA* = Ca and Sr and *TM* = Ti, Mo, W could be examined.

The mineralizer is necessary for different ammonothermal synthesis.[28, 33, 34] Still, the crucial role of the mineralizer is a matter of debate. It is unclear if the growth of crystals takes place in the melt of mineralizer or in the dissolved mineralizer of the solution medium inside the autoclave. First experiments in terms of mineralizers were done. By using suitable mineralizers in combination with reactive precursors like amorphous oxides obtained by the Pechini method, could notably lead to better growth rates and

exploration of new materials. The obtained crystals of nitride oxide perovskites were frequently found at the bottom of the liner in druse-like agglomerations.[28] This melt seems to be essential for the growth of µm-range crystals. First attempts of different mineralizers for the synthesis of $PrTaON_2$ with alkaline azides (Na, K, Rb, Cs) showed that NaN_3 provides the most appropriate mineralizer for crystals growth in form of cube-like crystals for the same reaction conditions concerning temperature and pressure. Other mineralizers did not lead to the desired nitride oxide perovskite neither in form of microcrystalline powder nor in form of crystals. Further attempts in different synthetic conditions (temperature, pressure, heating and cooling rates) should be examined in order to elucidate suitable crystals growth conditions. *In situ* measurements will additionally help to determine the dissolution temperature of the product. One problem is that the obtained crystals of nitrides and nitride oxides are often fused and twinned. Furthermore the employed metal liner provides a surface with many seeds. The final cooling leads to leave the Ostwald-Miers area were a supersaturation of the solution takes places. Thus, a lot of seeds are formed and many small crystals are grown instead of few large ones.[35]

The novel mixed-valence nitrogen-rich Ruddlesden-Popper phase $Eu_3Ta_2N_4O_3$ with n = 2 was discovered using Eu, Ta and ammonobasic mineralizers NaN_3 and NaOH as starting materials. This is the first Ruddlesden-Popper phase employing the ammonothermal approach. Remarkably, $Eu_3Ta_2N_4O_3$ crystallizes in the $SrTb_2FeO_7$ structure type and has two different europium cations. This mixed Eu valence (Eu^{II}/Eu^{III}) is new for this structure type ($SrTb_2Fe_2O_7$). The high oxidation state of Ta^V results in a high nitrogen content. Since the perovskite and related structures are very versatile and many different cations and anions can be substituted it seems likely that it could be possible to synthesize the analogue Nb compound in this system, as Nb and Ta are very similar in the chemical point of view. Additionally, Eu^{II}/Eu^{III} could be substituted by alkaline earth metals and lanthanides because several of them have the same radii and similar chemical behavior.[36] By elimination of residual side phases in the ammonothermal reaction to $Eu_3Ta_2N_4O_3$ the examination of magnetic properties and reasonable Mößbauer spectroscopy could be enabled.

Within this presented sesearch, the synthesis of crystals of $ATaN_2$ with *A* = Na, K, Rb and Cs system was possible. For example $RbTaN_2$ crystals of up to 200 µm were synthesized, which are the largest crystals of ternary nitrides synthesized with the ammonothermal method so far. The synthesis of the corresponding niobium

compounds was obtained by Jacobs and coworkers with sodium and cesium.[37, 38] The $KNbN_2$ compound was only accessible in gas flow ammonolysis.[17] Further experiments in this particular research field seems promising because alkali mineralizers are well soluble in supercritical ammonia.[39]

$NaTaN_2$ crystallizes in the layered delafossite structure. Layered and channelized structures are typically suitable for ion exchange reactions. Ion exchange reactions of $NaTaN_2$ with CuI were performed in flowing ammonia to obtain $CuTaN_2$.[40] Therefore the ammonothermal approach seems appropiate. The synthesis of $CuTaN_2$ crystals with the help of the ammonothermal synthesis could support the examination of electronic properties, yet only powders of $CuTaN_2$ and $CuNbN_2$ could be obtained. The ammonothermal synthesis of ternary nitrides is a promising research field, because these materials have suitable properties for solar energy conversion applications like photovoltaic and photoelectrochemical cells. In addition ternary and multinary nitrides are relatively unexplored. The ammonothermal approach therefore provides a vast opportunity for the discovery of new materials and expands the compositional space of latter. Through targeted synthesis in supercritical ammonia we estimate to obtain these as-yet unreported but thermodynamically stable compounds like ABN_2 (*A* = Cu, Ag, Au; *B* = Ta, Nb, V) in the future.[41, 42] This thesis showcases the synthesis of 14 different nitrides and nitride oxides crystal.[28, 33, 34, 43]

The redevelopment of the ammonothermal method after Jacobs and coworkers requires new autoclave systems providing the necessary synthetic parameters e.g. temperature, pressure and resistivity against corrosive reaction materials. With the help of the *Ammono-FOR* group new holistic autoclave systems were developed. Using high-temperature autoclaves, new compounds were obtained and attainable crystal sizes were extensively increased. Solid-state synthesis with gas flow ammonolysis and other typical solid-state reactions reach their limits and are often laborious and complicated. The decomposition of ammonia to N_2 and H_2 can considerably suppressed by applying the solution-based ammonothermal approach. If limits can be shifted further to higher temperatures and pressures the decomposition can be hampered in order to enhance solubilities by increased permittivity.[44] As a consequence other concepts including internally heated capsule based systems have to be considered because of commercially limited available materials.[7, 45]

The stated results provide a first insight of the ammonothermal synthesis of nitride and nitride oxide crystals including new compounds. Future experiments should lead to a significant extension of compositional space of new compounds with huge potential of the explorative ammonothermal synthesis of novel semiconductors and still has to be exploited. Based on the gained knowledge further investigations like *in situ* Raman and UV/VIS spectroscopy should to be performed.[46, 47] By using *in situ* ultrasonic velocity measurements the concentration can be determined. Therefore, solubility measurements will help to contribute to a holistic picture of the ammonothermal method. This will lead to a better understanding of this method to develop more sophisticated growth techniques for nitride and nitride oxides.

To summarize, this re-established explorative method is still relatively unexplored and the combined results will lead to a better understanding of a holistic picture besides innumerable novel compounds of functional nitride and nitride oxides crystals.

7.1 References

[1] E. Horvath-Bordon, R. Riedel, A. Zerr, P. F. McMillan, G. Auffermann, Y. Prots, W. Bronger, R. Kniep, P. Kroll, *Chem. Soc. Rev.* **2006**, *35*, 987-1014.

[2] T. Richter, R. Niewa, *Inorganics* **2014**, *2*, 29-78.

[3] D. R. Modeshia, R. I. Walton, *Chem. Soc. Rev.* **2010**, *39*, 4303-25.

[4] A. Rabenau, *Angew. Chem.* **1985**, *97*, 1017-1032; *Angew. Chem. Int. Ed. Engl.*, **1985**, *24*, 1026-1040.

[5] K. Byrappa, M. Yoshimura, *Handbook of Hydrothermal Technology*, Elsevier Science, **2012**.

[6] K. Byrappa, M. Yoshimura, *Handbook of Hydrothermal Technology - A Technology for Crystal Growth and Materials Processing*, William Andrew Publishing, Norwich, NY, **2001**.

[7] J. Häusler, W. Schnick, *Chem. Eur. J.* **2018**, *24*, 11864-11879.

[8] W. Schnick, *Angew. Chem. Int. Ed. Engl.* **1993**, *32*, 806-818; *Angew. Chem.* **1993**, *105*, 846-858.

[9] A. Fuertes, *Prog. Solid State Chem.* **2018**, *51*, 63-70.

[10] A. Fuertes, *J. Mater. Chem.* **2012**, *22*, 3293-3299.

[11] J. Odahara, A. Miura, N. C. Rosero-Navarro, K. Tadanaga, *Inorg. Chem.* **2018**, *57*, 24-27.

[12] L. Le Gendre, C. Le Paven-Thivet, J. Pinel, D. Fasquelle, J.-C. Carru, F. Cheviré, F. Tessier, R. Marchand, *Silic. Indus.* **2004**, *69*, 165-171.

[13] C. Le Paven-Thivet, L. Le Gendre, J. Le Castrec, F. Cheviré, F. Tessier, J. Pinel, *Prog. Solid State Chem.* **2007**, *35*, 299-308.

[14] D. Oka, Y. Hirose, H. Kamisaka, T. Fukumura, K. Sasa, S. Ishii, H. Matsuzaki, Y. Sato, Y. Ikuhara, T. Hasegawa, *Sci. Rep.* **2014**, *4*, 4987.

[15] Y. Masubuchi, S. K. Sun, S. Kikkawa, *Dalton Trans.* **2015**, *44*, 10570-10581.

[16] A. Hosono, Y. Masubuchi, T. Endo, S. Kikkawa, *Dalton Trans.* **2017**, *46*, 16837-16844.

[17] H. Yamane, F. J. DiSalvo, *Prog. Solid State Chem.* **2018**, *51*, 27-40.

[18] A. Zakutayev, *J. Mater. Chem.* **2016**, *4*, 6742-6754.

[19] M. Davi, F. Schrader, T. Scholz, Z. Ma, A. Rokicinska, R. Dronskowski, P. Kustrowski, A. Slabon, *ACS Appl. Nano Mater.* **2018**, *1*, 869-876.

[20] Z. Ma, T. Thersleff, A. Görne, N. Cordes, Y. Liu, S. Jakobi, A. Rokicinska, Z. Schichtl, R. H. Coridan, P. Kuśtrowski, W. Schnick, R. Dronskowski, A. Slabon, *ACS Appl. Mater. Interfaces* **2019**, *11*, 19007-19086.

[21] Y. Wu, P. Lazic, G. Hautier, K. Persson, G. Ceder, *Energy Environ. Sci.* **2013**, *6*, 157-168.

[22] R. Aguiar, D. Logvinovich, A. Weidenkaff, A. Rachel, A. Reller, S. G. Ebbinghaus, *Dyes Pigm.* **2008**, *76*, 70-75.

[23] K. Ueda, H. Kato, M. Kobayashi, M. Hara, M. Kakihana, *J. Mater. Chem.* **2013**, *1*, 3667-3674.

[24] J. Jacobs, F. Oehler, J. Schettlock, S. G. Ebbinghaus, *Z. Anorg. Allg. Chem.* **2018**, *644*, 1832-1838.

[25] S. G. Ebbinghaus, H.-P. Abicht, R. Dronskowski, T. Müller, A. Reller, A. Weidenkaff, *Prog. Solid State Chem.* **2009**, *37*, 173-205.

[26] M. Jansen, H. P. Letschert, *Nature* **2000**, *404*, 980-982.

[27] S. Y. Tee, K. Y. Win, W. S. Teo, L. D. Koh, S. Liu, C. P. Teng, M. Y. Han, *Adv. Sci. (Weinheim, Ger.)* **2017**, *4*, 1600337.

[28] N. Cordes, W. Schnick, *Chem. Eur. J.* **2017**, *23*, 11410-11415.

[29] V. M. Goldschmidt, *Naturwissenschaften* **1926**, *14*, 477-485.

[30] R. J. D. Tilley, *Perovskites: Structure–Property Relationships*, Wiley, United Kingdom, **2016**.

[31] N.-Y. Park, Y.-I. Kim, *J. Mater. Sci.* **2012**, *47*, 5333-5340.

[32] M. Ahmed, G. Xinxin, *Inorg. Chem. Front.* **2016**, *3*, 578-590.

[33] N. Cordes, T. Bräuniger, W. Schnick, *Eur. J. Inorg. Chem.* **2018**, *2018*, 5019-5026.

[34] N. Cordes, M. Nentwig, L. Eisenburger, O. Oeckler, W. Schnick, *Eur. J. Inorg. Chem.* **2019**, *2019*, 2304-2311.

[35] D. Ehrentraut, E. Meissner, M. Bockowski, *Technology of Gallium Nitride Crystal Growth*, Springer-Verlag GmbH Heidelberg, **2010**.

[36] R. Shannon, *Acta Crystallogr., Sect. A* **1976**, *32*, 751-767.

[37] H. Jacobs, B. Hellmann, *J. Alloys Compd.* **1993**, *191*, 277-278.

[38] H. Jacobs, B. Hellmann, *J. Alloys Compd.* **1993**, *191*, 51-52.

[39] J. Jander, H. Spandau, C. C. Addison, *Anorganische und allgemeine Chemie in flüssigem Ammoniak, Vol. 1*, F. Vieweg, **1966**.

[40] M. Yang, A. Zakutayev, J. Vidal, X. Zhang, D. S. Ginley, F. J. DiSalvo, *Energy Environ. Sci.* **2013**, *6*, 2994-2999.

[41] N. J. Szymanski, L. N. Walters, O. Hellman, D. Gall, S. V. Khare, *J. Mater. Chem.* **2018**, *6*, 20852-20860.

[42] A. K. Tareen, G. S. Priyanga, S. Behara, T. Thomas, M. Yang, *Prog. Solid State Chem.* **2019**, *53*, 1-26.

[43] N. Cordes, R. Niklaus, W. Schnick, *Cryst. Growth Des.* **2019**, *19*, 3484-3490.

[44] S. Pimputkar, S. Nakamura, *J. Supercrit. Fluids* **2016**, *107*, 17-30.

[45] S. Pimputkar, T. F. Malkowski, S. Griffiths, A. Espenlaub, S. Suihkonen, J. S. Speck, S. Nakamura, *J. Supercrit. Fluids* **2016**, *110*, 193-229.

[46] S. Schimmel, P. Duchstein, T. G. Steigerwald, A. C. L. Kimmel, E. Schlücker, D. Zahn, R. Niewa, P. Wellmann, *J. Cryst. Growth* **2018**, *498*, 214-223.

[47] T. G. Steigerwald, J. Balouschek, B. Hertweck, A.-C. L. Kimmel, N. S. A. Alt, E. Schluecker, *J. Supercrit. Fluids* **2018**, *134*, 96-105.

8 Summary

This chapter provides a short overview of the publications in this thesis and additional details obtained from further experiments of the ammonothermal synthesis of $PrNb(N,O)_3$ and the evaluation of alkali mineralizer system of $PrTaN_2O$ reactions.

The ammonothermal synthesis represents a fundamental approach for the explorative solid-state chemistry providing new sophisticated perspectives for the discovery of novel nitrogen based compounds. The development of new high-temperature autoclaves along with the systematic exploration of different elemental compositions, mineralizers and precursors, besides different synthetic parameters, strongly enlarge the explorative nature of the ammonothermal method. Within this thesis, the ammonothermal method emerged as a powerful tool for the preparation of 17 different compounds of functional ternary and multinary nitride oxides and nitrides. Thus, reveal the great potential of this solution-based crystal growth method in future. The following summaries reveal an overview of the presented work.

Figure 1: .Custom-built autoclave made from Inconel 718 with peripheral equipment.

8.1 Ammonothermal Synthesis of *EAM*O_2N (*EA* = Sr, Ba; M = Nb, Ta) Perovskites and ^{14}N Solid-State NMR Investigations of *AM*(O,N)$_3$ (*A* = Ca, Sr, Ba, La)

N. Cordes, T. Bräuniger, W. Schnick

Eur. J. Inorg. Chem. **2018**, *2018*, 5019–5026

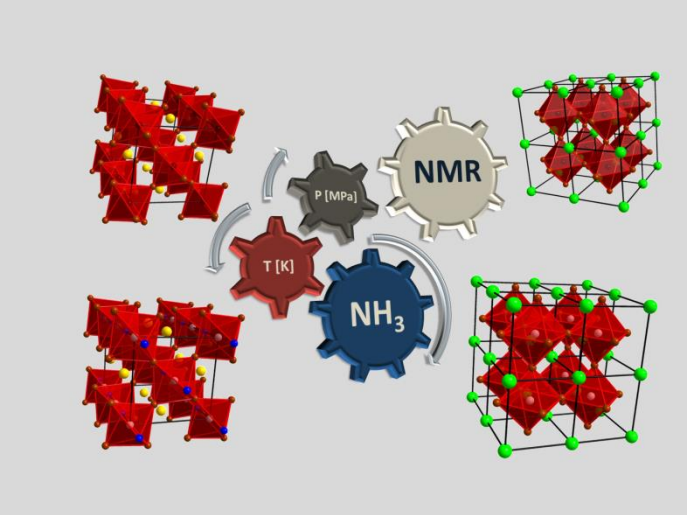

This chapter provides information about the ammonothermal synthesis of *EAM*O_2N with *EA* = Sr, Ba and *M* = Nb, Ta. Employing metals in combination with basic mineralizers (NaN_3, NaOH) in high-pressure autoclaves, phase pure highly crystalline nitride oxide perovskites were synthesized. These compounds are suitable for the investigation of material properties. Band gaps of $SrNbO_2N$ (1.9 eV), $BaNbO_2N$ (2.0 eV), $SrTaO_2N$ (2.1 eV) and $BaTaO_2N$ (2.1 eV) were determined by diffuse reflectance spectroscopy (UV/VIS) using the Kubelka-Munk function and corresponding Tauc plots. SEM pictures reveal cube-like crystals of up to 10 µm edge length. Further ^{14}N solid-state NMR investigations were performed on *AM*(O,N)$_3$ (*A* = Ca, Sr, Ba, La). Remarkably, all eight compounds show a single resonance at about 270 ppm. This is quite impressive because the electron density at the N^{3-} ions seems sufficiently high to mask all external influences. The chemical shift remains unaffected by cation substitution in this rigid structure.

8.2 Ammonothermal Synthesis of Crystalline Oxonitride Perovskites *Ln*$TaON_2$ (*Ln* = La, Ce, Pr, Nd, Sm, Gd)

N. Cordes, W. Schnick

Chem. Eur. J. **2017**, *23*, 11410–11415

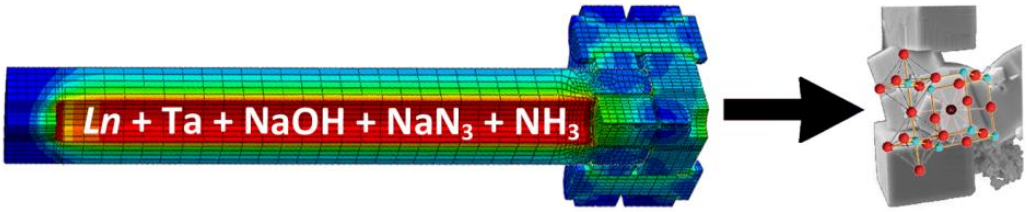

This section of the thesis gives a holistic picture of the accessible lanthanide tantalum based nitride oxide perovskites. These compounds with the composition *Ln*TaN_2O with *Ln* = La, Ce, Pr, Nd, Sm and Gd were synthesized by the ammonothermal method using custom-built autoclaves. Metal powders were reacted with NaOH and NaN_3 as mineralizers under supercritical conditions at 600 – 800°C at a maximum pressure of 3000 bar. Crystal structures, space group and lattice parameters were determined by powder X-ray diffraction and the Rietveld method. Cube-like crystals with up to 15 µm edge length and defined morphology were observed with SEM measurements. Additional EDX measurements were performed in order to investigate the elemental composition. The band gap values of the nitride oxide perovskites of $LaTaON_2$ (1.8 eV), $CeTaON_2$ (1.7 eV), $PrTaON_2$ (1.9 eV), $NdTaON_2$ (2.0 eV), $SmTaON_2$ (2.0 eV), and $GdTaON_2$ (1.8 eV) were estimated by using UV/VIS measurements and the Kubelka–Munk function. Furthermore, f-f transitions of Pr^{3+}, Nd^{3+} and Sm^{3+} were observed for the first time in nitride oxide perovskites in the visible to near-infrared part of the spectra.

8.3 Ammonothermal Synthesis of the Mixed-Valence Nitrogen-Rich Europium Tantalum Ruddlesden-Popper Phase $Eu^{II}Eu^{III}_2Ta_2N_4O_3$

Niklas Cordes, Markus Nentwig, Lucien Eisenburger, Oliver Oeckler, Wolfgang Schnick

Eur. J. Inorg. Chem. **2019**, *2019*, 2304–2311.

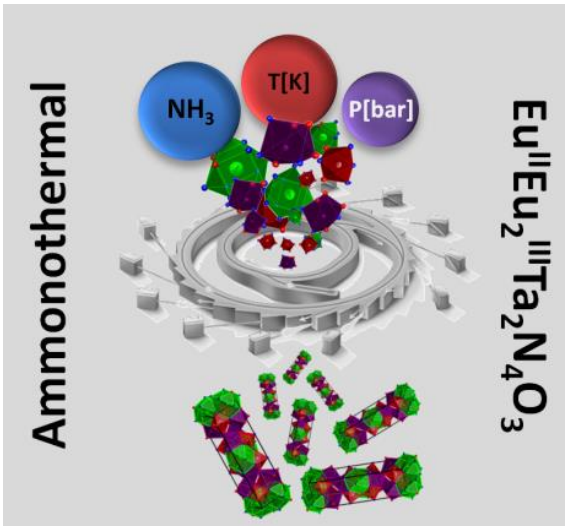

The first nitrogen rich Ruddlesden-Popper phase with mixed valence europium, namely $Eu_3Ta_2N_4O_3$ was synthesized under ammonobasic ammonothermal reaction conditions using custom-built high-temperature autoclaves. New developed high-temperature autoclaves used at a maximum temperature of 800 °C and 1700 bar enable the synthesis of the perovskite structure type related layered structure. TEM measurements reveal first indications of the new compound $Eu_3Ta_2N_4O_3$ crystallizing in a tetragonal cell with a = 5.7278(1), c = 19.8149(5) Å. X-ray diffraction using microfocused synchrotron radiation with subsequent crystal structure determination disclose the space group $P4_2/mnm$ (no. 136) and EDX analyses are consistent with crystal-chemical calculations with respect to $Eu^{II/III}$ and N/O ordering. Anion ordering was confirmed by MAPLE, BVS and CharDi calculations. According to diffuse reflectance spectra, the band gap amounts to 0.6 eV. SEM measurements demonstrate the advantages of the ammonothermal approach as a solution-based synthesis facilitate crystals of up to 50 µm.

8.4 Ammonothermal Crystal Growth of *A*TaN$_2$ with *A* = Na, K, Rb, Cs and their Optical and Electronic Properties

Niklas Cordes, Robin Niklaus, Wolfgang Schnick

Cryst. Growth Des. **2019**, *19*, 3484-3490.

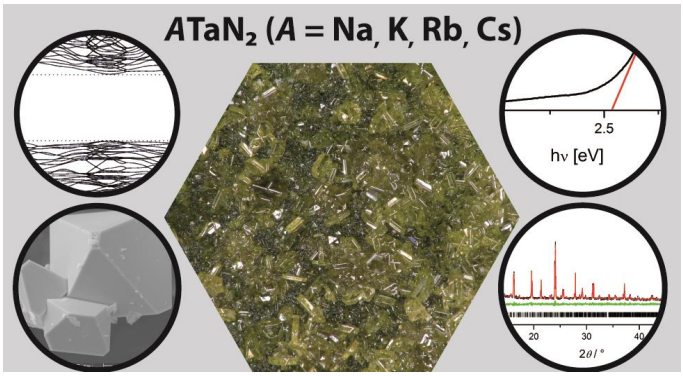

For the synthesis of *A*TaN$_2$ with *A* = Na, K, Rb, Cs, new developed high-temperature autoclaves were used. These autoclaves operate at 800 °C and a maximum pressure of 1700 bar. The ternary nitrides were synthesized from azides and tantalum powder in custom-built tantalum liners. A necessary second temperature step at the decomposition temperature of the respective mineralizer is required for the successful synthesis of crystals, due to formation of intermediates at lower temperatures. The employed liner prevents the autoclave from corrosion and presents a necessary substrate for the crystal growth of the mentioned ternary nitrides. The obtained nitride crystals were examined by powder X-ray diffraction and the Rietveld method. SEM and light microscope pictures were taken, revealing the hitherto largest ternary nitride crystals of up to 200 µm, but the obtained *A*TaN$_2$ crystals vary in size depending on the used alkali metal. The resulting crystals exhibited well developed crystal faces. The optical properties were investigated by UV/VIS measurements. Diffuse reflectance measurements employing the Tauc method revealed the band gaps of *A*TaN$_2$ with A = Na, K, Rb and Cs. Band gap values were supported by DFT-calculations.

8.5 Ammonothermal Synthesis of $PrNbN_2O$ and Evaluation of the Mineralizer Conditions for $PrTaN_2O$

The presented results provide a new important part of the ammonothermal approach of nitride oxide perovskites. The crystal growth of niobium based nitride oxide perovskites is less explored than the tantalum compounds. The ammonothermal synthesis of $PrNb(N,O)_3$ demonstrate a first prove of concept for the lanthanide niobium compounds. The general accessibility was demonstrated by powder X-ray diffraction and SEM measurements.

The examination of the mineralizer system of $PrTaN_2O$ entails the importance of the further investigation of the specific mineralizer conditions of ammonothermal reactions. By using a different mineralizer at the same reaction conditions a specific screening of suitable growth conditions was evaluated. Although $PrTaN_2O$ nitride oxides could be obtained with potassium and sodium azides as mineralizers, only NaN_3 led to the growth of rectangular crystals.

9 Appendix

9.1 Supplementary information for the publication: Ammonothermal Synthesis of Crystalline Oxonitride Perovskites *Ln*$TaON_2$ (*Ln* = La, Ce, Pr, Nd, Sm, Gd)

Published in: *Chem. Eur. J.* **2017**, *23*, 11410–11415.

Authors: Niklas Cordes, Wolfgang Schnick

9.1.1 $LaTaON_2$

9.1.1.1 Rietveld Refinement

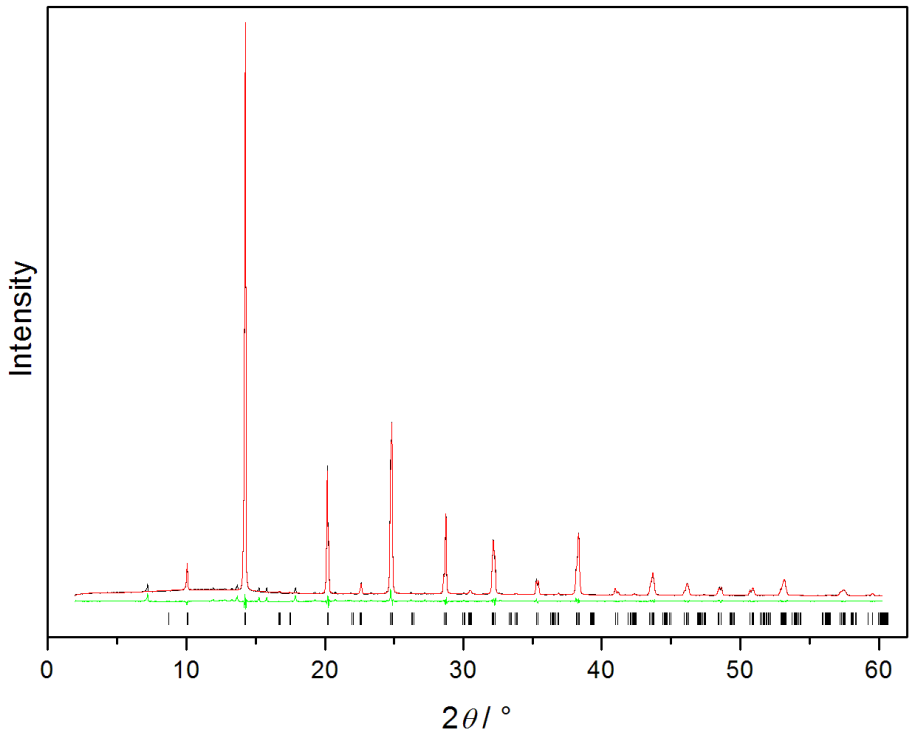

Figure S1. Rietveld refinement of X-ray powder diffraction pattern of $LaTaON_2$ profile with experimental data (black line), calculated pattern (red line), difference (green line), and positions of Bragg reflections (black bars).

9.1.1.2 Electron microscopy analysis

Table S1.

	La	Ta	O	N
	18	17	22	43
	20	20	19	41
	17	18	26	39
	21	19	23	37
Average	19	18.5	22.5	40

SEM measurements in atomic%.

9.1.2 $CeTaON_2$

9.1.2.1 Rietveld Refinement

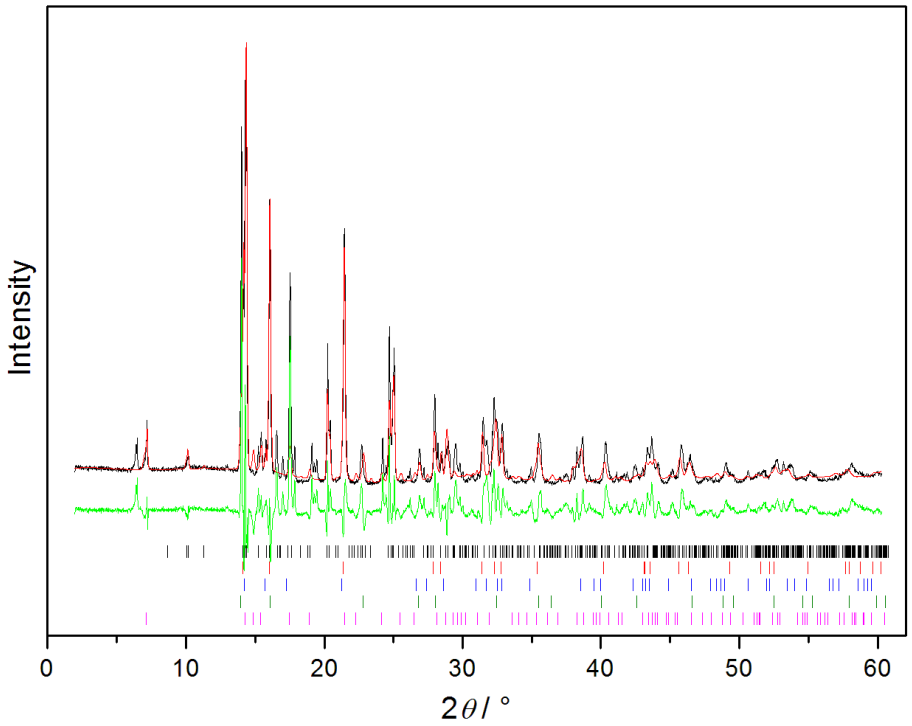

Figure S2. Rietveld refinement of X-ray powder diffraction pattern of $CeTaON_2$ profile with experimental data (black line), calculated pattern (red line), difference (green line), and positions of Bragg reflections (black bars: $CeTaON_2$ (45.8%), red bars: $TaN_{0.83}$ (33.6%), blue bars: Ta_2N (1.7%), olive bars: CeN (9%), pink bars: $NaTaN_2$ (9.9%)).

9.1.2.2 Electron microscopy analysis

Table S2.

	Ce	Ta	O	N
	12	19	17	52
	22	23	17	38
	23	26	16	35
	20	21	12	47
	17	17	13	53
Average	18.8	21.2	15	45

SEM measurements in atomic%.

9.1.3 $PrTaON_2$

9.1.3.1 Rietveld Refinement

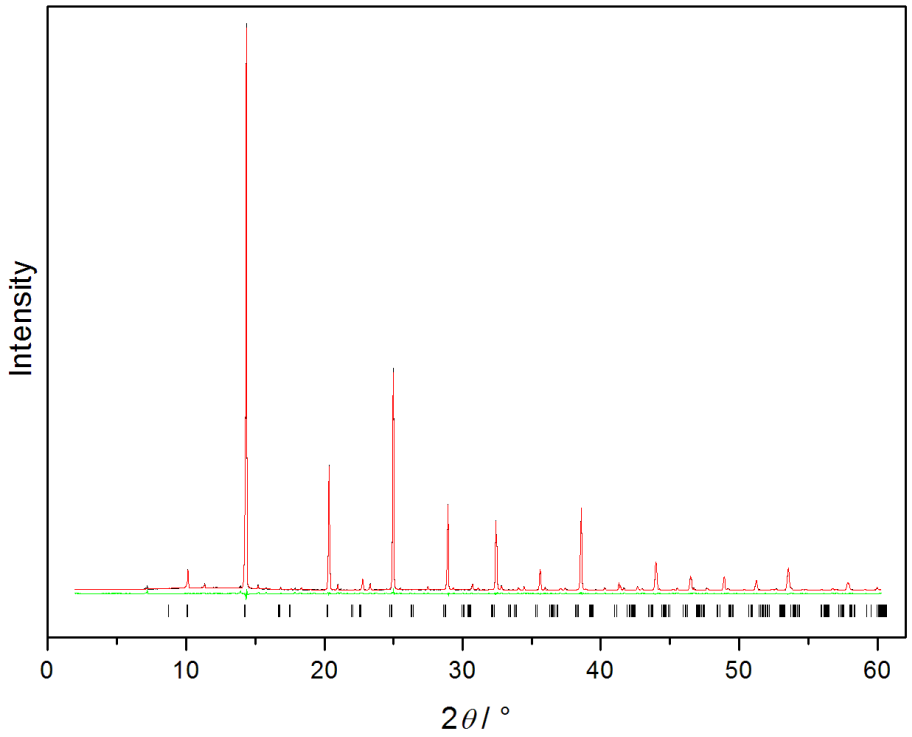

Figure S3. Rietveld refinement of X-ray powder diffraction pattern of $PrTaON_2$ profile with experimental data (black line), calculated pattern (red line), difference (green line), and positions of Bragg reflections (black bars).

9.1.3.2 Electron microscopy analysis

Table S3.

	Pr	Ta	O	N
	21	21	20	38
	21	23	19	37
Average	21	22	19.5	37.5

SEM measurements in atomic%.

9.1.4 $NdTaON_2$

9.1.4.1 Rietveld Refinement

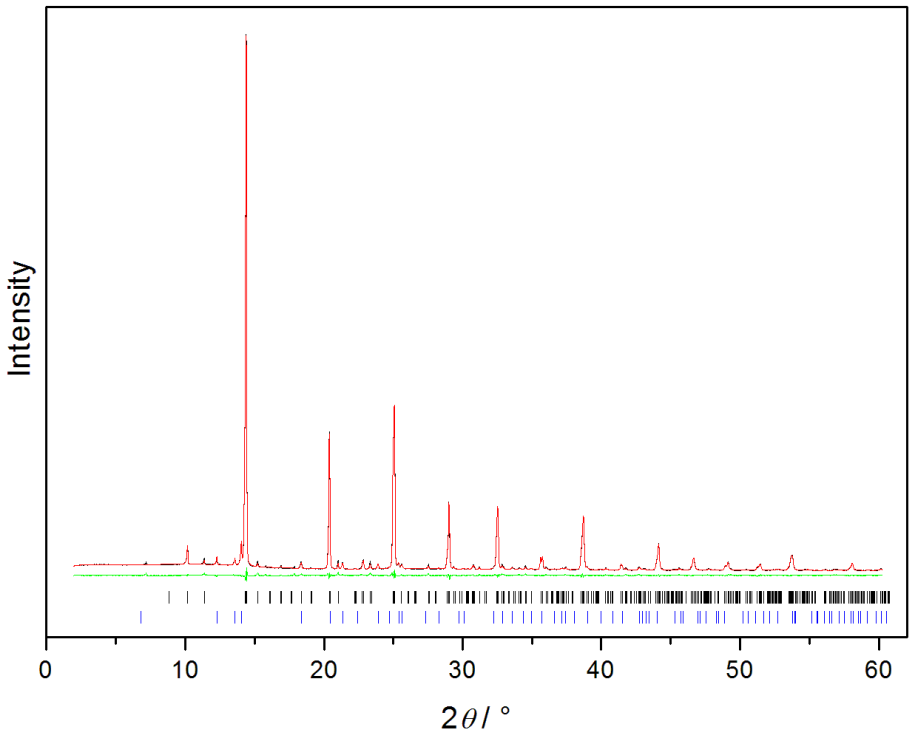

Figure S4. Rietveld refinement of X-ray powder diffraction pattern of $NdTaON_2$ profile with experimental data (black line), calculated pattern (red line), difference (green line), and positions of Bragg reflections (black bars: $NdTaON_2$ (97.4%) and blue bars: Nd_2O_3 (2.6%)).

9.1.4.2 Electron microscopy analysis

Table S4.

	Nd	Ta	O	N
	17	19	23	41
	17	20	24	39
	16	19	28	37
Average	16.66	19.34	25	39

SEM measurements in atomic%.

9.1.5 $SmTaON_2$

9.1.5.1 Rietveld Refinement

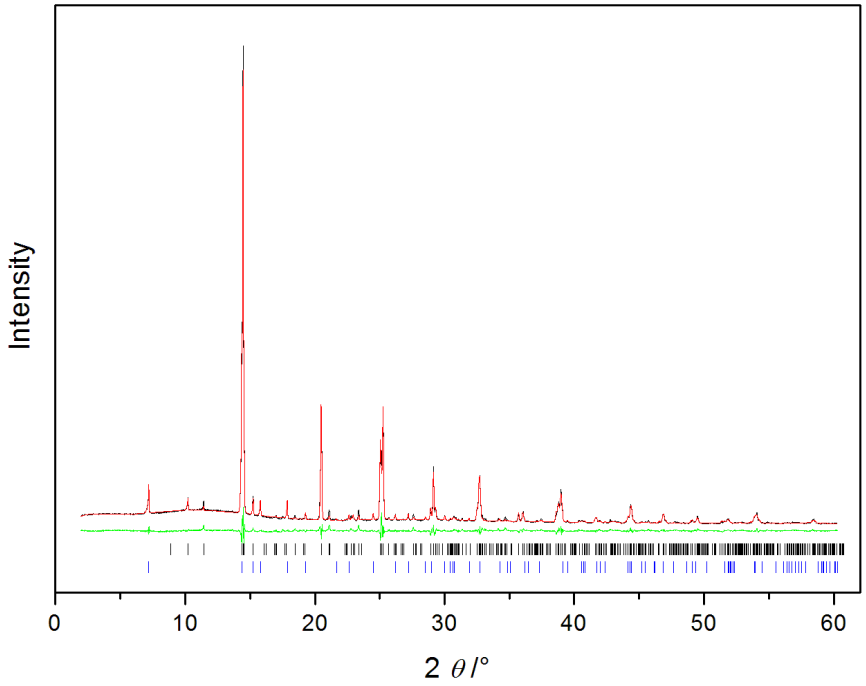

Figure S5. Rietveld refinement of X-ray powder diffraction pattern of $SmTaON_2$ profile with experimental data (black line), calculated pattern (red line), difference (green line), and positions of Bragg reflections (black bars: $SmTaON_2$ (91.5%) and blue bars: $NaTaN_2$ (8.5%)).

9.1.5.2 Electron microscopy analysis

Table S5.

	Sm	Ta	O	N
	18	20	22	40
	20	23	22	35
	17	19	22	42
Average	18.3	20.7	22	39

SEM measurements in atomic%.

9.1.6 $GdTaON_2$

9.1.6.1 Rietveld Refinement

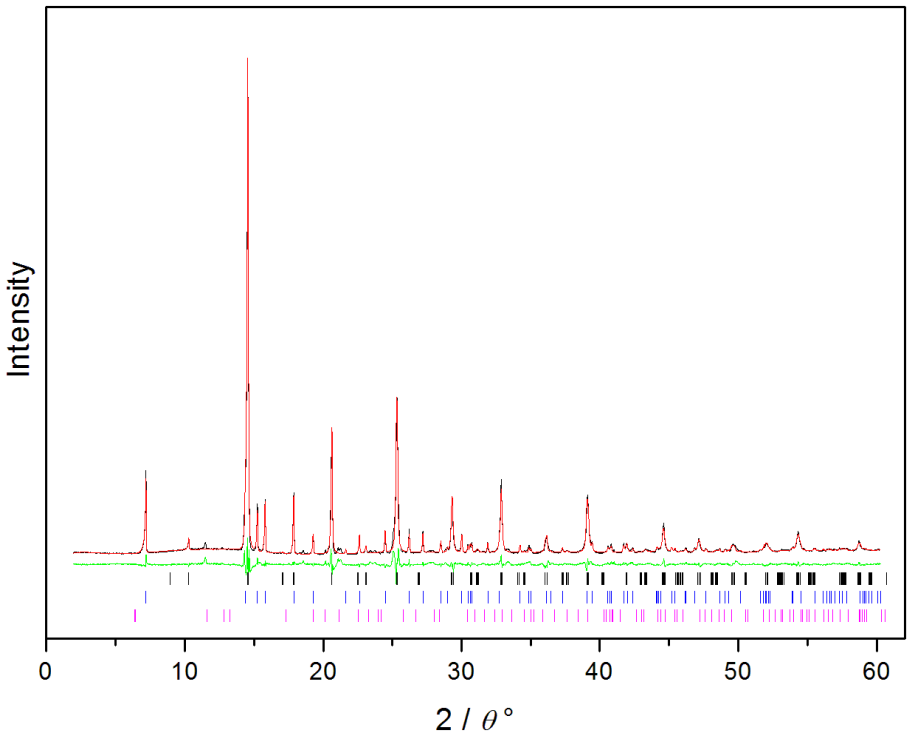

Figure S6. Rietveld refinement of X-ray powder diffraction pattern of $GdTaON_2$ profile with experimental data (black line), calculated pattern (red line), difference (green line), and positions of Bragg reflections (black bars: $GdTaON_2$ (85.2%), blue bars: $NaTaN_2$ (10.3%), pink bars: Gd_2O_3 4.5%).

9.1.6.2 Electron microscopy analysis

Table S6.

	Gd	Ta	O	N
	16	15	21	48
	26	29	10	35
	27	28	13	32
	19	20	17	44
	20	21	19	40
Average	21.6	22.6	16	39.8

SEM measurements in atomic%.

9.2 Supplementary information for the publication: Ammonothermal Synthesis of the Mixed-Valence Nitrogen-Rich Europium Tantalum Ruddlesden-Popper Phase $Eu^{II}Eu^{III}_2Ta_2N_4O_3$

Published in: *Chem. Eur. J.* **2019**, *2019*, 2304–2311.

Authors: Niklas Cordes, Markus Nentwig, Lucien Eisenburger, Oliver Oeckler, Wolfgang Schnick

9.2.1 TEM-BF Image of $Eu^{II}Eu^{III}_2Ta_2N_4O_3$

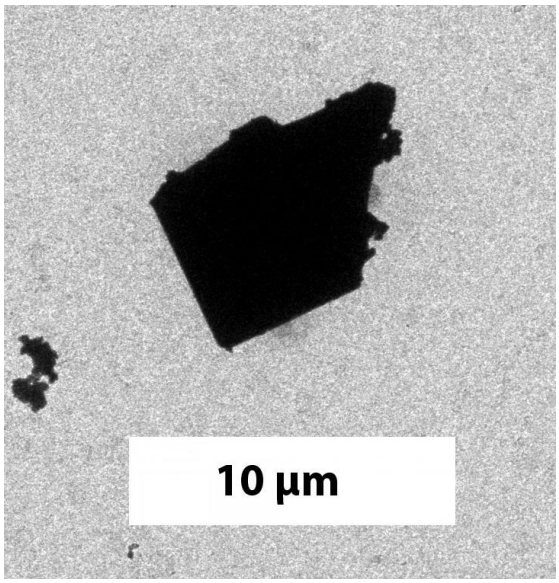

SI Figure 1. TEM-BF image of the single crystal of $Eu_3Ta_2N_4O_3$ used for structure determination by synchrotron diffraction.

9.2.2 Crystallographic data from the Rietveld refinement for $Eu_3Ta_2N_4O_3$.

SI Table 1. Crystallographic data from the Rietveld refinement for $Eu_3Ta_2N_4O_3$.

Formula	$Eu_3Ta_2N_4O_3$
Crystal system	tetragonal
Space group	$P4_2/mnm$ (no. 136)
Lattice parameters [Å]	a = 5.7125(3)
	c = 19.8621(13)
Cell volume [Å³]	648.15(7)
Formula units / cell	4
Density [g · cm³]	9.4467(10)
T [K]	293(2)
Diffractometer	STOE STADI P
Radiation [Å]	Mo-$K_{\alpha 1}$ (λ = 0.70930 Å)
θ range [°]	$2.0 \leq 2\theta \leq 60.7$
Data points	3886
Total number of reflections	577
Refined parameters	45
Background function	Shifted Chebyshev
R values [%]	R_p = 0.0591
	R_{wp} = 0.0858
	R_{Bragg} = 0.0290
Goodness of fit	3.566

9.2.3 Rietveld analysis

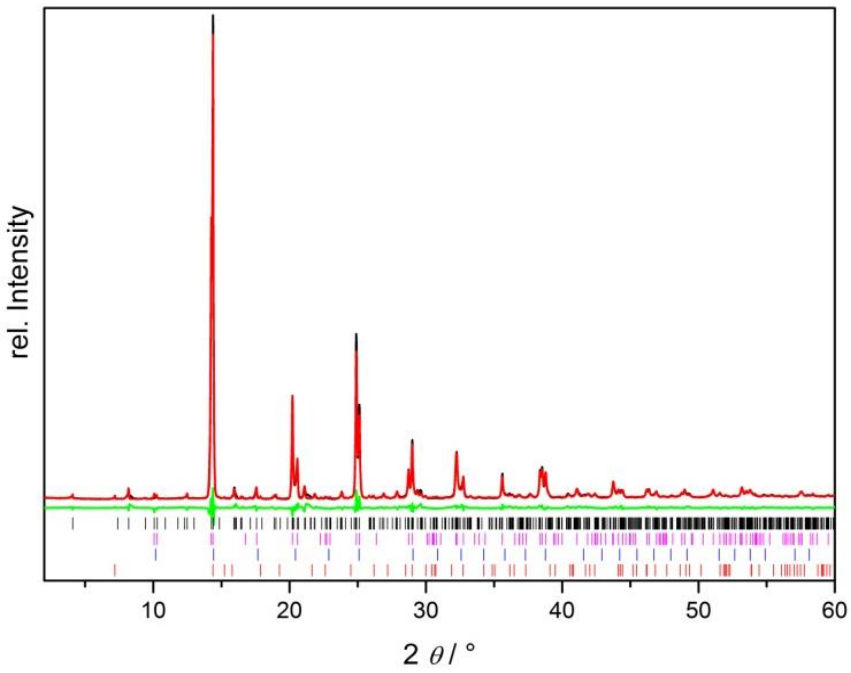

SI Figure 2: Rietveld analysis (linear scale of rel. intensity) of $Eu_3Ta_2N_4O_3$ with experimental data (black line) with calculated pattern (red line), difference profile (green line) and markers for Bragg positions ($Eu_3Ta_2N_4O_3$ black (60.6 wt%), $EuTaO_2N$ (tetragonal) magenta (23.0 wt%), $EuTaO_2N$ (cubic) blue (15.8 wt%) and $NaTaN_2$ red (0.6 wt%)).

9.2.4 Anisotropic displacement parameters

SI Table 2. Anisotropic displacement parameters (U_{iy} in $Å^2$) of $Eu_3Ta_2N_4O_3$ (standard deviations in parentheses).

Atom	U_{11}	U_{22}	U_{33}	U_{12}	U_{13}	U_{23}
Ta1	0.00883(13)	0.00883(13)	0.00681(18)	0.00118(5)	0.00134(4)	0.00134(4)
Eu2	0.01115(15)	0.01115(15)	0.0088(3)	0.00120(8)	0	0
Eu3	0.00833(14)	0.00833(14)	0.0049(2)	0.00020(7)	-0.00009(6)	-0.00009(6)
O1	0.0132(11)	0.0132(11)	0.0099(18)	-0.0022(14)	0	0
O2	0.0128(8)	0.0128(8)	0.0081(14)	-0.0015(12)	-0.0001(6)	-0.0001(6)
N3	0.0079(10)	0.0079(10)	0.012(2)	0.0013(13)	0	0
N4	0.0111(11)	0.0111(11)	0.003(2)	-0.0026(14)	0	0
N5	0.0087(13)	0.0092(13)	0.0059(16)	0.0016(10)	0	0

9.2.5 SEM-EDX point measurements

SI Table 3. SEM-EDX point measurements of $Eu_3Ta_2N_4O_3$ (in atom%) with calculated values in parentheses and average with standard deviation.

Eu (25)	**Ta (16.6)**	**N (33.4)**	**O (25)**	
24.1	19.9	31.3	24.7	
19.8	15.7	34.9	29.6	
20.8	16.2	35.6	27.4	
20.7	17.5	34.4	27.4	
26.2	19.3	29.1	25.4	
22.7	17.3	32.9	27.1	
24.7	18.5	31.0	25.8	
25.9	19.1	29.6	25.4	
24.0	17.6	32.4	26.0	
22.8	18.1	33.9	25.2	
25.0	19.1	30.9	25.0	
23.3	**18.0**	**32.4**	**26.3**	**Ø**
± 2.1	**± 1.3**	**± 2.1**	**± 1.4**	

9.2.6 N/O assignment

9.2.6.1 Bond valence sums

SI Table 4: Bond valence sums of anions and cations.

	O1	**O2**	**N3**	**N4**	**N5**	**Ta1**	**Eu2**	**Eu3**
BVS	1.96	1.75	3.15	2.98	3.09	4.90	1.77	3.11
Oxidation state	-2	-2	-3	-3	-3	+5	+2	+3

9.2.6.2 CHARDI

SI Table 5. CHARDI values calculated for each of the cations. With Δq as the fraction of the charge received by the ion, Q the total charge received by the ion, and q the formal charge (oxidation number).

Cation/Atom site	Δq	Q	q
Ta1			
O1	0.660	-2.506	-2
N5	0.910	-2.833	-3
N4	1.106	-2.981	-3
O2	0.404	-2.002	-2
N5	0.910	-2.833	-3
N3	1.011	-2.844	-3
Ta1		5.037	5

Cation/Atom site	Δq	Q	q
Eu2			
N4	0.258	-2.981	-3
N3	0.034	-2.844	-3
N3	0.034	-2.844	-3
N5	0.135	-2.833	-3
N5	0.135	-2.833	-3
N4	0.258	-2.981	-3
N4	0.127	-2.981	-3
N5	0.135	-2.833	-3
N5	0.135	-2.833	-3
N4	0.127	-2.981	-3
O1	0.311	-2.506	-2
O1	0.311	-2.506	-2
Eu2		1.915	2

Cation/Atom site	Δq	Q	q
Eu3			
N3	0.377	-2.844	-3
N5	0.371	-2.833	-3
O2	0.654	-2.002	-2
O2	0.472	-2.002	-2
N5	0.371	-2.833	-3
O2	0.472	-2.002	-2
O1	0.282	-2.506	-2
Eu3		3.006	3

10 Publications

The results complied in this thesis were published in scientific journals as detailed in the following list. The respective funding can be looked up in the publications themselves. The contributions of the following manuscripts are fully described below.

10.1 List of Publications within this Thesis

10.1.1 Ammonothermal Synthesis of *EAM*O_2N (*EA* = Sr, Ba; *M* = Nb, Ta) Perovskites and ^{14}N Solid-State NMR Investigations of *AM*(O,N)$_3$ (*A* = Ca, Sr, Ba, La)

N. Cordes, T. Bräuniger, W. Schnick

published in: *Eur. J. Inorg. Chem.* **2018**, *2018*, 5019–5026

In this contribution, the ammonothermal synthesis, structure elucidation from powder X-ray diffraction data and subsequent Rietveld refinements, diffuse reflectance spectroscopy with band gap determination, light microscope pictures, literature research, writing of the manuscript and sample preparation were carried out by Niklas Cordes. ^{14}N solid-state NMR measurements was performed by Thomas Bräuniger. Graphical material was created by Niklas Cordes. Wolfgang Schnick directed and supervised the research project. All authors revised the manuscript.

10.1.2 Ammonothermal Synthesis of Crystalline Oxonitride Perovskites *Ln*$TaON_2$ (*Ln* = La, Ce, Pr, Nd, Sm, Gd)

N. Cordes, W. Schnick

published in: *Chem. Eur. J.* **2017**, *23*, 11410–11415

For this manuscript, literature research and writing of the major parts was performed by Niklas Cordes. Sample synthesis by the ammonothermal approach and subsequent powder X-ray diffraction analysis with Rietveld refinement, UV Vis and IR measurements , spectroscopic transitions and band gap elucidation was carried out by Niklas Cordes, who also created the graphical material. Wolfgang Schnick directed and supervised the general work. Both authors revised the manuscript.

10.1.3 Ammonothermal Synthesis of the Mixed-Valence Nitrogen-Rich Europium Tantalum Ruddlesden-Popper Phase $Eu^{II}Eu^{III}_2Ta_2N_4O_3$

Niklas Cordes, Markus Nentwig, Lucien Eisenburger, Oliver Oeckler, Wolfgang Schnick

published in: *Eur. J. Inorg. Chem.* **2019**, *2019*, 2304–2311

In this publication, preparation of the ammonothermal synthesis obtained material, powder X-ray diffraction analysis, Rietveld refinements, diffuse reflectance spectroscopy and subsequent band gap determination by the Tauc method was performed by Niklas Cordes. Structure elucidation by TEM measurements and sample preparation for microfocused synchrotron measurements was performed by Lucien Eisenburger. The synchrotron measurements were done by Markus Nentwig and Lucien Eisenburger under supervision of Oliver Oeckler. Structure elucidation was performed by Markus Nentwig and confirmed by Lucien Eisenburger and Oliver Oeckler. Grapfical material was created by Niklas Cordes and Lucien Eisenburger. The manuscript was written by Niklas Cordes in a leading role and supported by Lucien

Eisenburger and Markus Nentwig. Wolfgang Schnick directed and supervised the research project. All authors revised the manuscript.

10.1.4 Ammonothermal Crystal Growth of *A*TaN_2 with *A* = Na, K, Rb, Cs and their Optical and Electronic Properties

Niklas Cordes, Robin Niklaus, Wolfgang Schnick

published in: *Cryst. Growth Des.* **2019**, *19*, 484–3490.

Development of the synthesis conditions, literature screening, writing of the main part of the manuscript, powder X-ray diffraction measurements with subsequent Rietveld refinements, spectroscopic measurements and band gap determination were carried out by Niklas Cordes. DFT calculations and evaluation of the results were performed by Robin Niklaus. Graphical material was created by Niklas Cordes and Robin Niklaus. Wolfgang Schnick directed and supervised this work. All three authors revised the manuscript.

10.2 Other publications

A Quaternary Core-Shell Oxynitride Nanowire Photoanode Containing a Hole-Extraction Gradient for Photoelectrochemical Water Oxidation

Z. Ma, T. Thersleff, A. Görne, **N. Cordes**, Y. Liu, S. Jakobi, A. Rokicinska, A. Schichtl, R. Coridan, P. Kuśtrowski, W. Schnick, R. Dronskowski, A. Slabon

ACS Appl. Mater. Interfaces **2019**, *11*, 19077–19086.

Ammonothermal Synthesis of Alkali-Alkaline Earth Metal and Alkali-Rare Earth Metal Carbodiimides: $K_{5-x}M_x(CN_2)_{2+x}(HCN_2)_{1-x}$ (M = Sr, Eu) and $Na_{4.32}Sr_{0.68}(CN_2)_{2.68}(HCN_2)_{0.32}$

M. Mallmann, J. Häusler, **N. Cordes**, W. Schnick

Z. Anorg. Allg. Chem. **2017**, *643*, 1956–1961.

Passivation of PbS Quantum Dot Surface with L-glutathione in Solid-State Quantum-Dot-Sensitized Solar Cells

A. N. Jumabekov, **N. Cordes**, T. D. Siegler, P. Docampo, A. Ivanova, K. Fominykh, D. D. Medina, L. M. Peter and T. Bein

ACS Appl. Mater. Interfaces, **2016**, *8*, 4600–4607.

Comparison of Solid-State Quantum-Dot-Sensitized Solar Cells with Ex Situ and In Situ Grown PbS Quantum Dots

A. N. Jumabekov, T. D. Siegler, **N. Cordes**, D. D. Medina, D. Böhm, P. Garbus, S. Meroni, L. M. Peter and T. Bein

J. Phys. Chem. C **2014**, *118*, 25853–25862.

Springer Series in Materials Science, unpublished.

Ammonothermal Synthesis and Crystal Growth of Nitrides – Chemistry and Technology

N. Cordes, M. Mallmann, W. Schnick

10.3 Contributions to Conferences, Seminars and Workshops

Seminar Schnick Group, Munich, Germany

03.12.2014

Master Thesis – Synthese von binären und höheren (Oxo)Nitriden mit dem Ammonothermalverfahren (talk)

Niklas Cordes, Wolfgang Schnick

1. Workshop zur Ammonothermalsynthese von Nitriden, Hopferau, Germany

19.02.2015

Synthesis of binary and higher (oxo)nitrides with the ammonothermal approach (talk)

Niklas Cordes, Wolfgang Schnick

Seminar Schnick Group, Munich, Germany

29.04.2015

Ammonothermal Syntheses in Supercritical NH_3 (talk)

Niklas Cordes, Wolfgang Schnick

Ammono-FOR researcher group meeting, Erlangen, Germany

27.07.2015

Synthesis of binary and higher (oxo)nitrides with the ammonothermal approach (talk)

Niklas Cordes, Wolfgang Schnick

Seminar Schnick Group, Munich, Germany

03.01.2016

Ammonothermal Syntheses in Supercritical NH_3 (talk)

Niklas Cordes, Wolfgang Schnick

2. Obergurgl Seminar Festkörperchemie, Obergurgl, Austria

26. – 29.01.2016

Ammonothermalsynthese neuer Oxonitridoperowskite (talk)

Niklas Cordes, Wolfgang Schnick

Ammono-FOR researcher group meeting, Stuttgart, Germany

10.02.2016

Synthesis of binary and higher (oxo)nitrides with the ammonothermal approach (talk)

Niklas Cordes, Wolfgang Schnick

Seminar Schnick Group, Munich, Germany

06.07.2016

Ammonothermalsynthese (talk)

Niklas Cordes, Wolfgang Schnick

Ammono-FOR researcher group meeting, Erlangen, Germany

26.10.2016

Synthesis of binary and higher (oxo)nitrides with the ammonothermal approach (talk)

Niklas Cordes, Wolfgang Schnick

2. Workshop zur Ammonothermalsynthese von Nitriden Hopferau, Germany

14. – 15.02.2017

Ammonothermal syntheses of multinary nitrides and oxonitride perovskites (talk)

Niklas Cordes, Wolfgang Schnick

Seminar Schnick Group, Munich, Germany

17.05.2017

Unbekanntes Flugobjekt (workshop)

Niklas Cordes, Wolfgang Schnick

Ammono-FOR researcher group meeting, Erlangen, Germany

19.07.2017

Synthesis of binary and higher (oxo)nitrides with the ammonothermal approach (talk)

Niklas Cordes, Wolfgang Schnick

Ammono-FOR researcher group meeting, Munich, Germany

13.11.2017

Synthesis of binary and higher (oxo)nitrides with the ammonothermal approach (talk)

Niklas Cordes, Wolfgang Schnick

Seminar Schnick Group, Munich, Germany

29.11.2017

Die Würfel sind gefallen – Neues aus dem Autoklaven (talk)

Niklas Cordes, Wolfgang Schnick

3. Obergurgl Seminar Festkörperchemie, Obergurgl, Austria

23. – 26.01.2018

Ammonothermalsynthese von Oxonitridoperowskiten (talk)

Niklas Cordes, Wolfgang Schnick

Ammono-FOR researcher group meeting, Stuttgart, Munich

13.03.2018

Ammonothermal synthesis of multinary nitrides and oxonitrides (talk)

Niklas Cordes, Wolfgang Schnick

Seminar Schnick Group, Munich, Germany

25.04.2018

Brückenbau (workshop)

Niklas Cordes

47. Hirschegg-Seminar Festkörperchemie 2018, Hirschegg, Austria

31.05. – 03.06.2018

Ammonothermalsynthese, früher und heute (talk)

Niklas Cordes, Markus Nentwig, Lucien Eisenburger, Oliver Oeckler, Wolfgang Schnick

Seminar Schnick Group, Munich, Germany

20.06.2018

Ammonothermal Syntheses in Supercritical NH_3 (talk)

Niklas Cordes, Wolfgang Schnick

Ammono-FOR researcher group meeting,Erlangen, Germany

13.07.2018

Synthesis of binary and higher (oxo)nitrides with the ammonothermal approach (talk)

Niklas Cordes, Wolfgang Schnick

16. Mitteldeutsches Anorganiker-Nachwuchssymposium, Jena, Germany

16.09 – 17.09.2018

Kationen- und Anionen-Ausordnung in der Ruddlesden-Popper-Phase $Eu^{2+}Eu^{3+}_2Ta_2N_4O_3$ (talk)

Lucien Eisenburger, Niklas Cordes, Markus Nentwig, Juliane Stahl, Theresa Block, Rainer Pöttgen, Dirk Johrendt, Wolfgang Schnick, Oliver Oeckler

Seminar Schnick Group, Munich, Germany

12.12.2018

Perowskite und andere Verbindungen aus dem Autoklaven – Auf die Größe kommt es an (talk)

Niklas Cordes, Wolfgang Schnick

4. Obergurgl Seminar Festkörperchemie, Obergurgl, Austria

29.01.-01.02.2019

Ammonothermalsynthese der Ruddlesden-Popper-Phase $Eu_3Ta_2N_4O_3$ (talk)

Niklas Cordes, Markus Nentwig, Lucien Eisenburger, Oliver Oeckler, Wolfgang Schnick

21st JCF Frühjahrssymposium and 2nd European Young Chemists' Meeting, Bremen, Germany

20.03.-23.03.2019

Ammonothermal Synthesis of Nitride Oxide Perovskites and Related Structures (poster)

Niklas Cordes, Wolfgang Schnick

10.4 Deposited crystallographic information

Crystallographic data (CIF) of investigated compounds were deposited at the Fachinformationszentrum (FIZ) Karlsruhe, 76344 Eggenstein-Leopoldshafen, Germany and are available on quoting the following CSD depository numbers.

The following table provides the compounds and associated deposited CSD numbers listed in this thesis.

Compound	CSD number
$SrNbNO_2$	434769
$BaNbNO_2$	434770
$SrTaNO_2$	434768
$BaTaNO_2$	434767
$LaTaN_2O$	433036
$CeTaN_2O$	433037
$PrTaN_2O$	433038
$NdTaN_2O$	433039
$SmTaN_2O$	433040
$GdTaN_2O$	433041
$Eu_3Ta_2N_4O_3$	1890993 (CCDC)
$NaTaN_2$	1915429 (CCDC)
$KTaN_2$	1915430 (CCDC)
$RbTaN_2$	1915431 (CCDC)
$CsTaN_2$	1915652 (CCDC)